OPTIMIZATION OF THERMAL ENERGY STORAGE SYSTEMS INTEGRATED WITH CONCENTRATED SOLAR POWER PLANTS

by

Zahra Razzaghpanah

A dissertation submitted to the faculty of
The University of North Carolina at Charlotte
in partial fulfillment of the requirements
for the degree of Doctor of Philosophy in
Mechanical Engineering

Charlotte

2019

Approved by:

_____
Dr. Nenad Sarunac

_____
Dr. Gloria Elliott

_____
Dr. Harish Cherukuri

_____
Dr. Charles Lee

_____
Dr. Shen-En Chen

ABSTRACT

ZAHRA RAZZAGHPANAH. Optimization of Thermal Energy Storage Systems integrated with concentrated solar power plants. (Under the direction of DR. NENAD SARUNAC)

Concentrated Solar Power (CSP) plants have been a major area of study for many years as an alternative to the conventional methods of power generation. High dependency of the global economy on fossil fuels rises sustainability concerns. Also, global climate change linked to the CO_2 emissions from burning fossil fuels, makes it very important to develop and deploy the carbon-free technologies, such as solar energy as a source of power. Utilizing reliable and renewable sources of energy in an economically sound and dependable way is perhaps one of the most important global challenges of the present time.

Solar energy, being inexhaustible and non-polluting in contrast to fossil fuels, has gained popularity among scientists and engineers around the world as a potential alternative. However, solar energy is variable and intermittent. Also, the peaks in solar irradiation and electricity demand typically do not coincide, resulting in a need for energy storage. Therefore, to utilize the solar energy most effectively, Thermal Energy Storage (TES) systems are needed for a steady and uninterrupted supply of energy.

A two-dimensional (2-D) steady-state numerical analysis of the sensible heat indirect TES comprising a heat exchanger immersed in the heat storage medium was performed to improve understanding of the thermal energy storage process, develop a better design of the high-efficiency TES, and improve utilization of solar energy by reducing its variability during the daytime and allowing its use during the periods of low or no solar irradiation. The statistical regression analysis was used to correlate the results.

This project focused on determining the optimum geometry of the heat exchanger(s) used in TES. Numerical simulations were performed for different geometries of the heat exchanger to determine the most efficient design and develop design criteria.

Numerical modeling and design analysis of the TES system was performed by employing ANSYS-Workbench [1] and StarCCM+ [2] Professional software packages.

DEDICATION

To my dearest parents, and my loving husband. Without their unrelenting support and love, none of this would be possible.

ACKNOWLEDGEMENTS

My research would not have been possible, without the encouragement and support from a number of people. I would like to take this opportunity to recognize them.

First and foremost, I would like to express my deepest gratitude to my graduate advisor, Dr. Nenad Sarunac. There is no doubt that I would not be able to complete this work without his support and guidance. I am deeply grateful for having the opportunity to collaborate with him during my PhD studies at the University of North Carolina at Charlotte.

I would also like to express my gratitude to Dr. Gloria Elliott, Dr. Harish Cherukuri, Dr. Charles Lee and Dr. Shen-En Chen for accepting to be on my doctoral committee and generously sharing their knowledge with me.

I would also like to express my gratitude to graduate school and Energy Production and Infrastructure Center (EPIC) at UNC Charlotte for supporting me by tuition scholarship (GASP) and Graduate Research scholarship during my PhD program.

TABLE OF CONTENTS

LIST OF FIGURES

LIST OF TABLES

NOMENCLATURE

D	Diameter of the cylinder (m)
H	Height (m)
S_L	Longitudinal (vertical) center to-center-cylinder distance
S_T	Transverse (horizontal) center-to-center cylinder distance
ϑ	Kinematic viscosity (m^2/s)
α	Thermal diffusivity (m^2/s)
μ	Dynamic viscosity ($N.s/m^2$)
k	Thermal conductivity (W/m.K)
c_p	Specific heat, (J/kg.K)
g	Acceleration due to gravity, (m/s^2)
T_w	The tube wall temperature (K)
T_∞	The fluid temperature (K)
β	The thermal expansion coefficient (K^{-1})
Ra	Rayleigh number
Ra^*	Modified Rayleigh number
Ra_D	Rayleigh number (based on cylinder diameter)
Ra_{S_L}	Rayleigh number (based on cylinder spacing)
$Ra_{S_L}{}^*$	Modified Rayleigh number (based on cylinder spacing)
Pr	Prandtl number
Nu	Nusselt number
$\overline{Nu}_D$	Average Nusselt number (based on cylinder diameter)
$\overline{Nu}_{S_L}$	Average Nusselt number (based on cylinder spacing)
q	Total heat transfer rate integrated over the surface of a cylinder (W)
q'	Volumetric Total heat transfer rate integrated over the surface of a cylinder (W/m^3)
$\tilde{q}$	Dimensionless volumetric heat transfer density
h	Convective heat transfer coefficient ($W/m^2.K$)

u, v	Velocity components (m/s)

SUBSCRIPTS

max	Maximum
min	Minimum
opt	Optimum
ref	Reference

ACRONYMS

ES	Energy storage
PT	Parabolic through
CSP	Concentrated solar power plant
TES	Thermal energy storage
HXE	Heat exchanger
HTF	Heat transfer fluid
HSF	Heat storage fluid
SHS	Sensible heat thermal energy storage
PCM	Phase change material TES, Latent heat thermal energy storage
TCS	Thermo-chemical energy storage

CHAPTER 1: INTRODUCTION AND PROBLEM STATEMENT

1-1. Overview

Utilizing reliable and renewable sources of energy in an economically sound and dependable way is perhaps one of the most important global challenges of the present time. Solar energy, being inexhaustible and non-polluting in contrast to fossil fuels, has gained popularity among scientists and engineers around the world as a potential alternative. However, the amount of solar energy available at a fixed point is not constant. Therefore, in order to utilize solar energy most effectively, solar energy storage systems are necessary for a steady and uninterrupted supply of energy.

Figure 1-1 represents different types of solar energy storage methods. Thermal energy storage system has come into focus as a method for temporary energy storage of heat to be used in concentrated solar power plants. The Crescent Dunes Solar Energy Project is an example of effective use of TES in combination with CSP [3].

TES systems have also been proposed to improve flexibility of fossil-fired power plants, especially coal-fired plants, which are due to the penetration of renewables required to follow the load (cycle), as well as operate at lower and lower minimum loads. Since most coal-fired power plants were not designed for cycling duty, this new mode of operation is resulting in a significant cycling damage to the equipment.

Figure 1-2 is a simple schematic representation of TES integration and application; TES system integrated with a power plant would reduce temperature variations caused by load changes and reduce cycling damage.

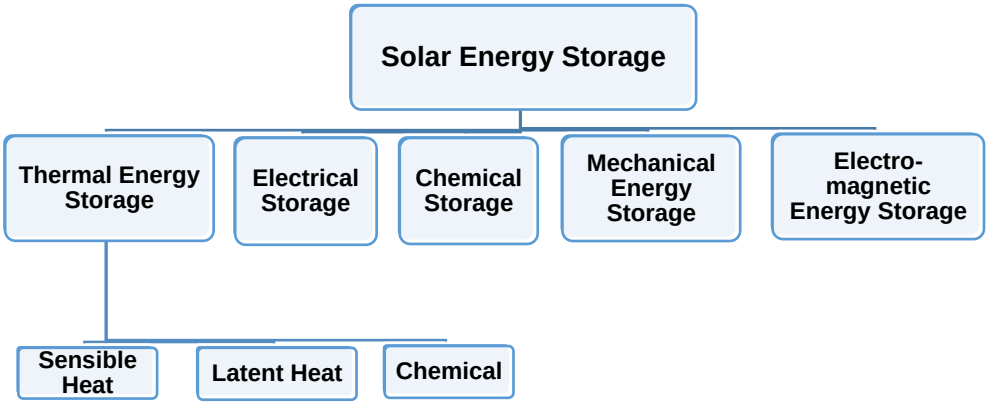

Figure 1-1 Solar energy storage classification.[4]

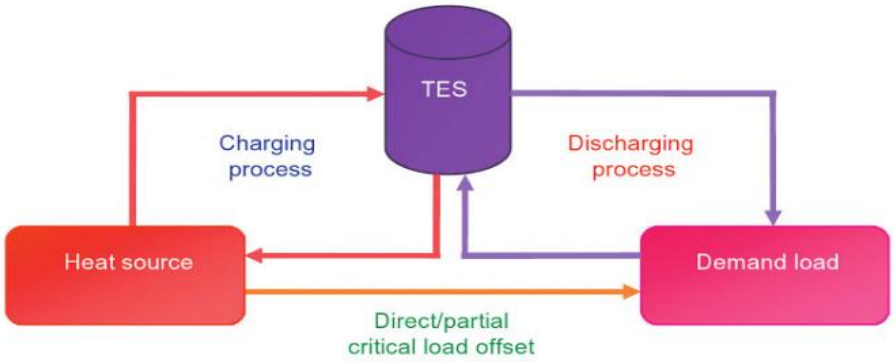

Figure 1-2 Simple schematic representation of TES integration and application. [5]

1-2. Concentrated Solar Power Technology

Finite resources of fossil fuels as well as the CO_2 emissions contributing to global warming, dictates a more efficient use of renewable energy resources such as solar energy. Concentrated solar power (CSP) as one of the most efficient renewable technologies for

generation of electricity is considered as a potential alternative to conventional electricity generating technologies.

Concentrating solar power (CSP) is a power generation technology that uses solar energy instead of fossil fuels to provide thermal energy input required to the thermodynamic power cycle. A concentrating solar power (CSP) system uses a large number of sun-tracking mirrors to concentrate the solar rays. In current CSP systems, concentrated solar energy is used to produce steam as the working fluid for the steam Rankine cycle. The electricity is then generated by a generator driven by the steam turbine. Depending on whether the solar rays are focused to a focal point or concentrated along a focal line, concentrated power plants are divided into two groups of the point-focusing and line-focusing systems, respectively [6]. Parabolic and Fresnel through technologies with a single-axis sun tracking system, which produce high-pressure superheated steam are the examples of the line-focusing systems. Solar tower technology with a two-axis tracking system is an example of the point focusing system [6].

1-2-1 Parabolic Through (PT)

The parabolic trough technology shown in Figure 1-3 uses highly reflective parabolic-shaped mirrors to concentrate solar rays to a heat transfer fluid (HTF) passing through a steel absorber tube located at the focal line of the mirror. Due to the single-axis nature of the line focusing systems, parabolic trough is aligned on north-south axis and rotates to track sun during the day. The 70 to 100 times concentrated sunlight heats the heat transfer fluid (synthetic oil or molten salt) up to the 350 to 550$^{\circ C}$. Parabolic trough is so far

the most mature technology with annual solar-to-electricity efficiency of about 10-15% [7].

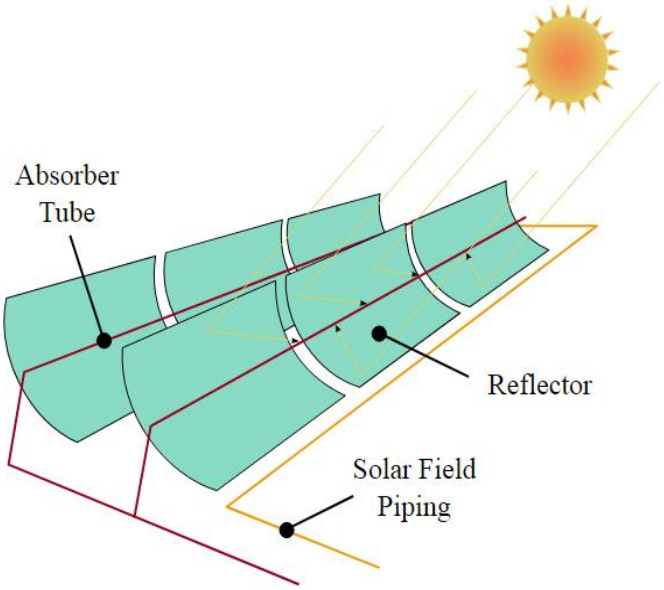

Figure 1-3 A diagram of a parabolic trough solar farm. [8]

1-2-2 Solar Power Tower Technology (CSP-T, or TCSP)

Solar power tower (thermal solar) or central receiver technology shown in Figure 1-4 consists of a large number of sun-tracking computer-controlled mirrors – heliostats – that reflect solar radiation to the central receiver positioned on the top of the tower. The 600 to 1000 times concentrated sunlight heats the heat transfer fluid, typically molten salt or liquid metal, up to the 800 to 1000˚C. Mineral or synthetic oils are used for maximum temperatures below 550^{o}C. New concepts are being developed where fluidized solid medium, such as sand is used as the heat transfer "fluid". The high temperature heat transfer fluid from the solar towers can be used to heat a working fluid (He, sCO_2, or air) for the Brayton cycle or generate steam for the steam Rankine cycle. Combined cycles, employing Brayton cycle as a topping cycle and steam Rankine cycle as a bottoming cycle are also

being developed for CSP applications. Solar tower technology has a mirror-to-electricity efficiency in the 20 to 35% range in the sunny regions [7].

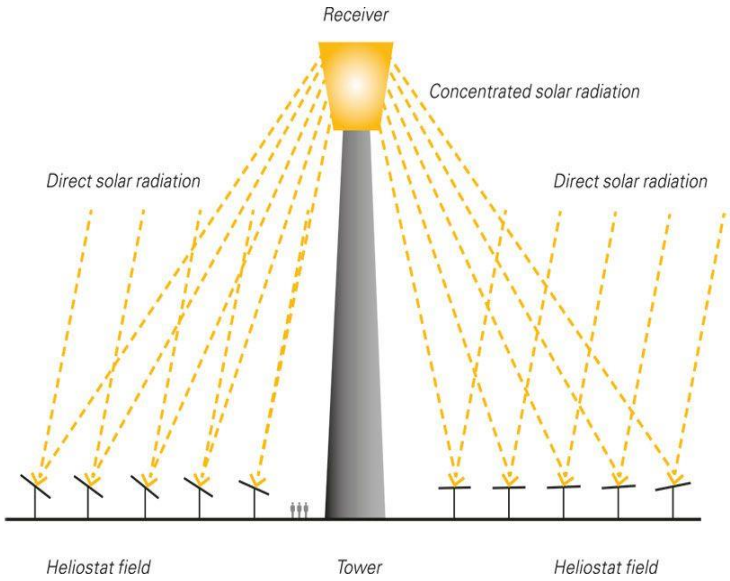

Figure 1-4 A diagram of a solar power tower farm. [9]

1-3. Thermal Energy Storage

Energy storage (ES) system is a system which stores energy in some form (potential, kinetic, electrical and thermal) and facilitates its recovery for later use [10]. Thermal energy storage is a technology that stores thermal energy (heat) for later use, such as improved utilization of solar energy. TES is a vital area of research in energy conversion applications. Nearly all conventional power generation plants generate heat as a precursor to electricity (i.e., through thermodynamic power generation cycles). The benefits of TES technologies include the following [5]:

- Reduced usage of fossil fuels.
- Reduction of the greenhouse gases emissions through energy conservation.
- Cost reduction of equipment and plant operation due to lower amount of fossil fuel-derived electrical energy.

- Reduced price of fuel and other economic risks.
- Increasing cooling/heating systems capacity and utility service through load shifting from on-peak to part load conditions.
- Increase operational flexibility and availability and thus, improve performance of the power plant by avoiding load cycling.
- Decreased installation cost achieved through reduction of redundant electrical/mechanical equipment for meeting the backup cooling or heating capacity of essential systems.
- Environmentally friendly.

1-3-1 TES in Concentrating Solar Thermal Power

Concentrating solar thermal power, commonly referred to as CSP, is unique among renewable energy generators because even though it is variable, like solar photovoltaics (PV) and wind, it can easily be coupled with thermal energy storage (TES) system, as well as conventional fuels, making it highly dispatchable [11]. Without TES the application of CSP would be limited to serving as an adjunct to fossil fuel plants, for example supplementing thermal energy generated by the natural gas combustion with solar heat to increase power output [12]. Roundtrip efficiencies for thermal energy storage systems can be quite high, on the order of 95% or higher, which makes the storage option for CSP much more attractive than for PV, where battery or fuel-production technologies are needed to implement storage [13].

Depending on the storage period required, economic viability, and operating conditions, different TES systems are designed. For storing thermal energy there are three

approaches that have been considered over the years in solar thermal systems. These are: sensible-heat storage (where a change of temperature occurs), latent heat storage (where a phase change occurs), and thermochemical energy storage (where a reversible chemical reaction takes place). Examples of different thermal energy storage approaches are shown in Figure 1-5. Depending on the type of the technology, TES has different key properties as presented in Table 1-1. Conventional storage systems predominately use sensible heat mechanisms; meaning, they depend solely on the heat capacity of the heat storage materials used. Typical examples include dual-tank systems (for liquid media) and thermoclines (for solid media) [14].

Table 1-1 The general values of the key properties for different storage technologies. [15]

Key Properties	Sensible Heat Storage	Latent Heat Storage	Thermo-Chemical Storage
Capacity (kWh/ton)	10-15	50-150	120-250
Power (MW)	0.001-10	0.001-1	0.01-1
Efficiency (%)	50-90	75-90	75-100
Storage Period (h,d,m)	d, m	h, d, m	h, d
Cost ($/kWh)	0.2-20	20-100	15-180

1-3-2 Sensible Thermal Energy Storage

Sensible heat refers to the energy transferred to either increase or decrease temperature and, therefore, internal energy content of the storage medium without a phase change. Sensible thermal energy storage systems work based on the sensible heat that is transferred due to the temperature gradient between the heat transfer fluid from the solar tower (for example) and the heat storage medium. Sensible TES uses a heat storage medium in a thermally isolated storage tank to store thermal energy.

The following characteristics and operational conditions of a storage medium must be taken into account to design a sensible TES: density, specific heat, thermal conductivity and diffusivity of the storage material, vapor pressure and stability, as well as, operational temperatures, heat loss coefficient as a function of the surface area-to-volume ratio, and cost [10].

1-3-3 Latent Heat Thermal Energy Storage

In order to reduce the cost of thermal energy storage, latent heat storage systems, which utilize phase change materials are of great appeal. PCMs allow for heat to be stored nearly isothermally due to the enthalpy change involved in phase transition, i.e., between solid and liquid, liquid and vapor, or solid and solid. This allows for a higher energy storage capacity when operating temperature range is relatively small or when change in enthalpy of the involved PCMs and their heat capacities is high [16].

1-3-4 Chemical Heat Thermal Energy Storage (TCS)

Chemical heat TES, or TCS is another cost-effective TES mechanism offering high energy density and longer storage duration. Chemical heat TES uses thermal energy from the solar tower to excite an endothermic reversible chemical reaction such as adsorption, where chemical energy is stored by increasing the temperature of reacting substances and then recovered in a chemically reverse reaction that leads to temperature reduction of the mentioned substances [10].

Table 1-2 and Figure 1-5 present detailed comparison of different thermal storage technologies in terms of their advantage and disadvantages along with the suggestions for future studies.

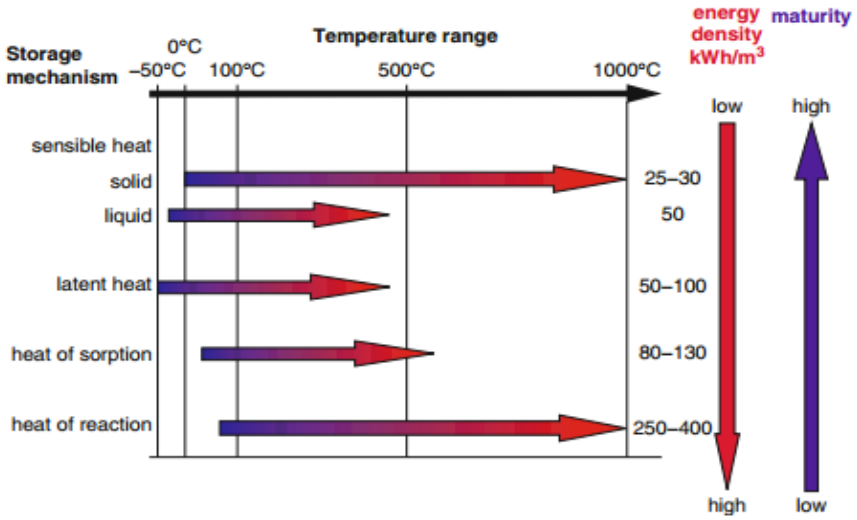

Figure 1-5 Comparison of TES Technologies [17].

Table 1-2 Comparison of TES Technologies [5].

	Sensible	Latent	Chemical
Storage medium	Water, gravel, pebble, soil...	Organics, inorganics	Metal chlorides, metal hydrides, metal, oxides…
Type	Water-based (water tank, aquifer) Rock or ground based	Active storage Passive storage	Thermal-sorption (adsorption-absorption) Chemical reaction (normally for high-temperature storage)
Advantage	Environmentally friendly cheap material	Higher energy density than possible heat storage Provide thermal energy at constant temperature	Highest energy density, compact system Negligible heat losses
Disadvantage	Low energy density, huge volumes required Self-discharge and heat losses problem Geological demonstration	Lack of thermal stability Crystallization Corrosion High cost of storage material	Poor heat and mass transfer property under high-density condition Uncertain cyclability High cost of storage material
Present status	Large-scale demonstration plants	Material characterization, laboratory-scale prototypes	Material characterization, laboratory-scale prototypes
Future work	Optimization of control policy to advance the solar fraction and reduce the power consumption Optimization of storage temperature to reduce heat losses Simulation of ground-/soil-based systems with the consideration of affecting factors (e.g., underground water flow)	Screening for better suited PCMs with higher heat of fusion Optimal study on store process and concept Further thermodynamic and kinetic study, noble reaction cycle	Optimization of particle size and reaction bed structure to get constant heat output Optimization of temperature level during charging/discharging process Screening for more suitable and economical materials

1-3-5 Active and Passive Thermal Energy Storage

In addition to sensible and latent, there is also a distinction between active and passive TES systems. An active storage system is characterized by the forced convection heat transfer into the heat storage material. The heat storage medium circulates through the storage system and the heat exchanger. Active systems are divided into the direct and indirect systems [18]. Active storage refers to storing solar energy in day time and using it when there is a lack of solar irradiation [19]. An active thermal storage system could be designed as a single- or a two-tank system [20].

In passive heat storage systems, a heat transfer fluid (HTF) carries thermal energy (heat) received from the energy source (solar tower or solar field) to the storage medium during charging. These systems are also called regenerators. The heat stored by the storage medium is released during discharging A major influencing factor on transfer of heat in the unit is allowing for the HTF to flow through the heat storage medium. When the heat transfer fluid is a liquid and the heat capacity of the solid in the storage system is not negligible, the system is called a dual storage system.

Passive storage systems may utilize inexpensive solids such as rocks, sand or concrete as sensible heat storage materials, or phase change materials. Passive type systems can be more challenging concerning heat transfer, compared to active types, since the storage medium is in solid phase rather than liquid phase. Several heat transfer systems are used, varying from embedding tubes or pipes in the storage medium to using a packed (fixed) bed of fluidized bed type storage unit where the heat transfer fluid is flowing directly through the storage medium with no heat exchanger required. If the storage

medium is a solid-liquid phase change material, the liquid medium ought to be separated from the heat transfer fluid. Types of solid containment studied and suggested are bulk storage in tank heat exchangers, macro encapsulation and microencapsulation [21].

1-4. Sensible TES

Unlike latent heat storage systems, sensible heat storage systems depend on thermal conductivity and heat capacity of the storage media. The vast majority of operational TES systems use sensible heat storage [16]. Sensible heat storage of thermal energy is perhaps, conceptually, the simplest form of storing thermal energy. It, however, requires large volumes because of its low energy density (i.e., three to five times lower than that of PCM and TCS systems, respectively). Furthermore, sensible heat storage systems require proper design to discharge thermal energy at constant temperature. A key issue in the design of a thermal energy storage system is its thermal capacity.

In the simplest configuration of a sensible heat TES, cold fluid contained in an insulated tank is heated by the hot fluid from the field of solar collectors as shown in Figure 1-6. Such a technique is quite similar to that of a residential solar hot water heater. In most industrial solar energy systems, the fluid in the collector field and the storage tanks is the same. This is not the case with storage concepts such as latent heat storage where the storage medium undergoes a phase change.

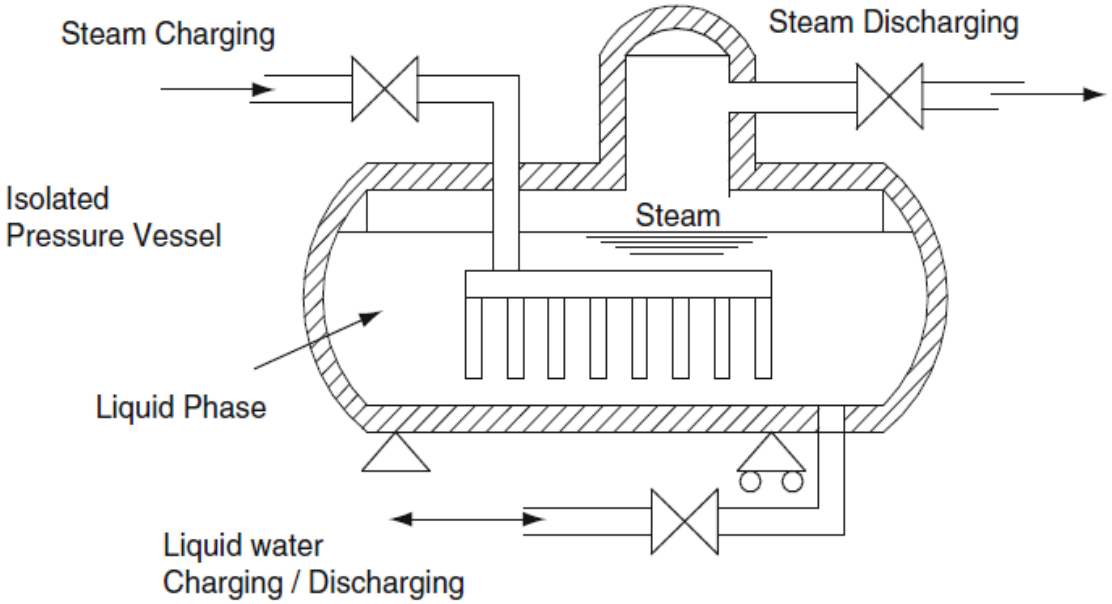

Figure 1-6 Variable-pressure (Ruths) steam accumulator [19].

1-4-1 Single-Tank Sensible Heat Storage System

A conceptual representation of the single-tank heat storage system is presented in Figure 1-7. The problem with the single-tank sensible-heat storage is that although the average temperature of heat storage fluid increases during charging, it does not reach temperature of the hot collector fluid. However, the quality (i.e., exergy) of thermal energy in a storage tank plays an important role in design of solar thermal energy systems. If the amount of thermal energy delivered by the collector field (e.g., on partially cloudy days) is insufficient to heat the entire storage tank to the desired temperature, a significant loss in energy quality (availability or exergy) can occur in the heat storage system. Therefore, to avoid reduction in the efficiency of the collector in high-temperature solar thermal energy systems, a two-tank storage system is used.

Most sensible-heat storage systems are design variations of the single- and two-tank storage systems shown in Figure 1-7 and Figure 1-8.

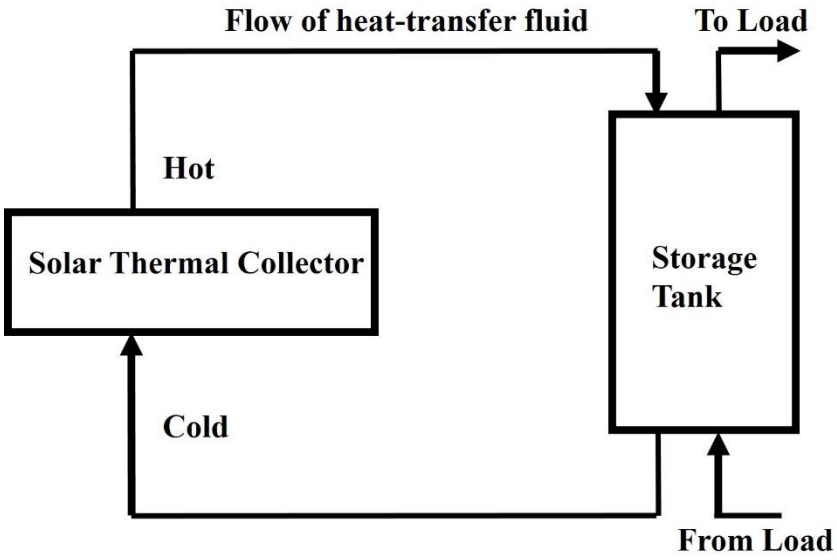

Figure 1-7 Single-tank sensible-heat storage system [22].

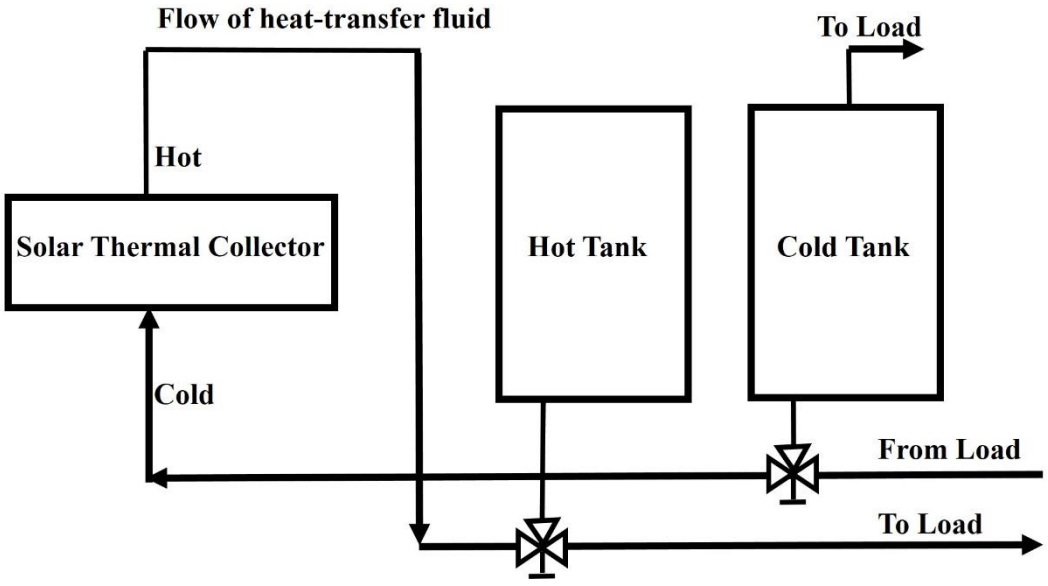

Figure 1-8 Two-tank sensible heat storage system [18].

1-4-2 Two-Tank Sensible Heat Storage System

In two-tank storage systems improved thermal control of the hot and cold fluids is achieved by keeping hot and cold heat transfer fluids separate as presented in Figure 1-9

[14]. The basic idea is that one tank holds cold HTF, returning from the power block, while the other tank holds hot HTF flowing from the solar field. The Solar Two power plant in Dagget, California using molten salts for the HTF, reached 97% round-trip storage conversion efficiencies with this arrangement [10]. The downside is that to maintain HTF at operating temperatures immersion heaters as well as a large amount of insulation materials is required [10].

The early two-tank direct system was used in the first Luz mirror plant, the Solar Energy Generating System (SEGS) I in California (Figure 1-10). It has two tanks, one of low and one of high temperature. Only one HTF, in this case mineral oil (Caloria), circulates from the low-temperature tank through the solar collectors picking up the heat. Part of the heat is used to generate the steam to run the turbine while the excess heat is stored in the high-temperature tank. After passing through a heat exchanger, the cooled HTF flows back to the low-temperature tank to be reused.

To achieve a higher operating temperature and thus a higher efficiency, SEGS use synthetic oil (a eutectic mixture of biphenyl-diphenyl oxide). However, in this case a two-tank direct system is no longer suitable. The unpressurized storage tank system used in SEGS is not suitable for the use of mineral oil having high vapor pressure, and pressurized storage tanks are very expensive. Additionally, the HTF cost is high and it cannot be used as a heat storage fluid.

The heat transfer fluid needs to be chosen based on the freezing point and local temperature (day and night). Figure 1-10 is the Solar Two power tower in California, which uses the two-tank system with molten salt as the HTF. At the Solar Two plant, the

intermediate heat exchanger (oil-to-salt) is not needed, which means a cost reduction of the power plant. The main disadvantage is the high quantity of oil required for storage tanks, increasing the cost of installation. Furthermore, pressurized tanks needed for the heat storage fluid (oil) imply a high cost due to its high vapor pressure. In Solar Two, the chosen thermal energy storage media is molten salt, composed of a mixture of 60% of sodium nitrate ($NaNO_3$) and 40% of potassium nitrate (KNO_3).

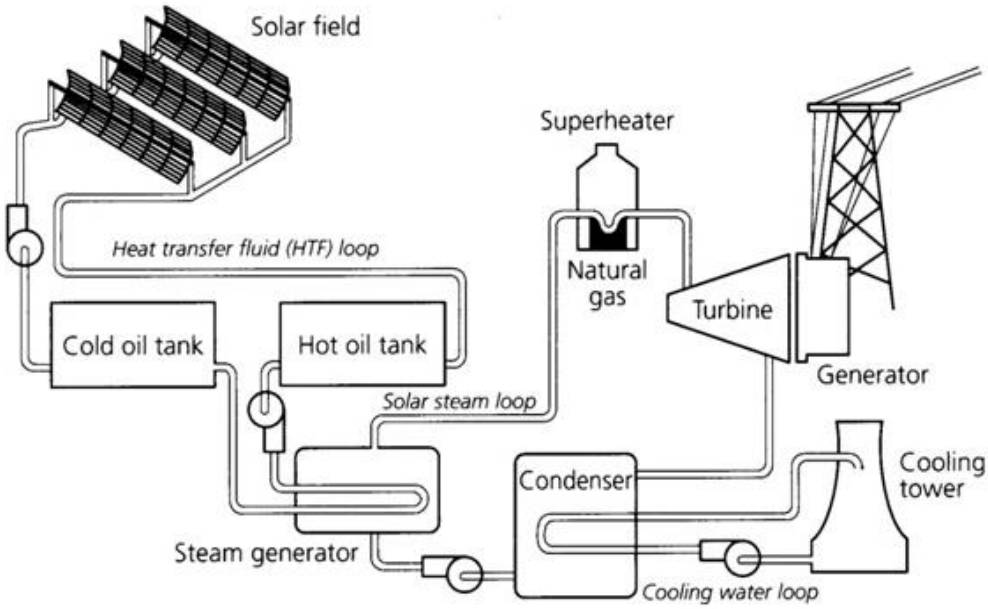

Figure 1-9 Conventional dual-tank storage system in a concentrating solar tower [19].

Figure 1-10 Solar Two power tower in California [23]

Although the above-mentioned heat storage systems are very reliable, they still pose a high overall cost. Alternative concepts with a lower cost are being explored and investigated. Research is under way to find more efficient and less costly storage materials for the one-tank systems.

1-4-3 Two-Tank Indirect Storage System

A two-tank indirect storage system, presented schematically in Figure 1-11, includes a HTF as well as a heat storage fluid (HSF) and an additional (primary) heat exchanger. The heat is transferred from the high-temperature HTF to the HSF leaving the low-temperature tank via the primary heat exchanger. The cycle continues as the high-temperature HSF flows to a high-temperature storage tank, and the low-temperature HTF flows back to the solar collector field. The-two tank indirect system with molten salt as the STF is dominant in most parabolic trough power plants despite its two main downsides: added costs of the second heat exchanger and lower temperature difference between the two tanks. It's referred to as an indirect system because the storage medium fluid is different

from the heat transfer fluid bringing heat from the solar field. Examples of the two-tank indirect storage systems are the Extresol I-II and Andasol I-II CSP plants.

Extresol I have been inaugurated in 2009 at Torre de Miguel Sesmero, Spain. It is a parabolic through mirror plant with a synthetic oil used as an HTF. The storage is molten salt two-tank system sized to drive the power block for 12 hours at nominal power. Andasol is another parabolic through system (Guadix, Spain). Andasol is placed on a plateau at about 1,000 meters above the sea level to decrease atmospheric scattering of solar irradiation. The site benefits from sunny weather for most of the year and available annual radiation reaches 2,000 kWh/m^2. In Andasol I synthetic oil is used in the solar field at a temperature ranging from 290 to 390^{o}C. TES system comprises a molten salt indirect two-tank configuration sized for 7.5 hours of full-load storage capacity. The temperature of the hot tank is 384^{o}C, while the temperature of the cold tank averages 291^{o}C. Each tank is 37 meters in diameter and 14 meters in height. Annual average mirror-to-electric efficiency is 14.7 %.

The indirect storage TES is usually used in conjunction with parabolic through mirrors. In this system, oil is used as the HTF, and molten salt as the heat storage medium. The use of molten salt in the parabolic through solar field requires particular attention because molten salt could freeze during the nighttime. Particular freezing protection, such as gas or electric heaters, is required; alternatively, recirculation of stored warm molten salt through the solar field is performed. An example of a molten salt parabolic trough is the 5 MW plant Archimede, Italy [24]. However, if molten salt is used in the solar field, direct storage is preferred because no expensive HTF-to-storage medium heat exchanger is

needed [25]. The 50MW AndaSol project in Granada, Spain and the 280MW Solana, in Gila Bend, Arizona, both use the molten salt thermal storage system. Andasol 1 and 2, for example, aim at a thermal storage capacity of 1,010 MWh, equivalent to 7.5 hours of full load operation. For high-temperature thermal storage, molten salt or liquid metal remain stable whereas organic HTFs thermally decompose. However, special operating procedure is required for molten salt because of its relatively high freezing temperature 121-221^{o}C to reduce the risk of freezing when ambient temperature is low [26].

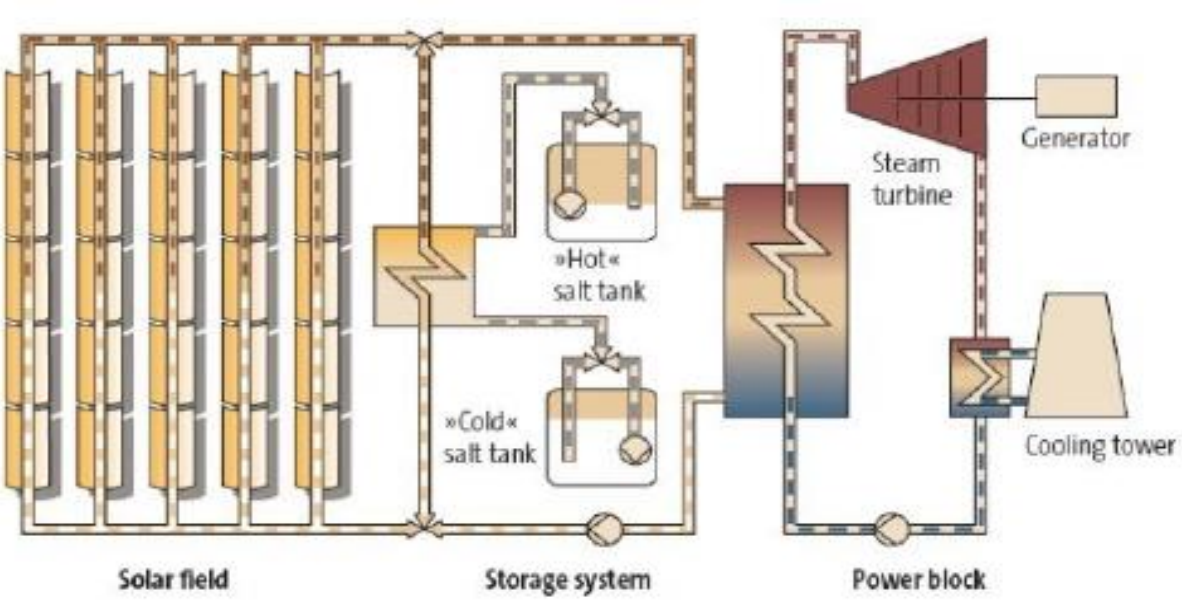

Figure 1-11 Diagram of parabolic trough CSP plant with indirect two-tank storage [22].

1-4-4 Single-Tank Thermocline

A single-tank thermocline storage system stores thermal energy in a solid medium, usually silica sand, located in a single tank. At any time during the operation, a portion of the medium is at high temperature and a portion at low temperature. The hot and cold temperature regions are separated by a temperature gradient or thermocline. The high

temperature heat transfer fluid flows from the top of the thermocline through the storage medium and is discharged at the bottom at low temperature. This moves the thermocline downward and adds thermal energy to the system for storage. Reversing the flow moves the thermocline upward and removes thermal energy to, for example, generate steam and electricity. Buoyancy effects create thermal stratification of the fluid in the tank, which helps stabilize and maintain the thermocline.

The thermocline technology has proven advantageous because the reduction of material used for tank construction decreases cost. Using a solid-state storage medium and only one tank reduces the cost relative to a two-tank system. The thermocline system was demonstrated at the Solar One power tower, where steam was used as the heat transfer fluid and mineral oil was used as the heat storage fluid. However, this technology is still undergoing development and requires more research before it becomes economically and technically viable [27]. For example, the thermocline storage system must maintain the thermocline zone in the tank, so that it does not expand to occupy the entire tank.

The research goal is now directing current R&D in solar thermal storage into developing heat-transfer fluid that can operate at higher temperature with low freezing point, resulting in a higher overall heat transfer efficiency of the thermal storage. Another goal is development of a storage fluid having high heat capacity to reduce the amount of fluid is needed in the storage system. A detailed analysis of the optimal design of the thermocline systems is provided in Reference [25].

1-4-5 Steam Accumulators

In addition to the use of synthetic oils and molten salts in active type heat storage, water can be used as the storage medium in systems called steam accumulators. In these systems, charging takes place when a superheated steam or saturated water enters a pressurized storage tank that initially contains saturated steam and saturated water. If the system is being charged with the superheated steam, the temperature and pressure of the water in the tank increases, thus changing the saturation state of the initial mass [28]. On the other hand, if the saturated liquid is used to charge the system, pressure and temperature remain constant yet the mass in the volume is increased. The discharging process takes place by reducing pressure in the storage tank. This results in flashing and production of saturated steam that decreases in pressure as the discharging process proceeds. If superheated steam is desired, a secondary storage system is needed to increase temperature of the steam. Steam accumulators are well-suited for the direct steam generation (DSG) CSP plants in which steam is produced directly in the solar field and then used in the power block to produce power. Steam that is produced in excess of what is needed by the turbine is diverted to the steam accumulator. These systems can also act as both the storage system and the phase separator in DSG plants that are run in a recirculation mode. In this mode, saturated steam is separated from the saturated liquid in a separator drum and then sent through another collector to get superheated.

As can be seen in the schematic in Figure 1-12, rather than using two distinct pieces of equipment, wet steam leaves the solar field and enters the combined steam accumulator/separator where the phases are separated and the pressure remains constant.

Since these systems require pressurized and hence expensive storage tanks, and also possess low volumetric energy densities (volumetric storage capacity for water is 20 to 30 kWh/m^3 compared to approximately 100 kWh/m^3 for PCMs), they are useful when low thermal storage capacity is needed, as is the case for buffer storage. In order to increase the storage capacity, it has been proposed that latent heat storage is used in conjunction with the steam accumulator by either placing PCMs directly in the steam accumulator or externally to the steam accumulator [29].

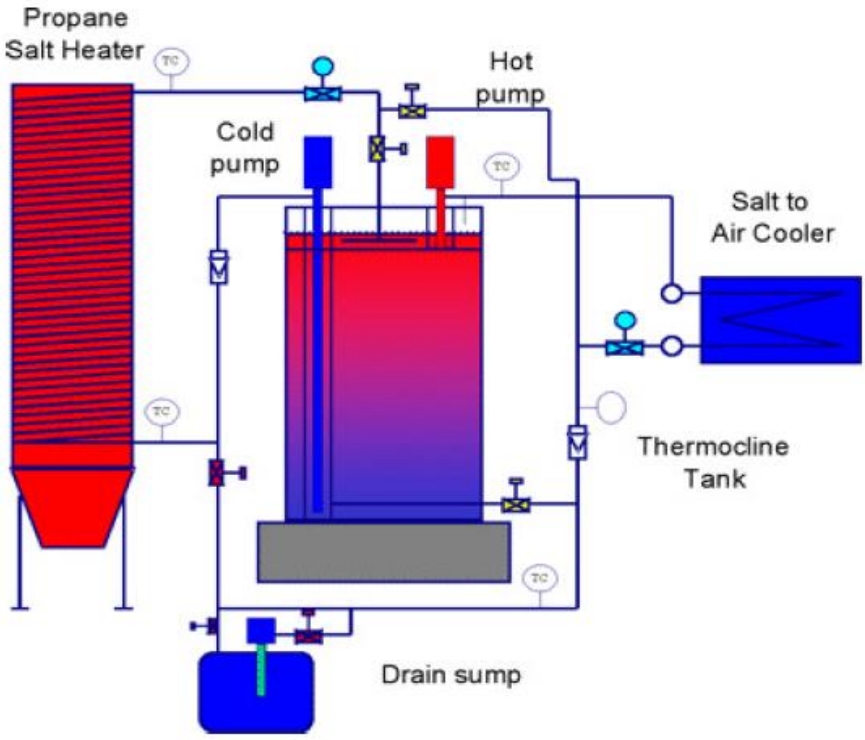

Figure 1-12 Thermocline test at Sandia National Laboratories [24]

1-4-6 Review of Research on Sensible Heat Storage Systems

A considerable amount of research work has been carried out on sensible heat storage materials and systems, and technology for their utilization is well developed. Beasley and Clark [30] have provided an excellent review of such efforts in the case of

packed bed SHS systems. Dincer et al. [31] presented a detailed investigation of the availability of SHS techniques for solar thermal applications, selection criteria for SHS systems, economics, and environmental impacts of the SHS systems. Thermal performances of solar water heating systems integrated with SHS system were investigated experimentally by the researchers Collares et al. [32], Sodha et al. [33] and Reddy et al. [34].

The following is a review [35] of some of the research carried out on various aspects of SHS.

Domanski and Fellah [36] considered advantages of employing a thermo-economic analysis of sensible heat storage systems to use the storage system at the minimum total cost of owning, maintaining and operating such system. The analysis extended to model the entire process of the charging-discharging cycle. The analysis provides an important engineering tool for selecting the proper storage unit for a given application. In a study by Badar et al. [37], an analytical method is presented for the second-law-based thermo-economic optimization of a sensible heat-storage system, in which energy is stored in a large liquid bath from a hot-gas source. Results are presented in terms of the optimum number of transfer units as a function of a dimensionless unit-cost ratio, charging time, and reduced temperature difference of the storage system.

Kuznetsov [38] obtained an analytical solution for heating a rectangular sensible heat storage packed bed by a non-thermal equilibrium flow of an incompressible fluid with a constant wall temperature. The physical model consists of a porous packed bed at uniform temperature filled with an incompressible fluid. The initial temperature of the packed bed

is kept constant; at the instant t=0 the high temperature fluid is allowed to flow through the bed. The analytical solution shows that the temperature difference between the solid phase and fluid consists of the steady and transient components. As the wave propagates downstream, its amplitude rapidly diminishes.

In a study by Prasad and Nandi [39], the waste energy dissipated during industrial manufacturing process was stored as a sensible heat in a heat storage system. The authors have applied the integral method to the specified storage system and obtained a closed form solution of the governing equation for a sensible heat storage system with heat conduction. The proposed sensible heat storage system consists of two semi-infinite plates of different materials with uniform yet different thermo-physical properties. The plates are at different temperatures and storage plate with lower temperature stores the sensible heat flowing from the hot plate which acts as a constant temperature heat reservoir.

In an experiment performed by Nallusamy et al. [40], performance of the combined heat storage system is compared to that of a conventional SHS system. The water used as the HTF flows from a constant temperature solar collector to the TES tank also acts as the SHS material. The TES unit also contains paraffin as PCM filled in spherical capsules packed in an insulated cylindrical storage tank. In this combined storage system batch discharging of hot water from the TES tank is best suited for applications where the requirement is intermittent. The experiments were performed to examine the effect of inlet fluid temperature and flow rate on TES performance for the constant and varying HTF inlet temperature. The results show that the uniform rates of charging and discharging can be achieved for a longer period of time compared to the conventional SHS system, which is

the major advantage of the combined heat storage system. It has also been shown that in the case of combined storage system the batch discharging process gives better performance compared to the continuous discharging process. This is because in case of a constant inlet HTF temperature the mass flow rate of HTF has only a small effect on the charging rate. It has been concluded that the combined storage system with direct mixing of the HTF with the hot water in the storage tank had better performance comparing to the conventional systems.

In a paper by Navarro et al. [41] alternative low cost materials are evaluated through the valorization of by-products derived from mining and metallurgical industry for solid sensible heat based energy storage systems. The materials studied are of high energy density and medium thermal conductivity. They are compared to other materials using the material selection methodology. Studied materials are cost-effective for industrial use as a storage medium in CSP. The paper by Bauer et al. [42] also presents thermal stability examinations of Solar Salt and $NaNO_3$ performed at different lab scale tests and thermal analysis measurements. Salt analysis showed a steadily increasing oxide level at a constant nitrite to nitrate ratio. The overview of corrosion aspects was also given. Thermo-physical properties of solar salt were studied, and consistent data were identified.

Ravaghi-Ardebili et al. [9] have performed a first comparison between two direct TES technologies: a single-tank storage and two-tank storage, both commonly adopted in CSP plants, by employing dynamic simulation of each system. A single-tank TES appears superior to a two-tank TES from the control and design standpoint, although it is less flexible from the operational and control viewpoints of steam production and power

generation. Medrano et al. [10, 43] presents a review of the storage media systems. This study mainly focuses on the type classifications and storage concepts of thermal storages. It also reviews materials and material properties enhanced for thermal energy storages. Case studies from other sources are presented and compared in the second paper.

1-5. Thermal Energy Storage Design Criteria

Some of the design criteria that have to be considered when deciding on the type and design of thermal storage include: storage duration, high energy density of the storage material (storage capacity); good heat transfer between heat transfer fluid (HTF) and storage medium (efficiency); mechanical and chemical stability of heat storage material (must support charging/discharging cycles), compatibility between HTF, heat exchanger and/or storage medium (safety), complete reversibility of the charging/discharging cycles (lifetime), low thermal losses, available space and ease of control. The most important parameters from the point of view of technology are: operation strategy, maximum load, nominal temperature and specific enthalpy drop in load, and integration with the power plant [10].

Of all the TES technologies, Sensible TES as an inexpensive option is the simplest in design. However, the huge volume and low energy density as well as the self-discharge and heat losses are disadvantages of this technology.

1-5-1. Desirable Properties of Thermal Energy Storage Medium

Of fundamental importance is the economic aspect of a sensible heat TES system in order to improve profitability of this technology in high-performance buildings. Even if the major part of capital cost is cost of the shell and tube heat exchanger, the total cost can

be significantly reduced by using alternative low-cost materials [44]. The cost of a storage material depends essentially on its properties, such as density, specific heat capacity, etc., and energy per total weight of the material employed in construction of the sensible heat TES module. In order to reduce the cost, lightweight but high thermal performance materials are required for large sensible heat TES system [45]. Sensible TES requires inexpensive materials that offer high thermal capacity (ρC_P), and maintain their physical state over the temperature range of the storage process.

Table 1-3 presents detailed overview of desirable properties of sensible heat storage materials.

Table 1-3 Desirable properties of sensible heat storage materials.

Properties	Desirable Characteristics
Thermo-Physical Properties	High energy density (per unit mass or volume), high thermal conductivity, high heat capacity, high density, long term thermal cycling ability
Chemical Properties	Long term chemical stability, non-toxic, non-explosive, low corrosion potential or reactivity to HTFs.
Economic properties	Cheap and abundant materials with low cost of manufacturing into suitable shapes
Mechanical	Good mechanical stability, low coefficient of thermal expansion, high fracture toughness, high compressive strength.
Environmental	Low manufacturing energy requirement and CO_2 footprint.

1-5-2. Available Options for Thermal Energy Storage Medium

Depending on the economics, operational temperature range and available space, sensible heat storage can be made out of solid media (rocks, metals) or liquid media (water, oil-based fluids, molten salt).

Solid media can store thermal energy in both low and high temperature ranges. However, the need for large storage tank and considerable amount of land are disadvantages of these materials. Highly conductive and fairly costly inorganic salts or metals are also proposed for high temperature (393-1673K) energy storage [46].

There are many liquid heat storage media suitable for different operating temperature range meeting the stability and safety requirements of the storage process. Different types of thermal energy storage fluids, their approximate working temperature ranges and specific heat capacities are presented in Table 1-4.

Water, being inexpensive and widely available with high specific heat is the most widely used storage media for low temperature range operation [46]. Petroleum-based oils and molten salts with higher thermal conductivity, lower vapor pressure and lower heat capacities (25-40% on a weight basis) compared to water, are used for thermal storage temperature ranges of 573K and higher. However, high potential for corrosion and high reactivity are downsides of these storage media [46].

Table 1-4 Molten salts and high temperature oils.

Storage Material	Working temperature (°C)	Specific heat capacity ($\frac{kJ}{kg\ K}$)
Water	0-100	4.18
Mineral Oil	200-300	1.67
Synthetic Oil	250-350	1.88
Silicon Oil	300-400	1.51
Molten Salts	142-600	1.53

1-5-3. State of Art Thermal Energy Storage Medium

Of all available options for the heat storage medium, molten salt (a eutectic mixture of 60% Sodium nitrate and 40% Potassium nitrate) as an inexpensive, nonflammable and nontoxic option with excellent thermal stability under high operational temperatures, low melting point and high thermal conductivity is one of the most popular choices for sensible heat storage medium. This medium is thermally stable to about 850K [47] and has a favorable combination of low vapor pressure, moderate specific heat, high density, low chemical reactivity, and low cost. Some of the physical properties and features of the molten salt are presented in Table 1-5. As shown in the phase diagram of the molten salt presented in Figure 1-13, the molten salt remains in a liquid phase throughout the desired temperature range for the thermal energy storage.

Using molten-salt in both the solar field and thermal energy storage system eliminates the need for expensive heat exchangers. It allows the solar field to be operated at higher temperatures compared to the current heat transfer fluids. This also results in a substantial reduction in the cost of the thermal energy storage (TES) system. Unfortunately, molten-salts freeze at relatively high temperatures 120 to 220 ^{o}C. This means that special care must be taken to ensure that the salt does not freeze in the solar field piping during the night, or when the unit is not running. The Sandia National Laboratory is developing new salt mixtures with the potential for freezing below 100 ^{o}C (212 ^{o}F). At 100 ^{o}C the freezing problem is expected to be much more manageable [48].

Thermo-physical properties of the molten salt at different temperatures can be calculated using correlations from the literature, such as [49]:

$\rho(T) = -0.635 \times T + 2089.9$ in kg/m^3

$\mu(T) = -1.474 \times 10^{-10} \times (T - 273)^3 + 2.28 \times 10^{-7} \times (T - 273)^2 - 1.2 \times 10^{-4} \times (T - 273) + 2.27 \times 10^{-2}$ in kg/ (m-s)

$C_p(T) = 0.172 \times T + 1443$ in J/ (kg-K)

$k(T) = 0.00019 \times T + 0.44$ in W/ (m-K)

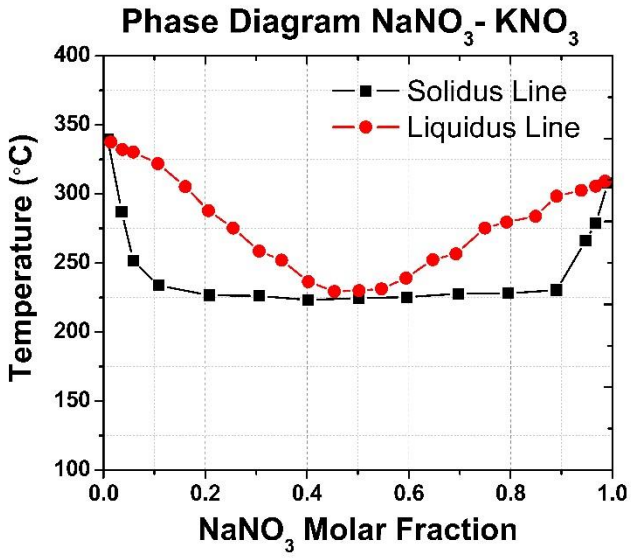

Figure 1-13 Phase Diagram of NaNO3-KNO3 System [50]

Table 1-5 Molten Salt Features and Physical Properties [50].

Salt Features	Salts Physical Properties
• Operative temperatures: 260-550°C. • Environmentally friendly, non-flammable and non-toxic stable fluid. • Low cost fluid. Good heat transport properties ○ High Coefficient of Heat Transfer. ○ High Heat Capacity. ○ High Density. ○ Low Operative Pressures.	• *Freezing Temperature: 221°C. • Heat of Fusion: 161 kJ/kg. • Volume Change on Fusion: 4 to 6%. *Corresponding to the $NaNO_3$ molar fraction of 0.6.

1-6. Research Objectives

1-6-1. Scope of Research Project

This study focuses on the indirect sensible heat TES system employed in CSP plants. The phase changing systems are not a subject of this study. The main objectives of this study include optimal heat exchanger design for efficient charging and discharging of thermal energy stored in a TES. More specifically, the aim of the study is to address the following questions:

- What is the mathematical relationship between heat transfer coefficient and stored energy per unit volume of the thermal storage fluid?
- What is the mathematical relationship between tube arrangement in the heat exchanger (HXE) and thermal energy stored in a thermal storage fluid?
- What is the optimal HXE geometry for a TES in terms of the tube spacing and their arrangement (in-line and staggered) needed to achieve the maximum storage efficiency?

1-6-2. Specific Objectives and Expected Outcomes

The specific objectives are:

- Perform numerical sensitivity calculations and statistical regression analysis of the results to develop relationships between the relevant design parameters for four different heat exchanger designs including: single horizontal row of cylinders, vertical column of cylinders, and the in-line and staggered tube bundle.
- Use the results to determine the optimum design of a heat exchanger immersed into the thermal energy storage fluid for an indirect TES system.

1-6-3. Research Phases

This study is divided into two main phases.

Phase 1

The first phase includes verification of the numerical model, method of analysis, and results. The analysis of the following geometries was performed to validate the results from this study by comparing them to the results published in the literature:

1- Free single cylinder (Molten Slat) - Compared with Kuehn and Goldstein [51].

2- Semi-confined single cylinder (Air) - Compared with Clifford [52], Morgan [53] and Fand et al. [54].

3- Two cylinders in a vertical column (Molten salt) - Compared with Lu et al. [55].

4- Multiple cylinders in a vertical column (Air) - Compared with Corcione [56].

5- Staggered tube bank (Water) - Compared with Ivanov et al. [57].

Phase 2

The second phase includes a steady-state simulation of the heat transfer in an indirect single-tank TES system and advances the idea proposed by Lu et al. [55] to a significantly more complex arrangements of horizontal circular cylinders representing heat transfer tubes in a heat exchanger.

Since a two-tank system is expensive and requires considerable amount of space, Lu et al. [55] proposed an indirect single-tank thermal energy storage system. As shown in Figure 1-14, the proposed single-tank TES design employs a tank filled with the heat storage medium and two heat exchangers. Heat exchanger 1 located at the bottom of the tank is transferring heat from the hot HTF (supplied by the solar tower or solar field)

flowing inside the heat exchanger tubes to the molten salt and charging the tank. Heat exchanger 2 is placed at the top of the tank to transfer heat from the storage medium to the working fluid flowing to the power block. Due to the buoyancy, a thermocline is established in the heat storage tank, with its bottom part acting as a cold tank and top part acting as a hot tank.

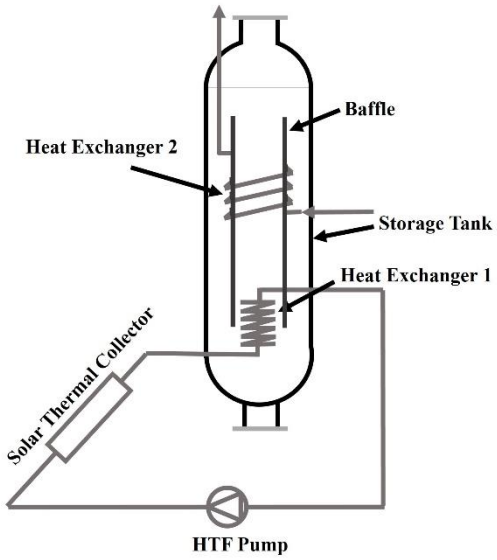

Figure 1-14 Schematic of the TES proposed by Lu et al. [55]

A series of numeric sensitivity calculations was performed in this study to investigate the effect of the heat exchanger geometry on heat transfer to the heat storage medium.

Considering the main design criteria for a TES design, such as: storage capacity; efficiency, complete reversibility of the charging/discharging cycles (lifetime), low thermal losses, and ease of control, the following four geometries were selected for the detailed analysis.

Task 2-1 Single row of horizontal tubes

A simple heat exchanger comprising a single row of horizontal tubes shown in Figure 1-15 immersed in a TES fluid was analyzed to determine relationships between heat transfer and storage capacity in terms of operating conditions (Rayleigh number, Ra_D) and heat exchanger (HXE) geometry (transverse tube spacing S_T, and dimensionless S_T/D ratio).

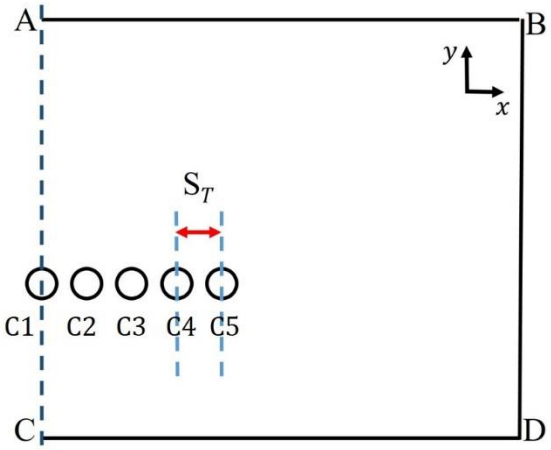

Figure 1-15 Schematic of the control volume for one row of horizontal cylinders

The following HXE geometry and operating conditions were analyzed:

- Molten salt for a range of $Ra_D = 10^4$ to 10^7 and S_T/D range from 1.2 to 20 for the total of 800 cases.
- Statistical regression analysis was performed to develop a set of correlations for the average $\overline{Nu}_D$ and optimal $\overline{Nu}_{D,opt}$ numbers for one horizontal row of five and nine horizontal circular cylinders immersed in a molten salt as functions of the Rayleigh number Ra_D and cylinder-to-cylinder spacing (S_T), expressed in a dimensionless form as S_T/D.

- Statistical regression analysis was also performed to develop a correlation for the optimal tube spacing $(S_T/D)_{opt}$ maximizing heat transfer to the TES medium for the Ra_D number values in the $10^5 \leq Ra_D \leq 10^7$ range.
- Statistical regression analysis performed to develop a correlation for maximum dimensionless volumetric heat transfer density $\tilde{q}_{max}$ for a horizontal row of nine to five cylinders as a function of the Ra_D number.

Task 2-2 Vertical column of cylinders

An elementary heat exchanger comprising one vertical column of two to ten circular cylinders, shown in Figure 1-16, immersed in a TES fluid was analyzed to determine relationships between heat transfer characteristics and storage capacity in terms of operating conditions (Rayleigh number, Ra_D) and heat exchanger (HXE) geometry (longitudinal tube spacing and dimensionless S_L/D ratio).

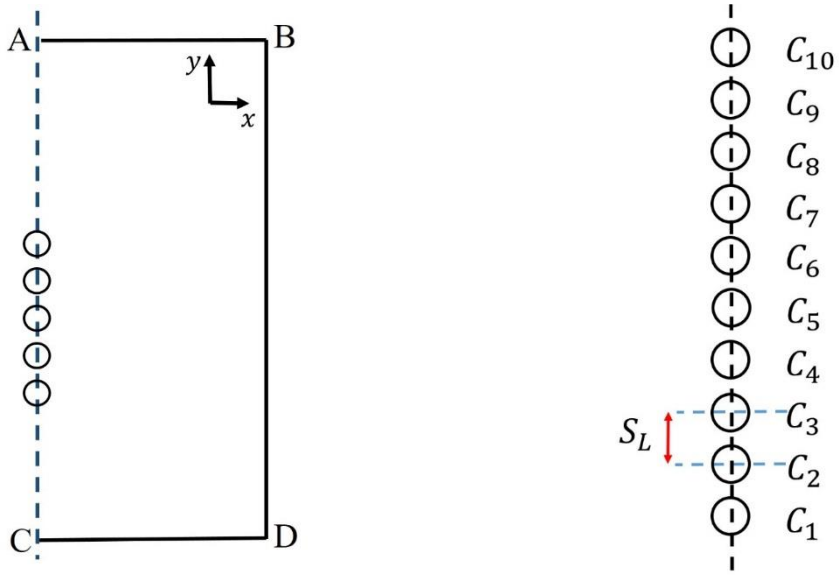

a) b)

Figure 1-16 Schematic of the control volume for one vertical column of ten circular cylinders.

The following HXE geometry and operating conditions were analyzed:

- Molten salt for a range of $Ra_D = 10^4$ to 10^7 and S_L/D range from 1.1 to 10 for the total of 800 cases.
- Statistical regression analysis was performed to develop correlations for the average Nusselt number for the entire column and for the individual cylinders in the column in terms of the Rayleigh number Ra_D and dimensionless cylinder spacing (S_L/D).

Task 2-3 Tube bank

An HXE comprising a bank of tubes immersed in a tank of the TES fluid was analyzed to determine the effect of tube bundle geometry, such as the tube arrangement (in-line or staggered) and tube spacing (lateral and longitudinal) on heat transfer. Sensitivity analyses were performed to determine the effect of the following geometrical parameters on TES performance:

- Rayleigh number, Ra_D
- Tube bundle arrangement (in-line and staggered arrangement)
- Transverse (S_T) and longitudinal (S_L) tube pitch

2-3-a. In-line Tube Arrangement

The heat transfer analysis of a stack of cylinders representing a tube bundle was performed for the in-line tube arrangement shown in Figure 1-17 over the following range of parameters:

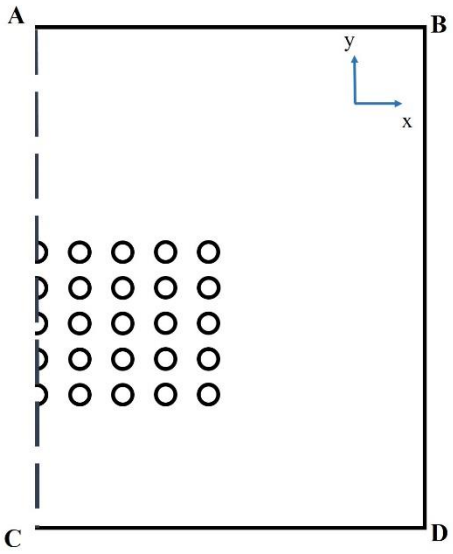

Figure 1-17 Schematic of the in-line arrangement of horizontal cylinders in a tube bank

- Molten salt for a range of $Ra_D = 10^4$ to 5×10^6 over the range of S_L/D and S_T/D values. The analysis was performed for the following values of the Rayleigh number: $Ra_D = 10^4, 5 \times 10^4, 10^5, 5 \times 10^5, 10^6$ for a total of 800 cases.
- Longitudinal and transverse tube spacings S_L/D and S_T/D were varied in the 1.1 and 10 range.
- Performance maps (contour diagrams) for the average Nusselt number and the dimensionless heat transfer volumetric density for the tube bundle were constructed as functions of the Ra_D number and tube spacings.
- Statistical regression analysis was performed to develop correlations for the dimensionless heat transfer volumetric density, maximum dimensionless volumetric heat transfer density $\tilde{q}_{max}$, and optimum dimensionless heat transfer volumetric density $\tilde{q}_{opt}$ for an in-line bundle of finite and infinite number of cylinders as functions of the Ra_D number and height H and width W of the bundle.

2-3-b. Staggered Tube Arrangement

The heat transfer analysis of a stack of cylinders representing a tube bundle in the staggered tube arrangement shown in Figure 1-18 was performed over the following range of parameters:

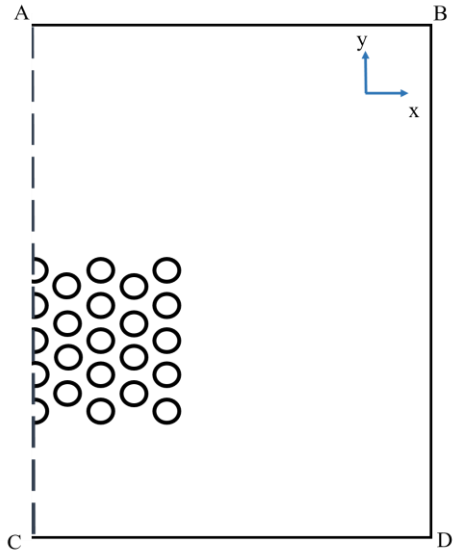

Figure 1-18 Schematic of the staggered arrangement of horizontal cylinders in a tube bank

- Molten salt for a range of Ra $= 10^4$ to 10^6 over the range of S_L/D and S_T/D values. The analysis was performed for the following values of the Rayleigh number: $Ra_D = 10^4, 10^5$ and 10^6 for a total of 430 cases.
- Longitudinal and transverse tube spacings S_L/D and S_T/D were varied in the 1.1 and 10 range.
- Performance maps (contour diagrams) for the average Nusselt number for the tube bundle and dimensionless heat transfer volumetric density were constructed as functions of the Ra_D number and tube spacings.

- Statistical regression analysis were performed to develop correlations for the dimensionless heat transfer volumetric density, maximum dimensionless volumetric heat transfer density $\tilde{q}_{max}$, and optimum dimensionless heat transfer volumetric density $\tilde{q}_{opt}$ for a staggered bundle of finite and infinite number of cylinders as functions of the Ra_D number and height H and width W of the bundle.

The physical model representing the computational domain and the boundary conditions chosen for the numerical analysis of the geometries described in Section 1-6-3 is discussed in the next chapter.

CHAPTER 2: PROBLEM DESCRIPTION

2-1 Overview

Physical model, modeling assumptions, and boundary conditions used in the numerical analysis are described in this section. As mentioned in Section 1-6-3, Phase 2 of the previous chapter, Lu et al. [55] proposed a simpler and cost-effective alternative to the two-tank indirect thermal energy storage system. The objective of this study is to advance the idea to four more complex HXE geometries.

A numerical model of a 2-D cavity representing a single-tank indirect TES system employing different tube configurations including one horizontal row of cylinders, one vertical column of horizontal cylinders, and a bundle of tubes in the in-line and staggered arrangement immersed in the thermal energy storage fluid was modeled to study the effect of the HXE geometry on heat transfer and thermal energy storage.

2-2 Physical Model

The analyzed geometries comprise a heat exchanger employing different configurations of circular cylinders immersed into the thermal energy storage fluid, representing an indirect TES consisting of the storage tank filled with molten solar salt. As discussed earlier, four heat exchanger geometries were analyzed in this study: a single horizontal row of five and nine circular cylinders, a vertical column of multiple horizontal circular cylinders, and a bundle of horizontal cylinders with the in-line and staggered tube (cylinder) arrangements. Due to the symmetry along the A-C line the analysis was performed for the right half ABCD of the domain. Horizontal circular cylinders of a

diameter D placed inside computational domain ABCD representing a heat exchanger immersed in heat storage fluid are presented in Figure 2-1.

Numerical simulations were performed where the cylinder-to-cylinder spacings S_T/D and S_L/D and Rayleigh number were varied to determine their effect on heat transfer and dimensionless volumetric heat density $\tilde{q}$. Predictions were obtained for the Rayleigh number Ra_D (based on cylinder diameter) range from 10^4 to 10^7 corresponding to the laminar flow regime (flow regime is laminar for $Ra_D < 10^8$ [51]), and over the range of cylinder to cylinder spacings S_T/D and S_L/D, and used to develop functional relationships between the Nusselt number $\overline{Nu}_D$ and $\tilde{q}$ as functions of the Rayleigh number and the S_T/D and S_L/D ratios.

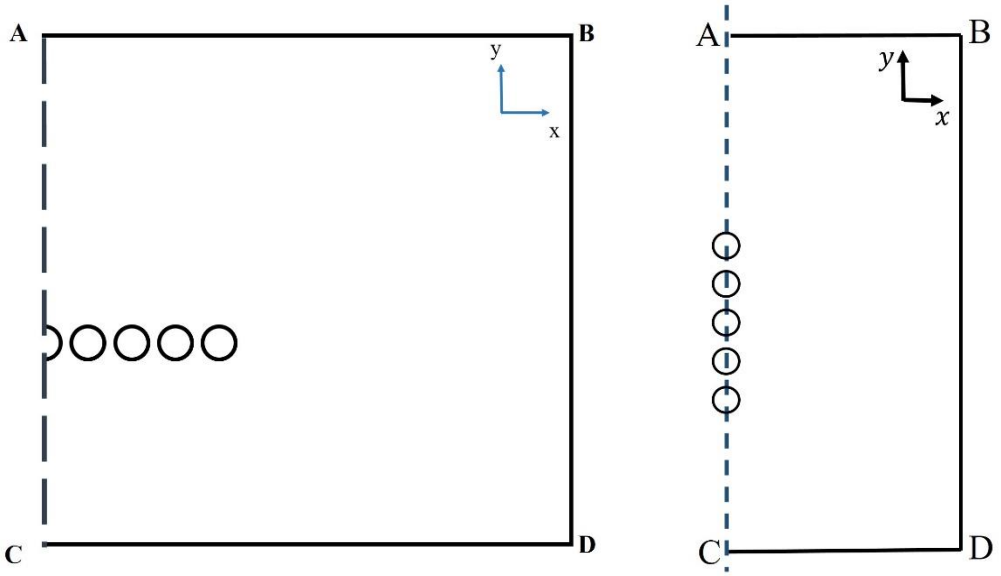

a) b)

Figure 2-1 Schematic of the control volume: (a) Single row of horizontal cylinders, (b) One vertical column of horizontal cylinders, (c) In-line bundle of horizontal cylinders, (d) Staggered bundle of horizontal cylinders.

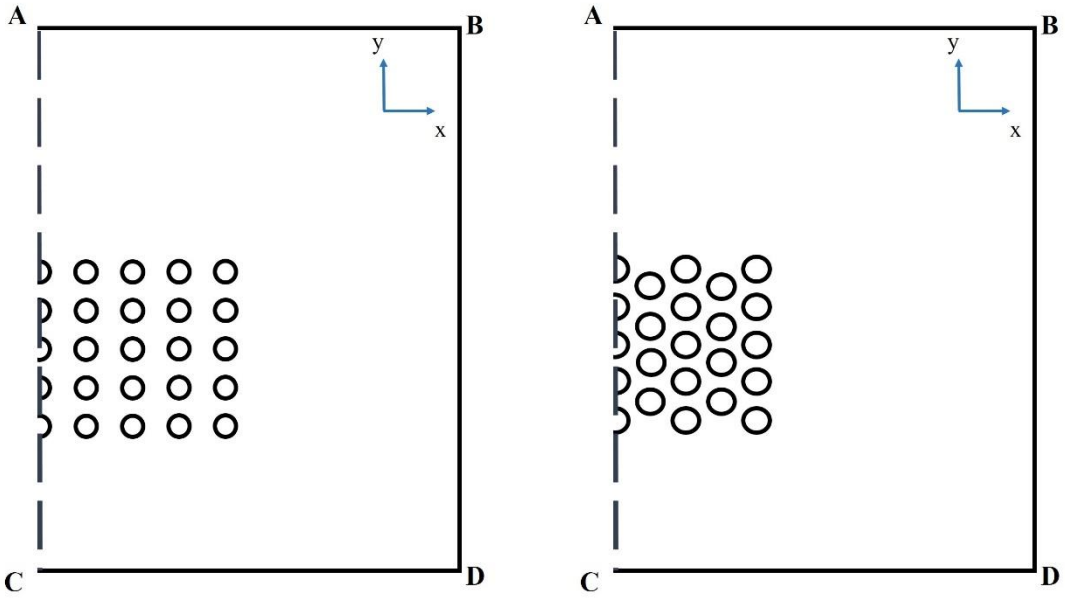

c) d)

Figure 2-1 cont.

The flow and temperature of the hot heat transfer fluid (HTF) passing through the HXE tubes were assumed to be uniform. Molten salt was used as a heat storage fluid. The heat storage fluid was assumed to be viscous and incompressible, and at rest before heat transfer commences. Also, frictional (viscous) heating was neglected. The numerical models were developed by discretizing governing equations over a fine mesh.

The numerical discretization scheme employs a cylindrical network of nodes around the cylinder and a Cartesian mesh for the rest of the computational domain. Since fineness of discretization mesh at the solid–fluid interface has a large effect on simulation results, the high fineness mesh near the cylinder wall was used.

2-3 Boundary Conditions

The following boundary conditions were applied to the system of governing equations for all investigated geometries:

Zero normal stress and vertical flow ($u = 0$) at the inlet to the computational domain ($x = 0$), free slip and no penetration at the left vertical boundary (symmetry line AB), no slip constant temperature wall at the right vertical boundary BD, no slip and no penetration at the cylinder surface, constant surface temperature (higher than temperature of the surrounding fluid), pressure inlet for the horizontal plane CD, pressure outlet for the horizontal plane AB, and free flow conditions.

It is well known that boundaries of a computational domain have to be sufficiently far from the physical boundaries of the modeled system to eliminate (or minimize) their effect on the numerical solution. This is especially true for the flows driven by weak body forces, such as natural convection-induced flows. However, "sufficiently" far is rather vague and depends on the nature of the problem being solved. Thus, determining the size of the computational domain needed to obtain the domain-independent numerical solution has received a special attention in this study.

To impose the free flow conditions, pressure outlet and pressure inlet were specified as boundary conditions at the inlet and outlet of the computational domain. The distance from the side walls of the domain to the center line of the column for one vertical column of horizontal cylinders, the center of the last cylinder in the row and the center of the last column in the bundle were chosen based on the analysis proposed by Warrington [35].

2-4 Solver Choice

The StarCCM+ [2] and ANSYS workbench software packages [1] used to solve the governing equations employ the control volume technique to discretize and solve the governing partial differential equations numerically. The control volume technique

subdivides the problem domain into a set of small non-overlapping control volumes with one control volume surrounding each nodal point. The governing equations are discretized to conserve each quantity within the control volume.

The pressure-based coupled solver (PBCS) and the standard laminar viscous flow model were used in this study. The pressure-based solver (PBCS) algorithm is presented in Figure 2-2. When using the PBCS, an algorithm for solving for the pressure-velocity coupling needs to be selected. The SIMPLE [58] solver was selected to derive an equation for pressure (or pressure correction) using a combination of continuity and momentum. The radiation heat transfer from the cylinders was assumed to be negligible. The residual convergence criteria for the continuity, momentum and energy equations were set to 10^{-5}. The average dimensionless heat transfer rate between the fluid and solid surface was also monitored for convergence.

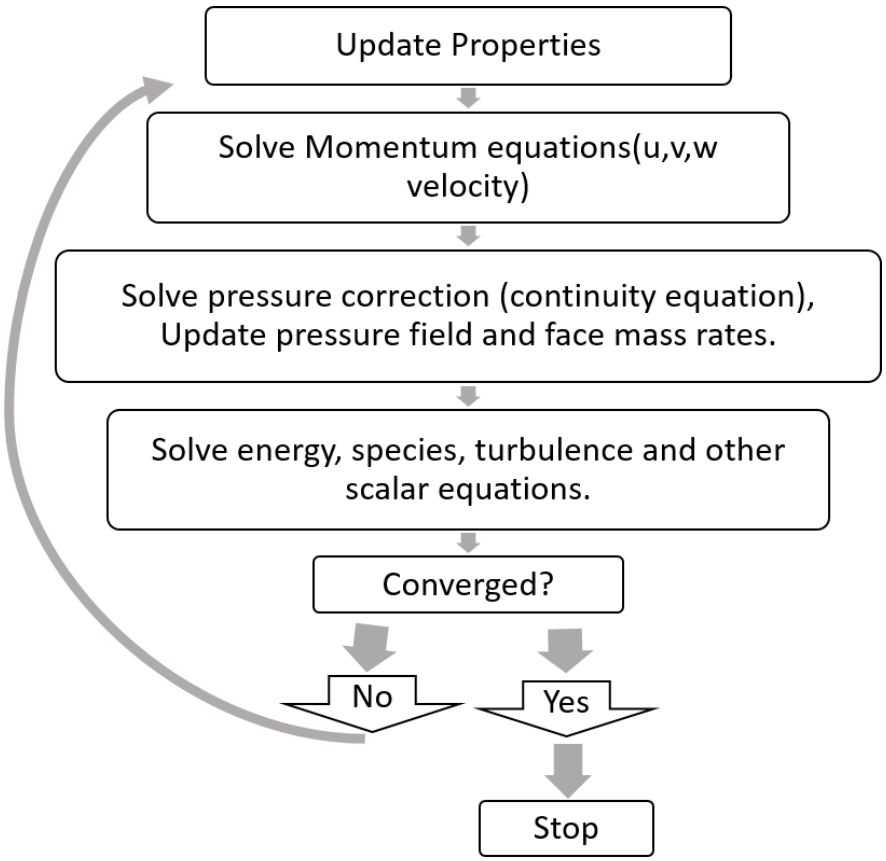

Figure 2-2 Pressure based solver algorithm. [52]

2-5 Grid Sensitivity Analysis

Since fineness of the discretization mesh, especially on the solid–fluid interface has a large effect on results, it is important to examine the accuracy of the numerical solution for the chosen mesh and boundary conditions. The numerical solution should be independent of the mesh size, i.e., discretization. In order to examine the effect of the mesh structure and accuracy of the results, the following mesh-independent analysis was performed.

- Run the initial simulation with initial mesh size and ensure convergence of residual error to 10^{-5}, the monitored points are steady, and imbalances are below 1%. Once the

convergence criteria above are met for the first simulation, the mesh is refined globally by using smaller cells throughout the computational domain.

- Run the simulation and ensure that the residual error drops below 10^{-5}, the monitored points are steady, and that the imbalances are below 1%.
- Compare the monitored point values from Step 2 against the values from Step 1. If they are the same (within the allowable tolerance), then the mesh at Step 1 is accurate enough to be used for numerical simulation. The solutions are compared in a graph where the average Nusselt number is plotted as a function of the number of cells used in the analysis. If the value of average Nu number predicted in Step 2 differs from the value obtained in Step 1 by less than the specified tolerance, the solution is independent of the mesh fineness.
- If the value of average Nu number predicted in Step 2 differs from the value obtained in Step 1 by more than the specified tolerance, the solution is dependent of the mesh fineness, the mesh needs to be further refined, and the process needs to be repeated until the mesh-independent solution is achieved.

Figure 2-3 shows the results of the grid sensitivity analysis obtained for the analyzed geometries. The total average Nusselt number is the average $\overline{\mathrm{Nu}}_{\mathrm{D}}$ number for all cylinders in the domain, calculated from the peripherally-averaged $\overline{\mathrm{Nu}}_{\mathrm{D}}$ numbers obtained for individual cylinders.

Based on the results, 2.2×10^5 cells are needed for a grid-independent solution for one horizontal row of nine cylinders for $S_T/D=2$ and $\mathrm{Ra}_{\mathrm{D}} = 10^4$, a minimum of 4.2×10^5 cell numbers are needed to achieve a grid-independent solution for a vertical column of ten

horizontal cylinders for $S_L/D=2$ and $Ra_D = 10^5$. For the in-line and staggered arrangement of tubes in a bundle 5×10^6 cells are needed for $S_L/D= S_T/D =2$ and $Ra_D = 10^6$.

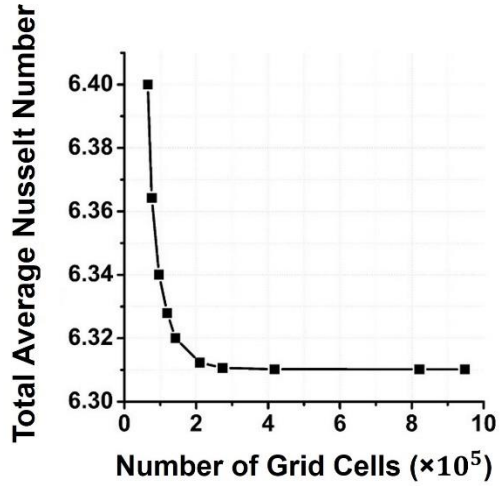

a) Horizontal row

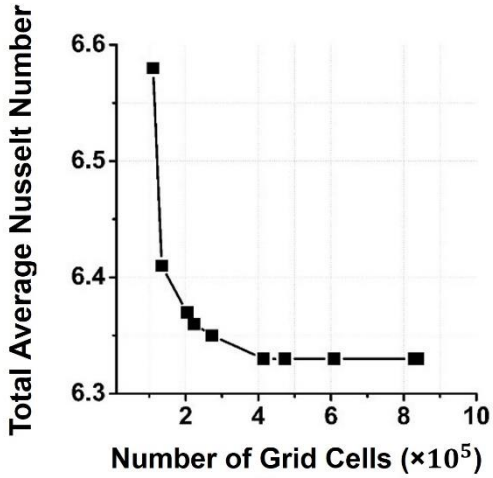

b) Vertical column

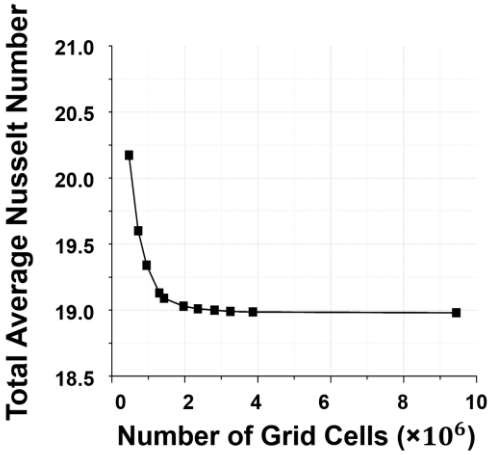

c) In-line bundle

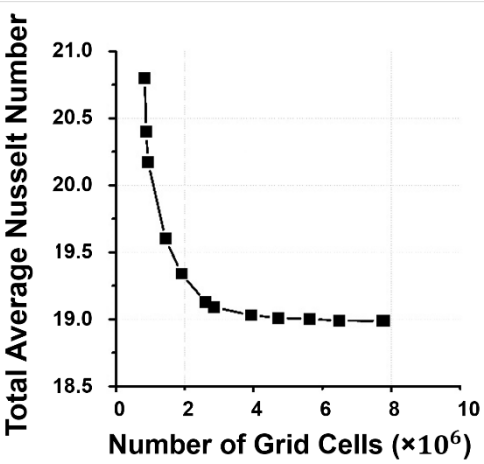

d) Staggered bundle

Figure 2-3 The total average Nusselt number vs. the number of grid cells for a) A horizontal row of five cylinders and $S_T/D=2$ and $Ra_D = 10^6$, b) A vertical column of ten horizontal cylinders and $S_L/D=2$ and $Ra_D = 10^5$, c) In-line bundle of horizontal cylinders and $S_T/D=2$, $S_L/D=2$ and $Ra_D = 10^6$, d) Staggered bundle of horizontal cylinders and $S_T/D=2$, $S_L/D=2$ and $Ra_D = 10^6$.

The equations, dimensionless parameters, statistical analysis, correlations from the published literature, and optimization approach used in this study to determine the optimal heat exchanger design are presented and discussed in the next chapter.

CHAPTER 3: MATHEMATICAL ANALYSIS AND OPTIMIZATION OF TES

3-1. Overview

The mathematical analysis and optimization approach for thermal energy storage systems are described in this section.

3-2. Governing Equations and Data Analysis of Thermal Energy Storage Systems

The following equation is an expression for the thermal energy Q stored in a thermal energy storage fluid having volume V_f as a function of time (assuming constant V_f):

$$Q(t) = \rho_f \cdot V_f \cdot c_f(T) \cdot \Delta T(t) \qquad \text{Eqn. 3-1}$$

Where in Eqn. 3-1, ΔT is the difference of temperature between the cylinder (tube) surface the heat storage fluid. Information regarding the maximum average temperature and the temperature profile within the heat storage fluid is needed to calculate the total amount of stored heat.

The total amount of stored heat can be calculated as:

$$Q = \int_0^t Q(t)dt \qquad \text{Eqn. 3-2}$$

The total energy Q_0 recovered from the TES, based on the TES efficiency η_{TES} is

$$Q_0 = Q\eta_{TES} \qquad \text{Eqn. 3-3}$$

ANSYS-Workbench [33] and StarCCM+ software packages [34] were used to solve governing equations: conservation equations for mass, momentum, and energy and determine the flow and temperature fields in the heat storage medium and heat transfer between the isothermal circular cylinders, representing tubes of a heat exchanger immersed in the heat storage fluid (molten solar salt).

The equations for conservation of mass (continuity equation), momentum, and energy for incompressible and compressible flows are the following:

$$\frac{\partial \rho}{\partial t} + \frac{\partial(\rho u)}{\partial x} + \frac{\partial(\rho v)}{\partial y} = 0 \qquad \text{Eqn. 3-4}$$

Momentum equation in x direction

$$\rho\left(\frac{\partial u}{\partial t} + u\frac{\partial u}{\partial x} + v\frac{\partial u}{\partial y}\right) = -\frac{\partial p}{\partial x} + \mu\left(\frac{\partial^2 u}{\partial x^2} + \frac{\partial^2 u}{\partial y^2}\right) \qquad \text{Eqn. 3-5}$$

Momentum equation in y direction

$$\rho\left(\frac{\partial v}{\partial t} + u\frac{\partial v}{\partial x} + v\frac{\partial v}{\partial y}\right) = -\frac{\partial p}{\partial y} + \rho g\beta(T - T_\infty) + \mu\left(\frac{\partial^2 v}{\partial x^2} + \frac{\partial^2 v}{\partial y^2}\right) \qquad \text{Eqn. 3-6}$$

Energy Equation (neglecting viscous dissipation)

$$\left(\frac{\partial T}{\partial t} + u\frac{\partial T}{\partial x} + v\frac{\partial T}{\partial y}\right) = \alpha\left(\frac{\partial^2 T}{\partial x^2} + \frac{\partial^2 T}{\partial y^2}\right) \qquad \text{Eqn. 3-7}$$

Variation of fluid density induced by temperature plays a central role in the evaluation of the buoyancy-induced flows. Molten salt is considered as an incompressible fluid with constant density calculated at film temperature, therefore the pressure work and viscous dissipation are negligible. Due to the small temperature changes, to account for the buoyancy effects in the y-momentum equation, the Oberbeck-Boussinesq [58] approximation was employed in Eqn. 3-6 to linearize the relationship between density and temperature in the buoyancy force term. The dimensionless parameters used in the study are the following:

$$Pr = \frac{\vartheta}{\alpha} = \frac{c_p \mu}{k} \qquad \text{Eqn. 3-8}$$

$$Ra_D = \frac{g\beta}{\vartheta\alpha}(T_w - T_\infty)D^3 \quad \text{Eqn. 3-9}$$

$$Ra_D^* = Ra_D \times \overline{Nu}_D \quad \text{Eqn. 3-10}$$

The dimensionless natural convection heat transfer around the cylinder can be expressed in terms of the peripherally-averaged Nusselt number [53] as:

$$\overline{Nu}_D = CRa_D^n \quad \text{Eqn. 3-11}$$

$$\bar{h} = \frac{k(T) \times \overline{Nu}}{D} \quad \text{Eqn. 3-12}$$

$$Q = h \cdot A \cdot \Delta T \quad \text{Eqn. 3-13}$$

Dimensionless temperature is defined as:

$$\theta = \frac{T - T_\infty}{T_w - T_\infty} \quad \text{Eqn. 3-14}$$

The physical properties of molten salt at different temperatures are calculated using correlations from the literature, as discussed in Section 1-5-3.

Dimensionless heat transfer volumetric density $\tilde{q}$ is a dimensionless form of volumetric total heat transfer rate q" integrated over the surface of a cylinder.

$$q'' = \frac{q}{HLW} \quad \text{Eqn. 3-15}$$

$$\tilde{q} = \frac{q}{HLW} \times \frac{D^2}{k(T_w - T_\infty)} \quad \text{Eqn. 3-16}$$

Dimensionless longitudinal and transverse lengths ($l_L^* = \frac{x}{S_{L-D}}$ and $l_T^* = \frac{x}{S_{T-D}}$) shown in Figure 3-1, represent the ratio of the radial distance of a point located on the cylinder surface to the radial distance between the cylinder surface and the adjacent cylinder at a specific (given) angle.

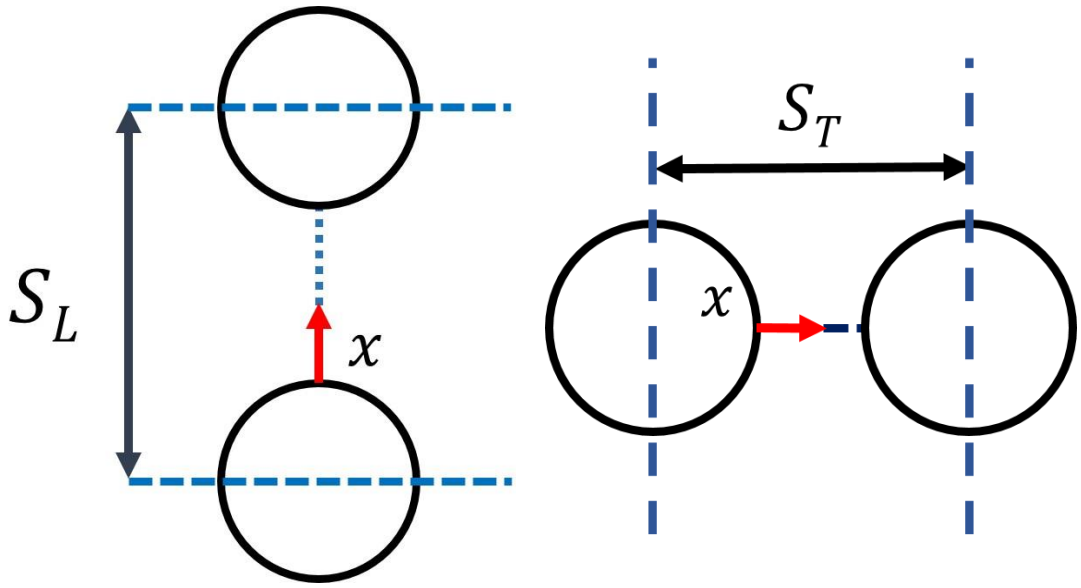

a) b)

Figure 3-1 Dimensionless longitudinal and transverse lengths a) $l_L^* = \frac{x}{S_L - D}$ b) $l_T^* = \frac{x}{S_T - D}$

3-3. Existing Correlations for Natural Convection Heat Transfer from Circular Cylinders

A correlation for the laminar natural convection heat transfer from a single horizontal cylinder in a free flow valid for any Rayleigh and Prandtl number was proposed by Kuehn and Goldstein [51]. Verified with the experimental data, this equation was obtained by solving the Navier-Stokes and energy equations using an elliptic numerical procedure [51].

$$\frac{2}{\overline{Nu}_0} = \ln\left[1 + \frac{2}{\left[\left\{0.518Ra_D^{0.25}\left[1 + \left(\frac{0.559}{Pr}\right)^{3/5}\right]^{-5/12}\right\}^{15} + \left(0.1Ra_D^{1/3}\right)^{15}\right]^{1/15}}\right] \quad \text{Eqn. 3-17}$$

For a single horizontal row of cylinders, the heat Transfer Enhancement HTE is defined as the ratio of $\overline{Nu}_D$ for a single row of horizontal cylinders to the Nusselt number Nu_0 for a single cylinder in a free flow calculated from Eqn. 3-17.

$$\frac{\overline{Nu}_D}{\overline{Nu}_0} = f\left(\frac{S_T}{D}, Ra_D\right) \quad \text{Eqn. 3-18}$$

$$\overline{Nu}_D = \overline{Nu}_0 \times f\left(\frac{S_T}{D}, Ra_D\right) \quad \text{Eqn. 3-19}$$

For a vertical column of cylinders, the Heat Transfer Enhancement HTE is defined as the ratio of $\overline{Nu}_D$ for a vertical column of horizontal cylinders to the Nusselt number Nu_0 for an unconfined single cylinder in a free flow calculated from Eqn. 3-17.

$$\frac{\overline{Nu}_D}{\overline{Nu}_0} = f\left(\frac{S_L}{D}, Ra_D\right) \quad \text{Eqn. 3-20}$$

$$\overline{Nu}_D = \overline{Nu}_0 \times f\left(\frac{S_L}{D}, Ra_D\right) \quad \text{Eqn. 3-21}$$

For a tube bundle, the Heat Transfer Enhancement HTE is defined as the ratio of $\overline{Nu}$ for a bundle of horizontal cylinders to the Nusselt number Nu_0 for a single cylinder in a free flow calculated from Eqn. 3-17.

$$\frac{\overline{Nu}}{\overline{Nu}_0} = f\left(\frac{S_T}{D}, \frac{S_L}{D}, Ra_D\right) \quad \text{Eqn. 3-22}$$

$$\overline{Nu}_D = \overline{Nu}_0 \times f\left(\frac{S_T}{D}, \frac{S_L}{D}, Ra_D\right) \quad \text{Eqn. 3-23}$$

The only correlations concerning natural convection heat transfer from a row of horizontal cylinders published in the literature are proposed by Bello-Ochende and Bejan [59]. They proposed two correlations for the optimal cylinder spacing $(S_T/D)_{opt}$ and the

corresponding maximum volumetric heat transfer density $\tilde{q}_{max}$ as functions of Ra_D number for a row of infinite horizontal cylinders immersed in air.

$$(S_T/D)_{opt} = 1.32Ra_D^{-0.22} \quad \text{Eqn. 3-24}$$

$$\tilde{q}_{max} = 0.65\ Ra_D^{0.3} \quad \text{Eqn. 3-25}$$

Corcione [56] proposed a correlation based on experimental data for the average $\overline{Nu}_{D,N}$ number for a vertical column of N unconfined horizontal cylinders. The correlation given by Eqn. 3-26 has standard error of 2.25% with the error range of -4.79 to 5.27%.

$$\overline{Nu}_{D,N} = {Ra_D}^{0.235}\left[0.292 \ln \left[\frac{\left(\frac{S_L}{D}\right)^{0.4}}{N_i^{0.2}}\right] + 0.447\right] \quad \text{Eqn. 3-26}$$

$$2 \le N_i \le 6$$

$$\left(\frac{S_L}{D}\right) \le 10 - \log Ra_D$$

$$5 \times 10^2 \le Ra_D \le 5 \times 10^5$$

Corcione [56] also proposed a correlation for the Nusselt number for individual cylinders in a vertical column of horizontal cylinders. Correlation for the peripherally-averaged Nusselt number for the i^{th} cylinder in the column given by Eqn. 3-27 has a standard error of 3.19% with the error range from −5.07 to 7.97%.

$$\overline{Nu}_{D,i} = {Ra_D}^{0.25}\left[0.364 \ln \left[\frac{\left(\frac{S_L}{D}\right)^{0.4}}{N_i^{0.9}}\right] + 0.508\right] \quad \text{Eqn. 3-27}$$

$$2 \le N_i \le 6$$

$$2(\overline{Nu}_{D,i} - 1) \le \left(\frac{S_L}{D}\right) \le 8 + N_i$$

$5 \times 10^2 \leq \mathrm{Ra_D} \leq 5 \times 10^5$

Based on his numerical analysis, Lu et al. [55] proposed correlations for the Nu number for the first (lower) $\mathrm{Nu_L}$, and second (upper) $\mathrm{Nu_U}$ cylinder from the bottom in the vertical column of two horizontal cylinders for $10^2 \ll \mathrm{Ra} \ll 10^6$. Correlations given by Eqn. 3-28 and Eqn. 3-29 have standard error of 5%.

$$\overline{\mathrm{Nu}}_{\mathrm{D,L}} = 0.63357 + 0.44681 \times \mathrm{Ra_D}^{0.2566} \qquad \text{Eqn. 3-28}$$

$$\overline{\mathrm{Nu}}_{\mathrm{D,U}} = 2.4414 + 0.3659 \times (\frac{\mathrm{S_L}}{\mathrm{D}})^{0.2334} \times \mathrm{Ra_D}^{0.2539} \qquad \text{Eqn. 3-29}$$

Based on his experimental data, Kitamura et al. [60] proposed a correlation for the average Nusselt number based on the cylinder spacing $\overline{\mathrm{Nu}}_{(\mathrm{S_L-D})}$ for individual cylinders in a vertical column of N horizontal cylinders in air. Correlation for the peripherally-averaged $\overline{\mathrm{Nu}}_{(\mathrm{S_L-D}),\mathrm{i}}$ number for the i[th] cylinder in the column, given by Eqn. 3-30, has a standard error of 4.8 %.

$$\overline{\mathrm{Nu}}_{(\mathrm{S_L-D}),\mathrm{i}} = 0.45 \times [\mathrm{Ra}^*_{(\mathrm{S_L-D})} \times \frac{1}{\mathrm{N_i}} \times \left({}^{\mathrm{S_L}}/_{\mathrm{D}} - 1\right)] \qquad \text{Eqn. 3-30}$$

$2 \leq \mathrm{N_i} \leq 10$

$2 \times 10^2 \leq \mathrm{Ra}^*_{(\mathrm{S_L-D})} \leq 10^5$

3-4. Optimization of a TES System

Since a sensible TES stores thermal energy by heating the storage medium, its performance strongly depends on heat transfer, which in turn depends on thermo-physical properties of the storage medium (such as specific heat and thermal conductivity), operating conditions (such as temperature difference), and design parameters, such as heat

exchanger design, amount of the heat storage medium, and other [61]. To improve TES performance, heat transfer from the heat transfer fluid via heat exchanger to the storage medium has to be increased. Higher heat transfer and energy storage rates in a TES can be achieved by optimizing design of the heat exchanger to a cost-effective smaller size geometry with higher heat transfer. Since molten salt as an inexpensive material with high thermal conductivity is one of the most popular choices for sensible heat storage medium, accurate information on heat transfer and effect of tube spacing for that storage medium is important for the optimal design of a TES heat exchanger.

Prior to optimizing heat exchanger geometry, the results from this study needed to be verified by comparing them to the results published from the literature. Verification of the numerical model, analysis procedure, and the results is described in the next chapter.

CHAPTER 4: MODEL VALIDATION

4-1. Overview

This section describes verification of the numerical model and results. The following analysis was performed to compare the results from this study to the results published in the literature and validate the numerical model and method of analysis.

4-2. Natural Convection Heat Transfer from an Unconfined Single Cylinder.

The analysis of a two-dimensional natural convection heat transfer from a single unconfined horizontal circular cylinder immersed in molten salt, representing a free flow condition, was performed over the Ra_D number range. The numerically obtained values of peripherally-averaged Nusselt number $\overline{Nu}_D$ were compared to the results obtained from the Kuehn and Goldstein (K&G) correlation [51] represented by Eqn. 3-17. As the results presented in Table 4-1 show, there is an excellent agreement between numerical predictions from this study and K&G correlation over the investigated range of Ra_D numbers. The average relative error is 1.5%, much lower compared to the uncertainty of the correlation.

The numerical results obtained from the StarCCM+ software packages were also compared to the results obtained from ANSYS. The difference in numerical predictions obtained by these two software packages is less than one percent.

Table 4-1. Comparison of the predicted average Nusselt number $\overline{Nu}_D$ values and results from the Kuehn and Goldstein [51] correlation.

Ra_D number	Nusselt number $\overline{Nu}_D$		
	Ref. [51] - Eqn. 3-17	This Study (Numerical Analysis)	Percentage Difference %
10^4	5.78	5.75	-0.52
10^5	9.56	9.64	0.83
5×10^5	13.83	13.97	1.01
10^6	16.26	16.41	0.92

4-3. Natural Convection Heat Transfer from a Semi-Confined Single Cylinder.

Two-dimensional natural convection heat transfer from a single semi-confined horizontal circular cylinder (horizontal cylinder placed inside a vertical channel of width W) shown in Figure 4-1 was analyzed for the confinement ratio C (defined as W/D) of 18. The results were compared to the results published by Clifford et al. [52], and correlations for a single unconfined cylinder by Fand et al. [62] and Morgan [53]. The comparison is presented in Table 4-2.

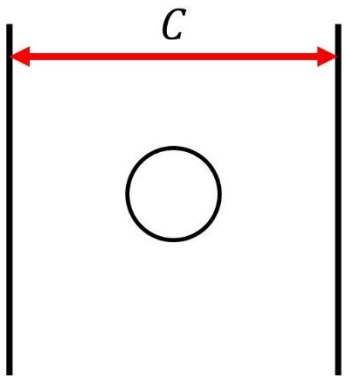

Figure 4-1 A single semi-confined horizontal circular cylinder placed inside a vertical channel of width W

Table 4-2 shows an excellent agreement with the average relative error of ± 5% between the predicted peripherally-averaged Nusselt $\overline{Nu}_D$ values from this study and the

numerical study by Clifford et al. [52]. Table 4-2 also compares peripherally-averaged Nusselt values for a single unconfined cylinder determined from the correlations proposed by Morgan [53] and Fand et al.[62]. This comparison shows that for the confinement ratio of 18 the presence of the confinement walls degrades heat transfer because channel walls affect the velocity and temperature fields, resulting in lower heat transfer.

However, for the confinement ratio of 18 confinement walls are relatively far from the cylinder and they have a small effect on heat transfer. Therefore, there is a good agreement between the results obtained from correlations for a single unconfined cylinder and numerical predictions for the semi-confined cylinder,

Table 4-2 Comparison of the predicted average Nusselt number values obtained from the numerical analysis and three references.

Ra_D	Nusselt number $\overline{Nu}_D$, Numerical analysis Confined Cylinder		Nusselt number $\overline{Nu}_D$, Correlation Unconfined Cylinder	
	This Study	Ref [52]	Ref [62]	Ref [53]
100	1.87	1.9	2.02	2.13
1000	2.96	3.01	3.12	3.26
10000	4.72	4.7	4.82	5.4
100000	8.08	8	8.54	8.55

4-4. Natural Convection Heat Transfer from Two Vertically Aligned Horizontal Cylinders Immersed in Molten Salt.

Computational domain shown in Figure 4-2 was used for a numerical study of two-dimensional natural convection heat transfer from two vertically aligned horizontal cylinders immersed in molten salt, representing a free flow condition. This analysis was performed for a range of Ra_D numbers from $Ra_D = 10^5$ to $Ra_D = 7.5 \times 10^6$ and a constant dimensionless cylinder spacing of $S_L/D = 2$.

Although molten salt was used as the heat storage medium in this study and in the study by Lu et al. [55], Lu assumed $\mathrm{Pr} = 14$, while in this study Prandtl number varied with temperature from 6 to 10.

Table 4-3 and Figure 4-3a and b show that considering the difference in Prandtl number, there is a very good agreement between the results obtained from Lu's correlations (Eqn. 3-28 and Eqn. 3-29) and numerical results from this study. The difference of less than 2% between the results is well within the error range of 5% reported by Lu [55]. Both

Table 4-3 and Figure 4-3 show that the heat transfer rate and value of the average Nusselt number $\overline{\mathrm{Nu}}_{\mathrm{D,L}}$ for the lower (first) cylinder in the column predicted by both studies is the same as for a single cylinder in a free flow obtained from Kuehn and Goldstein's correlation [51] given by Eqn. 3-17. Also, heat transfer from the lower cylinder is not affected by the downstream (upper) cylinder.

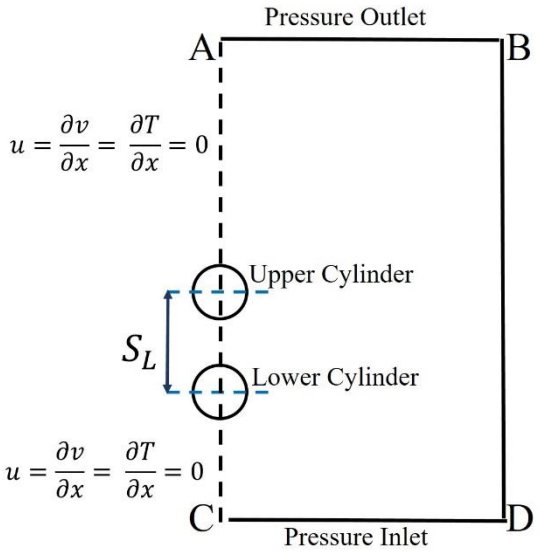

Figure 4-2 Computational domain for the study of natural convection from two vertically aligned horizontal cylinders immersed in molten salt.

Table 4-3 Comparison of the predicted average Nusselt number $\overline{Nu}_D$ values from two vertically aligned horizontal cylinders between the results obtained by Lu et al. [55] (Eqn. 3-28 and Eqn. 3-29) and this study.

$S_L/D=2$	This Study	Ref. [55] Eqn. 3-28	Percentage difference	This Study	Ref. [55] Eqn. 3-29	Percentage difference
Ra_D	Nu_{L1}	Nu_{L2}	$\frac{\overline{Nu}_{D_{L1}} - \overline{Nu}_D}{\overline{Nu}_{D_{L2}}} \times 100$	Nu_{U1}	Nu_{U2}	$\frac{\overline{Nu}_{D_{U1}} - \overline{Nu}_{D_U}}{\overline{Nu}_{D_{U2}}} \times 100$
10^5	9.45	9.21	**2.6**	8.15	8.24	**-1.09**
5×10^5	13.85	13.59	**1.9**	12.34	12.28	**0.49**
10^6	16.38	16.11	**1.67**	14.77	14.6	**1.16**
5×10^6	24.03	24.03	**0.0**	22.41	21.85	**2.56**

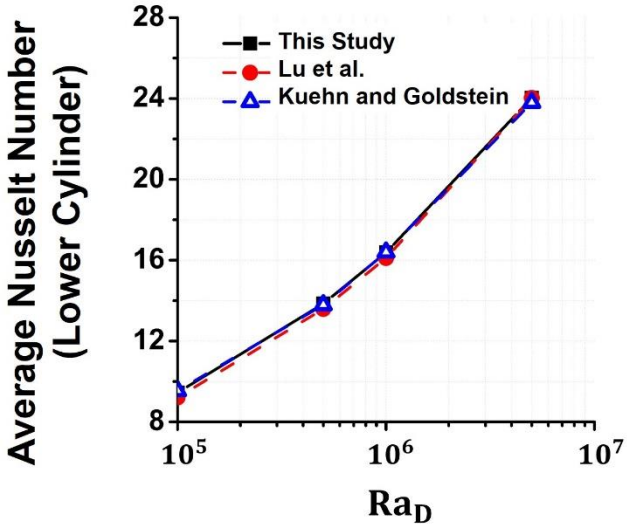

a)

Figure 4-3 Comparison of the predicted peripherally-averaged Nu values for two vertically aligned horizontal cylinders from this study to the results obtained by Lu et al. [55] and correlation proposed by Kuehn and Goldstein for a single free cylinder [51].

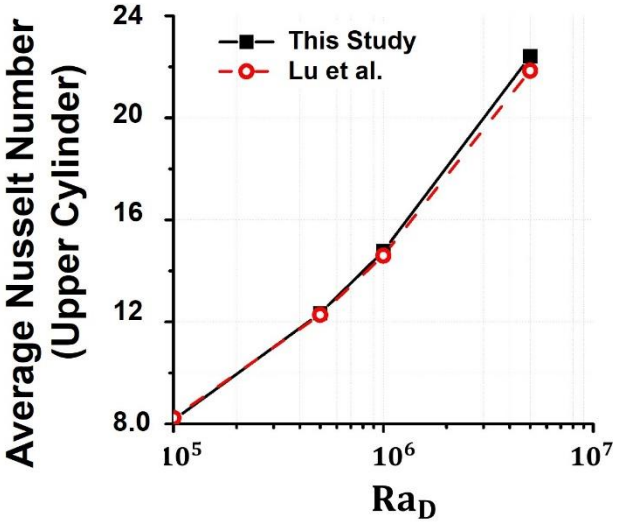

b)

Figure 4-3 cont.

4-5. Natural Convection Heat Transfer from a Vertical Column of Five Horizontal Cylinders.

Numerical analysis of a two-dimensional natural convection heat transfer from a vertical column of five horizontal cylinders immersed in air, representing a free flow condition shown schematically in Figure 4-4 was performed for $Ra_D=10^4$ and dimensionless cylinder spacing of $S_L/D = 2$. The results were compared to the results reported by Corcione [56] and are presented in Table 4-4 and Figure 4-5. The comparison of results shows an excellent agreement between the two studies; with the maximum difference being less than standard error of the correlation.

Also the heat transfer enhancement ($\overline{Nu}_D/\overline{Nu}_0$)values for the first cylinder in the column presented in Table 4-4 show that the heat transfer (Nu number) from the first cylinder in the column is the same as for a single cylinder in a free flow and is not affected by the presence of the downstream (upper) cylinder.

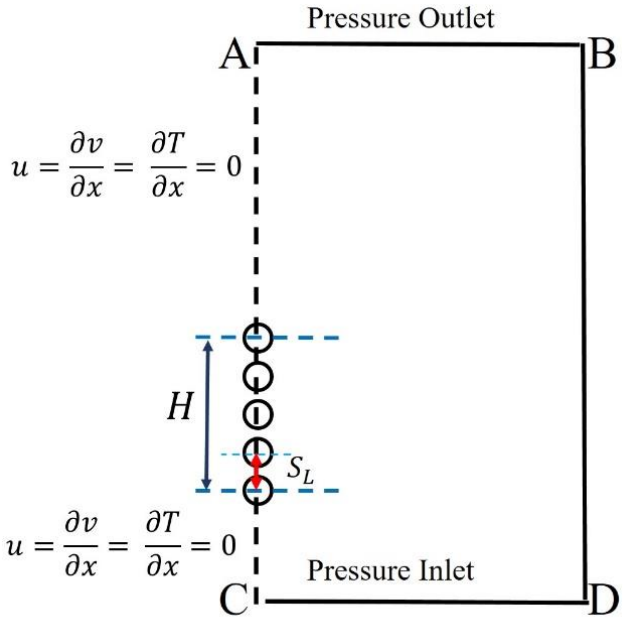

Figure 4-4 Schematic of the computational domain for the study of natural convection from a vertical column of five horizontal cylinders immersed in the heat storage fluid.

Table 4-4 Comparison of the heat transfer enhancement($\overline{Nu}_D/\overline{Nu}_0$) based on the predicted average $\overline{Nu}_D$values from a vertical column of five horizontal cylinders and the results obtained from Eqn. 3-27 proposed by Corcione [56].

(i^{th} cylinder)	This Study	Ref. [56] (Eqn. 3-27±5%)	Ref. [56] (Figure 10, from the paper)
1	1	1	1
2	0.76	0.79	0.76
3	0.63	0.73	0.63
4	0.57	0.65	0.56
5	0.56	0.59	0.55

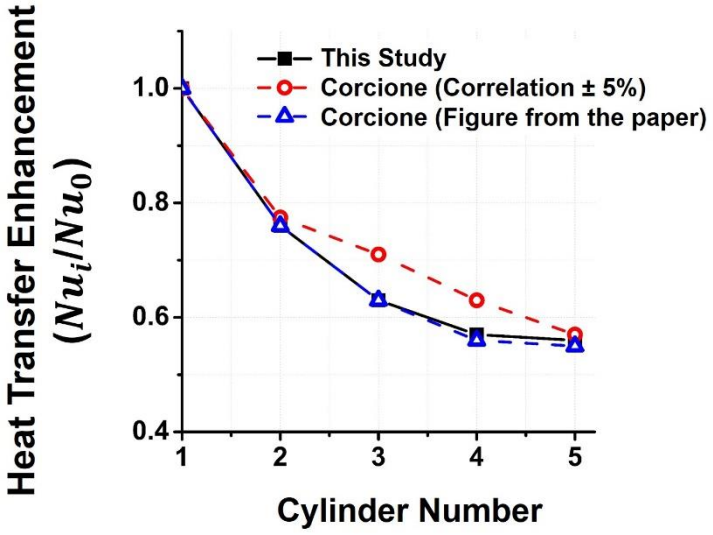

Figure 4-5 Comparison of the predicted average Nusselt number$\overline{Nu}_D$values from a vertical column of five horizontal cylinders and the results obtained from Eqn. 3-27 proposed by Corcione [56] and $Ra_D=10^4$.

4-6. Numerical Modeling of Buoyancy-Induced Fluid Flow and Heat Transfer in a Staggered Tube Bundle

The analysis of a two-dimensional steady-state buoyancy-induced heat transfer from a staggered tube bank (bundle of cylinders) immersed in water, with infinite number of cylinders in the transverse direction and twelve cylinders in the vertical direction, was performed for $\mathrm{Ra_D} = 1.2 \times 10^6$. The computational domain includes the space between three vertical columns, one complete column and two half columns of cylinders as shown in Figure 4-6. The numerically obtained values of peripherally-averaged Nusselt number (average Nu number) for the twelve cylinders of the middle column were compared to the results by Ivanov et al. [57]. The predicted average Nusselt number ($\overline{\mathrm{Nu}}_{\mathrm{D,i}}$) values for individual cylinders in a staggered tube bank (bundle of cylinders) presented in

Table 4-5 shows a very good agreement between the results obtained by Ivanov et al. [57] and this study, with maximum error of 2.78% for cylinder number 4.

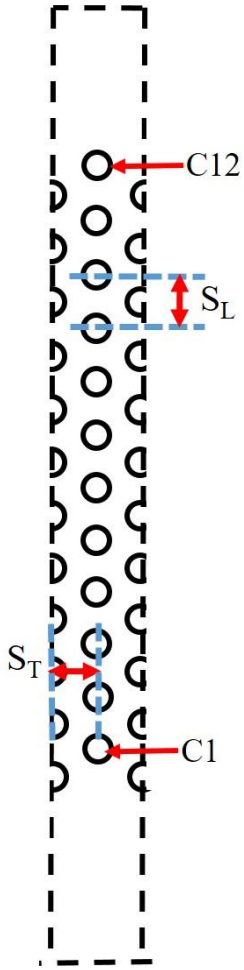

Figure 4-6 Schematic of the control volume, cylinders are numbered from the bottom up.

Table 4-5 Comparison of the predicted average Nusselt number $\overline{Nu}_{D,i}$ values for individual cylinders in a staggered tube bank (bundle of cylinders) between the results obtained by Ivanov et al. [57] and this study.

Cylinder number n	Ivanov et al. [57] $\overline{Nu}_{D,i}$	This Study $\overline{Nu}_{D,i}$	Percentage Difference %
1	24.4	25.01	2.44
2	15.3	15.7	2.55
3	12.7	13.02	2.46
4	11.9	12.24	2.78
5	11.1	11.4	2.63
6	11.2	11.32	1.06
7	10.6	10.89	2.66
8	10.5	10.72	2.05
9	10.4	10.6	1.89
10	10.1	10.26	1.56
11	10	10.11	1.09
12	11.6	11.4	-1.75

The next chapter presents the literature review of the experimental and numerical studies concerning the natural convection heat transfer from one horizontal row of cylinders. The physical model, a detailed analysis of the steady-state temperature and velocity distributions around the cylinders as well as statistical regression analysis of the numerical results are presented and discussed.

CHAPTER 5: SINGLE ROW OF HORIZONTAL CYLINDERS

5-1. Overview

Buoyancy driven flows and natural heat transfer phenomena from unconfined horizontal cylinders has been widely studied both experimentally and numerically [51, 53, 54, 63-68]. Churchill and Chu [69] proposed a correlation for the average Nusselt number for a single horizontal isothermal cylinder in a free flow for any value of the Ra and Pr numbers.

Cesini et al. [70] investigated the effect of Rayleigh number and geometry of the cavity on the natural convection heat transfer from a horizontal cylinder inside a rectangular cavity. Their experimental data were in an excellent agreement with analytical predictions based on the finite element analysis (FEM). Alinnawi et al. [71] numerically investigated the effect of the cross section shape of the cylinder located inside the cavity on heat transfer and concluded that a cylinder of the circular cross section has higher heat transfer rate compared to the square and triangular shapes.

Kim et al. [72] performed two-dimensional transient numerical analysis for horizontal heated circular cylinders placed into a colder cavity with isothermal walls and showed that the cylinder location in the cavity and Rayleigh number are important parameters affecting natural convection heat transfer between the cylinders and cavity walls. Roychowdhury et al. [73] observed that for a circular cylinder inside a cavity, the flow patterns, thermal stratification, and heat transfer rate are significantly dependent on the boundary conditions, Prandtl number, and aspect ratio of the cavity.

A few studies investigated the natural convection heat transfer from a single row of isothermally heated cylinders [59, 74, 75]. However, no correlations or performance maps were developed for the average Nusselt number Nu for a single row of horizontal cylinders. Using correlations developed for natural convection heat transfer from a single cylinder in a free flow would result in large errors in heat transfer for a single row of horizontal cylinders. Thus, correlations for the average Nusselt number Nu for a single row of horizontal cylinders are needed for more accurate design of heat exchangers used in solar and other thermal systems.

The use of molten salt for thermocline thermal energy storage systems has been focus of many recent studies [25, 49]. However, only a few studies considered the steady-state natural convection heat transfer from horizontal circular cylinders representing heat exchanger tubes immersed in a molten solar salt [55, 68] and [26]. Although heat transfer by natural convection from a row of infinite number of cylinders surrounded by air was studied previously [59, 74] for low values of Ra number, very little information is available for the molten solar salt, finite number of cylinders, and high Ra numbers.

The steady-state laminar natural convection heat transfer from a two-dimensional TES heat exchanger comprising one row of horizontal circular cylinders representing a heat exchanger immersed in a heat storage medium was investigated in this study with objective to determine heat transfer characteristics of a realistic heat exchanger used in a TES system.

5-2. Physical Model

Figure 5-1a shows schematic of a single-tank TES proposed by Lu et al. [55] with a more complex HXE geometry involving a single row of horizontally-aligned horizontal circular cylinders representing heat transfer tubes and molten salt as the storage medium. The analyzed heat exchanger geometry involves a single horizontal row of five and nine circular cylinders of diameter D placed in the computational domain ABCD presented in Figure 5-1b. Due to the symmetry along the A-C line, the analysis was performed for the right half (ABCD domain) of the storage tank.

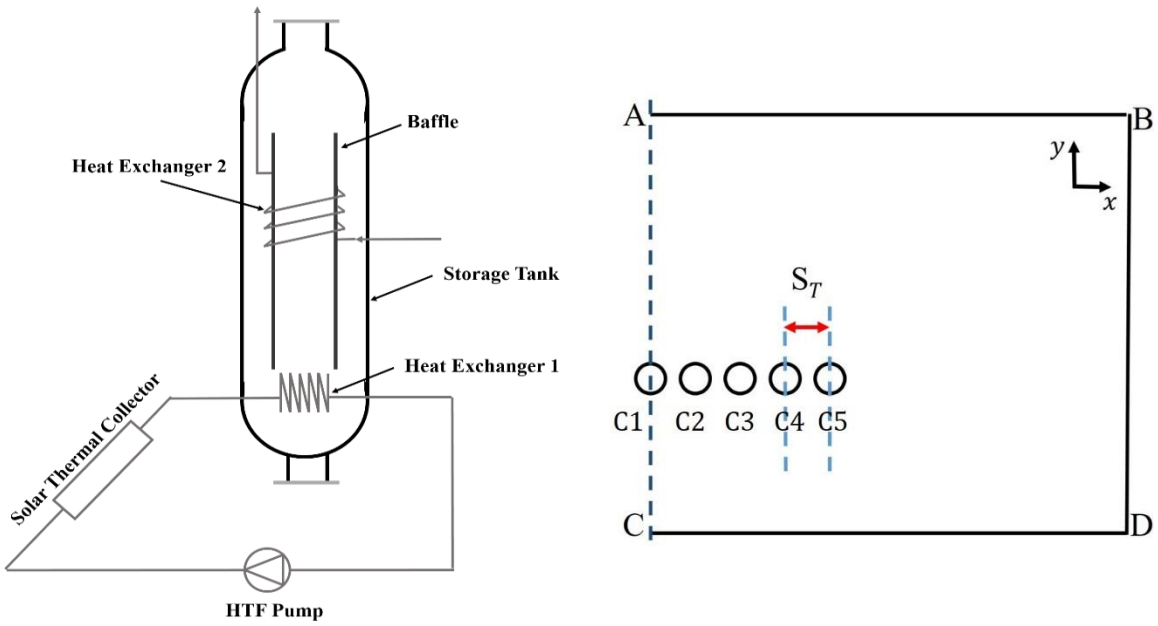

a) b)

Figure 5-1 Schematic of the: (a) Thermal Energy Storage, (b) Control volume for a single row of nine horizontal cylinders with cylinder numbers specified.

Based on the analysis proposed by Warrington [76], the distance from the side walls of the domain to the center of the last cylinder in the row (for example, cylinder C_5 in Figure 5-1b) was set to 5 times the diameter of the cylinder for very small cylinder

spacing to provide a domain-independent solution. This value was increased for larger cylinder spacing. The effect of the distance between the inlet to the computational domain (line CD) to the center of the cylinder row (the inlet, or the upstream distance) and the outlet of the computational domain, line AB (the outlet, or downstream distance) was investigated by performing a series of parametric numerical calculations where these distances were varied. The results of numerical simulations presented in Table 5-1 for $S_T/D = 2$ and $Ra_D = 10^4$ show that for the wall distance of 5 times the cylinder diameter or more, the heat transfer from a single row of horizontal cylinders is unaffected by the side walls.

Table 5-1 The effect of the side wall distance on heat transfer for a horizontal row of five cylinders for $Ra_D = 10^4$ and $S_T/D = 2$.

Wall distance	C1	C2	C3	C4	C5
D	6.54	6.70	6.23	6.22	6.32
1.5D	6.98	7.12	7.02	6.77	6.05
2D	6.10	6.66	6.75	6.66	6.10
5D	5.95	6.57	6.67	6.57	5.95
6D	5.95	6.57	6.67	6.57	5.95

5-3. Steady-State Temperature and Velocity Distribution Around Circular Cylinders

It has been observed in this study and the study performed by Farouk et al. [74] that in the case of a single cylinder in a free flow, for high Rayleigh numbers ($Ra_D \gg 10^5$) most of the flow enters the control volume (computational domain) from the sides instead at the bottom, as shown in Figure 5-2. The heat transfer in this case is expected to be affected by the presence of adjacent cylinders in a row and spacing between the cylinders [74].

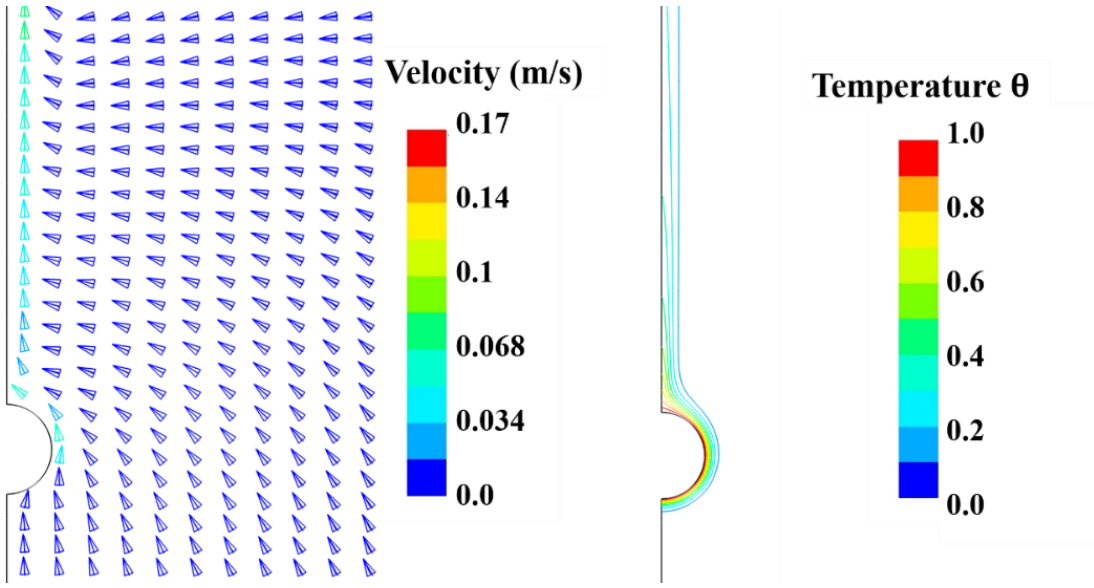

a) b)

Figure 5-2 A single circular cylinder in a free flow for $Ra_D = 10^5$. a) Flow field b) Dimensionless temperature contours.

The results presented in Figure 5-2a and b show that the flow and temperature fields around a single cylinder in a free flow predicted in this study are similar to the results from the previous studies conducted by Farouk et al. [74] and Cianfrini et al. [75], with most of the flow entering the control volume from the side and turning upwards, forming a plume at upper surface of the cylinder. Figure 5-3 shows the velocity and temperature contours predicted in this study for a single horizontal row of five cylinders for a low value of $Ra_D = 10^4$ and tight cylinder spacing $S_T/D = 1.4$. As the results presented in Figure 5-3a show, natural convection is driving the flow around the cylinders and inwards towards the center cylinder where the flow turns and accelerates in the vertical direction. The flow velocity is the highest along the centerline at the exit from the computational domain. Since the flow is induced by the temperature gradients and corresponding changes in fluid density, plumes rising from individual cylinders interact and merge forming a single distinct plume as

presented in Figure 5-3b. As discussed in the study by Cianfrini et al. [75], the "suction effect" between cylinders causes rotation of the warm plumes rising from the individual cylinders towards the center cylinder, their interaction, and merging into a single plume.

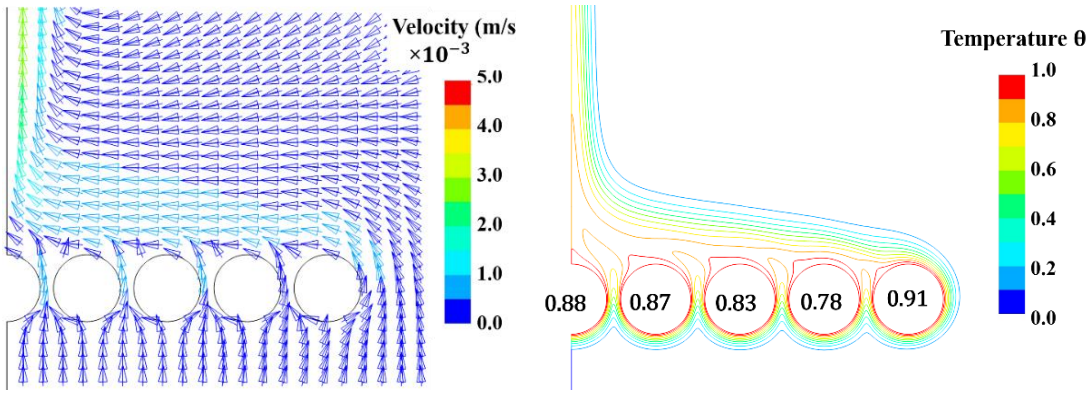

a) b)

Figure 5-3 Horizontal row of five cylinders$Ra_D = 10^4$ and (S_T/D)=1.4 a) Velocity b) Dimensionless temperature contours with heat transfer enhancement HTE values for each cylinder.

Presence of the adjacent cylinders affects temperature and flow fields around individual cylinders resulting in uneven heat transfer, as presented in Figure 5-3. For small values of S_T/D where cylinder spacing is smaller than thickness of the velocity boundary layer, interference of the thermal boundary layers and the bulk fluid flow reduces temperature gradient between two adjacent cylinders (Figure 5-3b and Figure 5-5a) resulting in a decrease in heat transfer and lower average Nusselt number $\overline{Nu}_D$. As shown in Figure 5-3a, Figure 5-4 and Figure 5-5b, for the smallest analyzed cylinder spacing of S_T/D = 1.2 there is virtually no flow between adjacent cylinders and heat transfer in this region is dominated by conduction, with natural convection occurring only at the top of the cylinders.

By increasing the cylinder spacing to values close to the thickness of velocity boundary layer, through-flow resistance is decreased, and buoyancy force drives stronger natural convection between the cylinders leading to the formation of weak plumes around individual cylinders. Stronger natural convection results in higher heat transfer rate and higher average Nusselt number $\overline{Nu}_D$. The effect of adjacent cylinders diminishes as cylinder spacing increases, and for large spacings individual plumes do not merge into a single plume as shown in Figure 5-4. For spacing much larger than thickness of the velocity boundary layer, individual cylinders behave like single cylinders in a free flow.

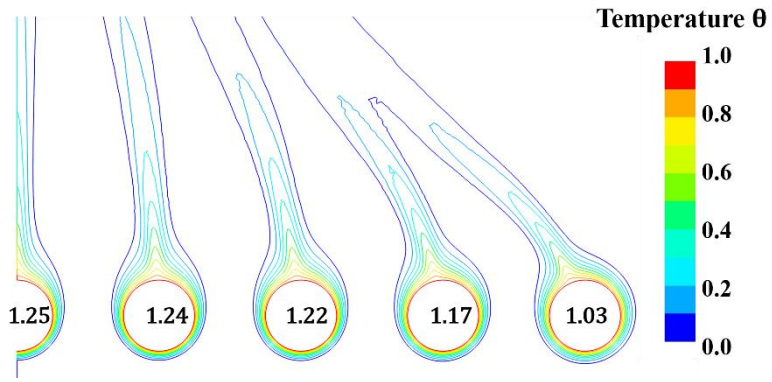

a) S_T/D= 2

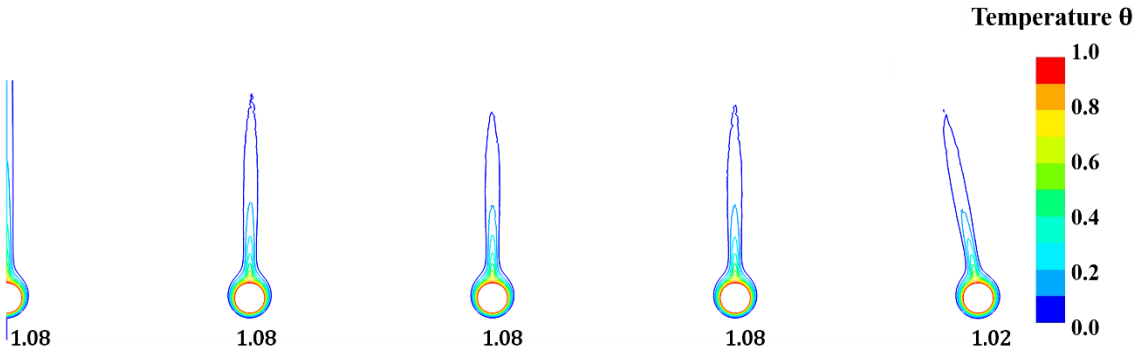

b) S_T/D= 8

Figure 5-4 Dimensionless temperature contours of heat transfer enhancement for each cylinder for a horizontal row of nine cylinders for $Ra_D = 10^4$ and two values of cylinder spacing, S_T/D= 2 and 8.

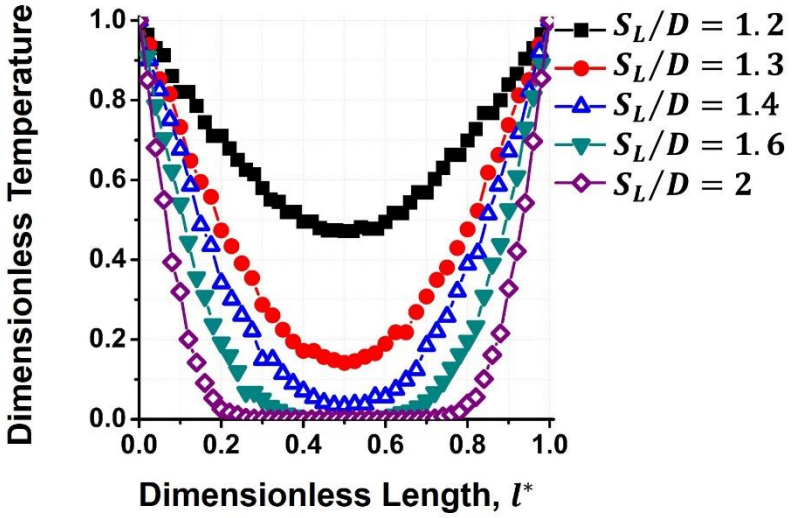

a)

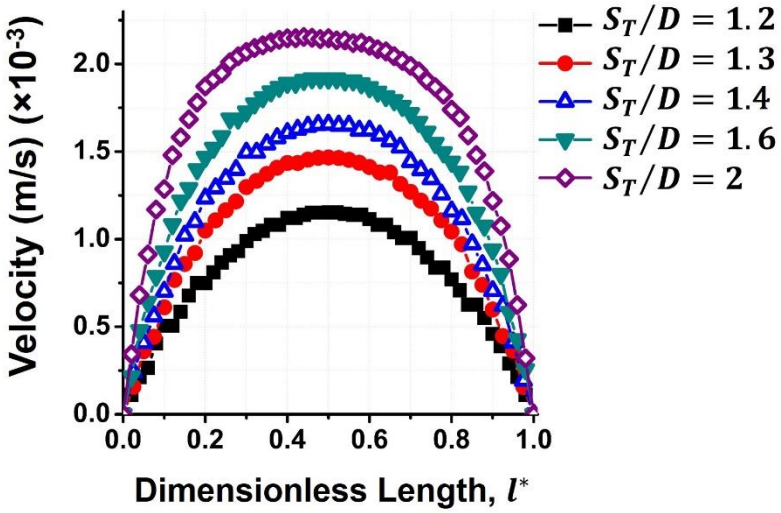

b)

Figure 5-5 a) Dimensionless temperature vs. dimensionless length l*. b) Velocity magnitude vs. dimensionless length for $Ra_D = 10^4$ between cylinders C_1 and C_2 in a row of nine horizontal cylinders for different cylinder spacing, S_T/D=1.2, 1.3, 1.4, 1.6 and 2.

The outer, semi-confined cylinders in a horizontal row behave differently compared to the inner cylinders. As shown in Figure 5-6a, depending on the cylinder spacing (S_T/D) heat transfer for the outer, semi-confined cylinder in the row may be lower or higher

compared to the inner cylinders. For the smallest analyzed spacing of $S_T/D = 1.2$ heat transfer from the outer, semi-confined cylinder is higher compared to the inner cylinders where conduction dominates heat transfer between cylinders. For $S_T/D > 1.2$ heat transfer for the inner cylinders is higher compared to the outer cylinder due to the increase in through-flow velocity and thinner boundary layers, as shown in Figure 5-6a. For the range of Ra_D numbers analyzed in this study, heat transfer is the lowest from the outer cylinders in the row, increases towards the center of the cylinder row, and reaches the maximum value for the center cylinder. For the symmetric boundary conditions, the heat transfer distribution is symmetric with respect to the center cylinder.

In summary, for a finite number of cylinders in a horizontal row of circular cylinders, heat transfer for individual cylinders is not uniform. The degree of non-uniformity depends on the cylinder spacing and Rayleigh number. A general solution for an infinite number of horizontal cylinders may be obtained by neglecting heat transfer from the outer, semi-confined cylinders. The heat transfer enhancement, HTE, for individual cylinders in a row of nine horizontal cylinders is presented in Figure 5-6b for a cylinder spacing of $S_T/D=2$ and values of Rayleigh number $Ra_D = 10^4, 10^5, 10^6$. As the results show, HTE increases with Ra_D number due to higher flow velocities, thinner boundary layers, and longer more slender plumes. The thinner boundary layers reduce interaction between the adjacent cylinders and, therefore the cylinders behave like a free single cylinder at smaller spacings compared to lower Ra_D number. Figure 5-6a also suggests that there is optimum cylinder spacing for each Rayleigh number corresponding to the highest HTE.

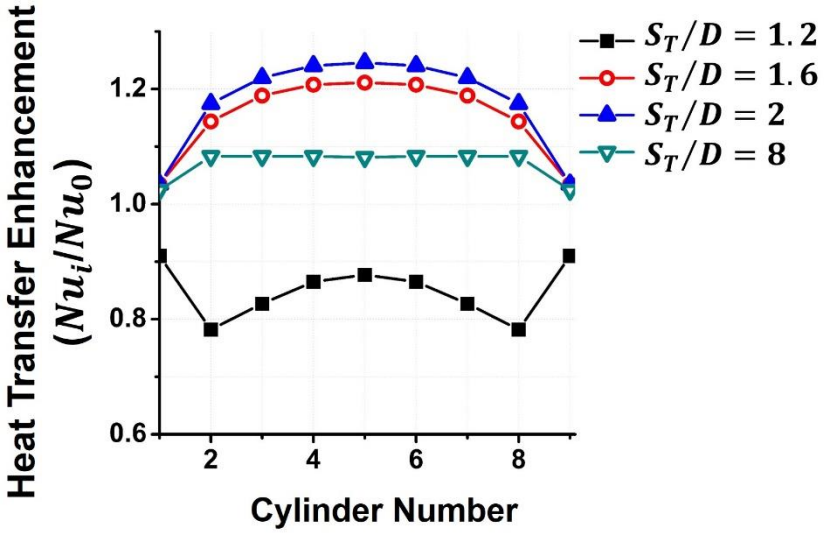

a)

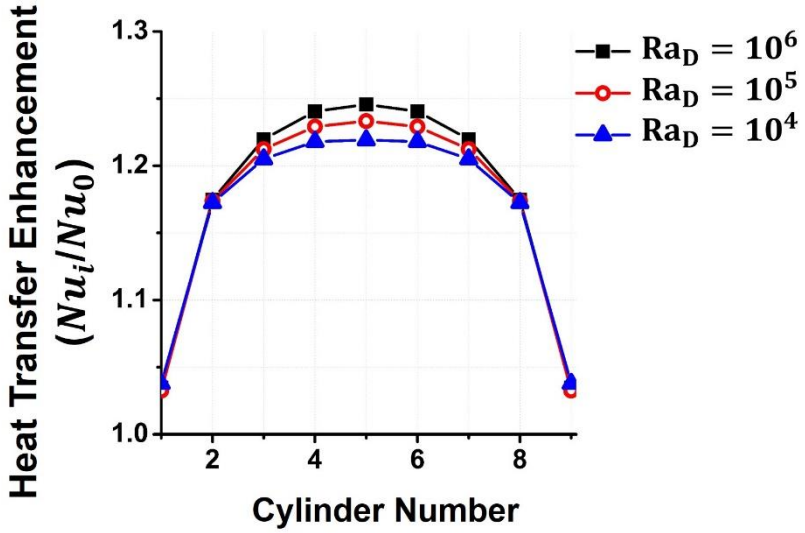

b)

Figure 5-6 Heat transfer enhancement vs. cylinder number in a horizontal row of nine cylinders for a) $Ra_D=10^4$ and cylinder spacing S_T/D of 1.2, 1.4, 1.6, 2 and 8 b) $S_T/D=2$ and three $Ra_D=10^4$, 10^5, 10^6.

The results presented in Figure 5-7 show that despite the different number of cylinders considered in this study and the study by Cianfrini et al [40], the heat transfer enhancement follows the same trend. Due to the suction effect described earlier, heat

transfer from the cylinder(s) located at the middle of the row is highest compared to other cylinders in the row. Also, heat transfer from the side, semi-confined cylinders is the lowest. Figure 5-7, also shows that heat transfer enhancement for the molten salt ($6 < \mathrm{Pr} < 10$) is higher compared to air ($\mathrm{Pr} = 0.7$).

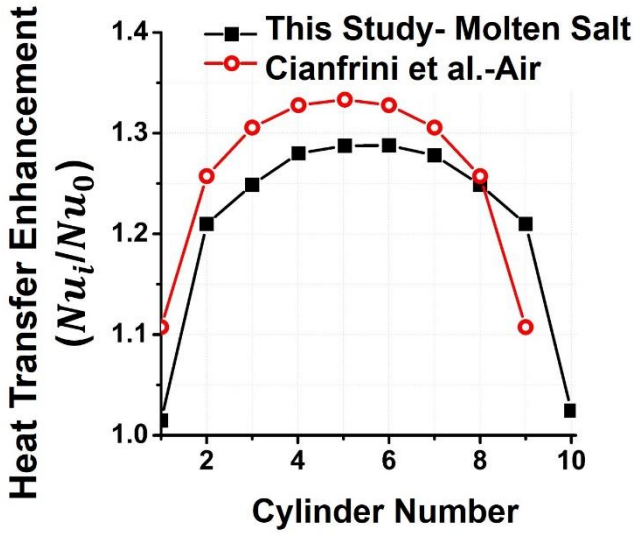

Figure 5-7 Comparison of HTE for individual cylinders in a horizontal row of N cylinders, between this study (N=9) and Cianfrini et al. [75] (N=10) , $\mathrm{Ra_D} = 10^4$ and S_T/D=2.

The effect of the cylinder spacing on HTE for individual cylinders (C_1 to C_5) in a horizontal row of nine cylinders and the average HTE is presented in Figure 5-8 for $\mathrm{Ra_D} = 10^4$ and 10^7. As the results show, HTE depends on the cylinder spacing S_T/D and $\mathrm{Ra_D}$ number. There is an optimum value of the cylinder spacing $(S_T/D)_{opt}$ at which HTE reaches the maximum value which is a weak function of the $\mathrm{Ra_D}$ number; for $\mathrm{Ra_D} = 10^4$ and $(S_T/D)_{opt} = 2$, while for $\mathrm{Ra_D} = 10^7$ $(S_T/D)_{opt} = 1.6$. For spacings larger than optimal, HTE decreases, asymptotically reaching constant value as cylinders get too far apart to affect each other. For spacings smaller than the optimal value, the heat transfer enhancement

decreases due to competing effects of S_T/D on temperature gradient and velocity discussed earlier. Since cylinder C_5 is the outer, semi-confined cylinder, it is affected less by the presence of the adjacent cylinders and shows lower amount of heat transfer enhancement compared to the inner cylinders.

While the optimal value of cylinder spacing is weakly dependent on the Ra_D number, the maximum value of the Nu number increases as Ra_D number is increased. For spacings larger than optimal, Nu number decreases, asymptotically reaching the value corresponding to a single cylinder in an unbounded Boussinesq fluid (free flow) for large spacings since cylinders no longer affect reach other. For spacings smaller than the optimal value, the average Nusselt number decreases because of the competing effects of wall temperature gradient and velocity.

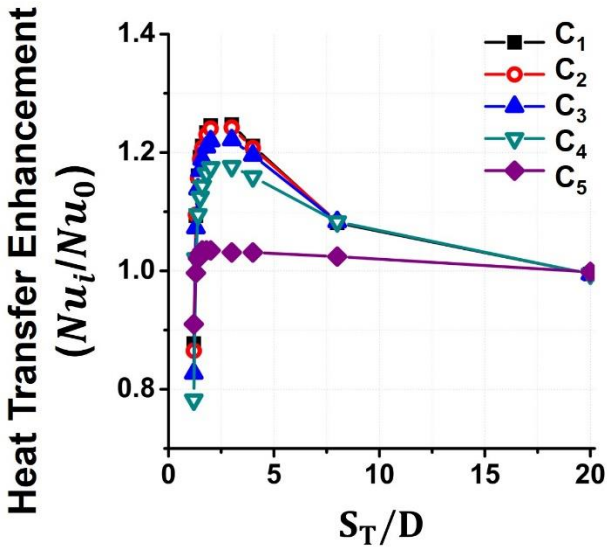

a)

Figure 5-8 Variation of the heat transfer enhancement in a horizontal row of nine cylinders vs. spacing S_T/D for a) $Ra_D = 10^4$, b) $Ra_D = 10^7$.

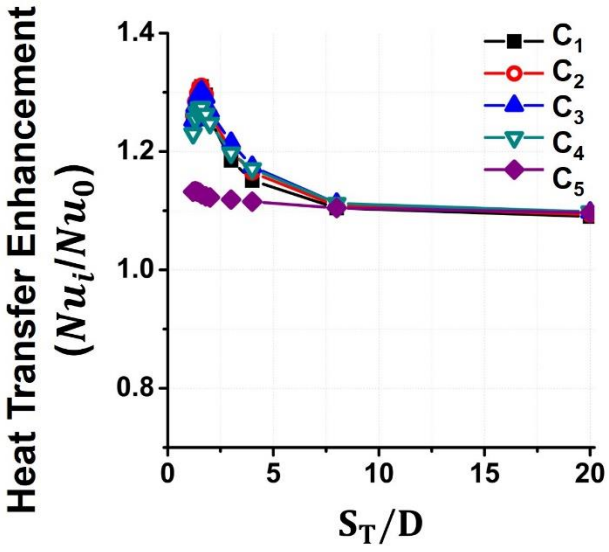

b)

Figure 5-8 cont.

5-4. Correlations for the Natural Convection Heat Transfer and Molten Salt

To improve design of heat exchangers used in TES and other thermal systems for solar and other applications, correlations were developed in this study for heat transfer from a single row of horizontal cylinders immersed in molten solar salt.

Numerical results obtained in this study and statistical regression analysis were used to develop correlations for the average Nusselt number $\overline{Nu}_D$ as functions of the Rayleigh number Ra_D and cylinder spacing S_T/D valid over the range of Ra_D numbers from 10^4 to 10^7 and the S_T/D range from 1.2 to 30.

The proposed form of the correlation for $\overline{Nu}_D$ for a horizontal row of nine circular cylinders immersed in a molten solar salt is given by Eqn. 5-1 as a function of the Ra_D number and parameter A, where A is a function of the cylinder spacing.

$$\overline{Nu}_D = A\, Ra_D^{0.242} \qquad \text{Eqn. 5-1}$$

Where:

$$A = -0.024 \times \ln\left(\frac{S_T}{D}\right) + 0.68 \qquad \text{Eqn. 5-1a}$$

Expressions given by Eqn. 5-1 and Eqn. 5-1a are valid for $1.2 \leq S_T/D \leq 30$ and $10^4 \leq Ra_D \leq 10^7$.

Eqn. 5-1 shows that there is an exponential variation of the average Nusselt number with Ra_D number while its variation with the cylinder spacing is logarithmic.

The average relative error between the correlation and the numerical results is less than 3.77 %. The average relative error is defined as:

$$\text{Error}=\sum\left(\frac{f_{simulation} - f_{correlation}}{f_{simulation}} \times 100\right) \qquad \text{Eqn. 5-2}$$

Eqn. 5-1 and 5-1a, can also be used for predicting heat transfer for a horizontal row of less than nine cylinders with the average relative error of less than 5%.

The generalized form of Eqn. 5-1, given by Eqn. 5-3, applicable to a horizontal row of the infinite number cylinders was obtained by omitting the semi-confined edge cylinders from the regression analysis, leading to Eqn. 5-3a for parameter A_∞.

$$\overline{Nu}_{D,\infty} = A_\infty \, Ra_D^{0.242} \qquad \text{Eqn. 5-3}$$

$$A_\infty = -0.033 \times \ln(\frac{S_T}{D}) + 0.7 \qquad \text{Eqn. 5-3a}$$

Eqn. 5-3 and 5-3a are valid over the same range of Ra_D numbers and cylinder spacings as Eqn. 5-1 and Eqn. 5-1a, with the average relative error less than 3.7%.

As the results presented in Figure 5-9a show, there is a very good agreement between values of the Nusselt number obtained from numerical predictions and correlation Eqn. 5-1; the maximum difference is less than 5%. The difference is the largest for the lowest analyzed Rayleigh number ($Ra_D = 10^4$) and for cylinder spacing $S_T/D \leq 2$. This is because for small Ra_D number and small cylinder spacing conduction is dominant mode of heat transfer between cylinders. As Ra_D number and cylinder spacing increase, heat transfer by convection becomes dominant. If needed for design purposes, the more accurate correlations could be developed by dividing numerical solutions into the conduction-dominated and convection-dominated regions.

Variation of parameters A and A_∞ with cylinder spacing is presented in Figure 5-9b. The results show that values of both parameters decrease monotonically with S_T/D and, for large values of cylinder spacing, asymptotically approach constant values: $A \rightarrow 0.55$, $A_\infty \rightarrow 0.53$. This is because for large spacings, cylinders no longer affect each other and, as discussed earlier, behave as isolated cylinders in a free flow.

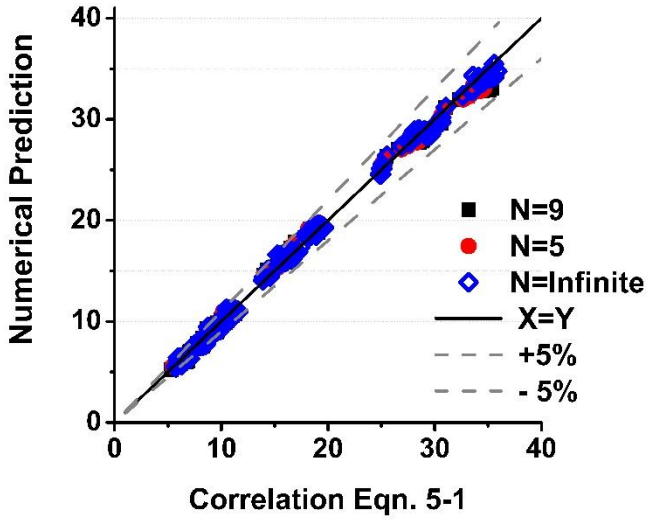

a)

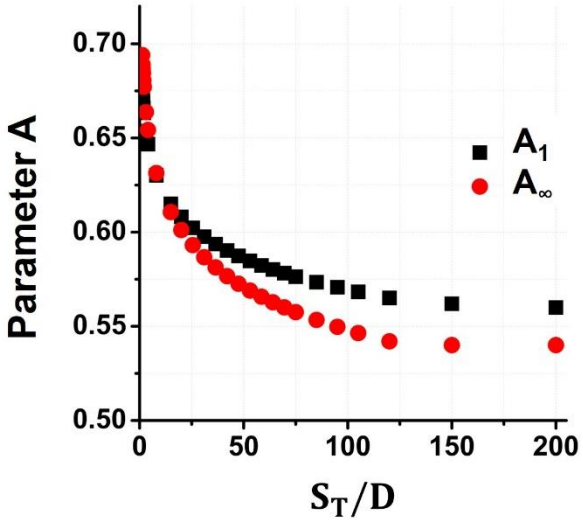

b)

Figure 5-9 a)Average Nusselt number comparison between numerical predictions vs. correlation (Eqn. 5-1) b) Variation of parameters A and A_∞ vs. cylinder spacing (S_T/D).

The maximum average Nusselt number $\overline{Nu}_{D,opt}$ and optimal cylinder spacing $(S_T/D)_{opt}$ for a horizontal row comprising nine to five cylinders are shown in Figure 5-10 as functions of the Ra_D number. As Figure 5-10a shows, the maximum value of the average Nusselt number at optimal cylinder spacing, $\overline{Nu}_{D,opt}$ increases exponentially as Ra_D

number is increased. For the Ra_D number in the $10^4 \leq Ra_D \leq 10^7$ range, $\overline{Nu}_{D,opt}$ may be determined from Eqn. 5-4.

$$\overline{Nu}_{D,opt} = 0.75\, Ra_D^{0.236} \qquad \text{Eqn. 5-4}$$

The results for the optimal cylinder spacing presented in Figure 5-10b show that for the Ra_D number range from 10^4 to 10^5 the value of optimal spacing is constant and equal to 2, i.e., $(S_T/D)_{opt}$ =2. For the Ra_D number values in the $10^5 \leq Ra_D \leq 10^7$ range the optimal spacing decreases with the Ra number and may be determined from Eqn. 5-5.

$$(S_T/D)_{opt} = 3.55\, Ra_D^{-0.05} \qquad \text{Eqn. 5-5}$$

For the Ra_D number in the $10^4 \leq Ra_D \leq 10^7$ range the value of dimensionless maximum heat transfer volumetric density $\tilde{q}_{max}$ for a horizontal row of nine to five cylinders may be determined from Eqn. 5-6.

$$\tilde{q}_{max} = 1.54\, Ra_D^{0.26} \qquad \text{Eqn. 5-6}$$

The expression for $\tilde{q}_{max}$ represented by Eqn. 5-6 determined in this study is in a reasonable agreement with Eqn. 5-7 developed from the dimensional analysis for a cylinder in a laminar natural convection flow and $Pr > 1$ proposed by Bello-Ochende and Bejan [59] where dimensionless volumetric heat transfer density is proportional to the $Ra_D^{0.25}$.

$$\tilde{q} \sim \frac{q' D^2}{k(T_w - T_0)} \sim Ra_D^{0.25} \qquad \text{Eqn. 5-7}$$

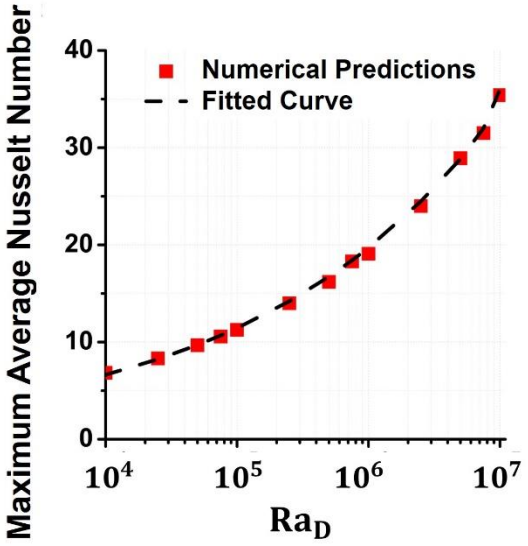

a)

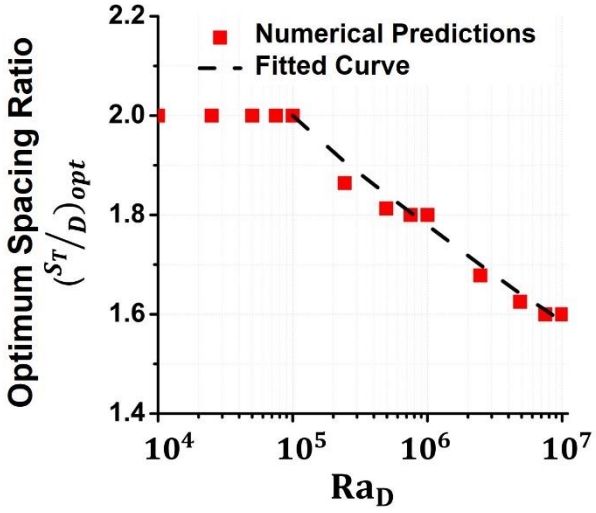

b)

Figure 5-10 Single horizontal row of nine cylinders: a) Maximum average Nusselt number vs. Ra_D number, b) Optimal cylinder spacing vs. Ra_D number.

Table 5-2 shows a comparison between Eqn. 3-24 and 3-25 proposed by Bello-Ochende and Bejan [59] and Eqn. 5-5 and Eqn. 5-6, from this study. As shown in Table 5-2, equations proposed by the Bello-Ochende and Bejan [59] for natural convection from air significantly under-predict values of the optimal spacing and maximum dimensionless

volumetric heat transfer density for natural convection from molten salt. This disagreement is likely due to different optimization criteria: minimum heat exchanger volume vs. maximum volumetric heat storage used in these studies.

Table 5-2 Comparison between Eqn. 3-24 and Eqn. 3-25proposed by Bello-Ochende and Bejan [59] and Eqn. 5-5 and Eqn. 5-6 from this study.

Ra	Ref. [59]	This Study		Ref. [59]	This Study	
	Eqn. 3-24	Eqn. 5-5	%Difference	Eqn. 3-25	Eqn. 5-6	%Difference
	$(S_T/D)_{opt}$			$\tilde{q}_{max}$		
10^4	1.17	2.3	48.96	10.30	16.73	34
10^5	1.10	1.99	44.48	20.55	30.38	32.35

As shown in the previous figures and by the form of correlations developed in this study, an increase in the Ra_D number results in an increase in the value of average $\overline{Nu}_D$ number for the row of horizontal cylinders, and for individual cylinders in the row. The cylinder spacing S_T/D has a complex effect on heat transfer and, depending on the Ra_D number, it may either enhance or degrade it.

Previous studies concerning natural convection heat transfer from a horizontal row of circular cylinders have mainly focused on the temperature and flow patterns, and no correlations were reported in the literature for the average heat transfer rate and heat transfer enhancement for this geometry valid for any fluid.

The values of Nusselt number predicted by the correlations developed in this study, expressed by Eqn. 5-1 and Eqn. 5-3, are compared to the results by Farouk et al. [74] and

Cianfrini et al. [75] obtained for a horizontal row of cylinders in Figure 5-11, and also to the results by Corcione [56] obtained for a vertical row of cylinders.

The results presented in Figure 5-11 show that for a horizontal row of cylinders, heat transfer enhancement monotonically decreases as cylinder spacing S_T/D is increased.

Figure 5-11 also shows that for the same Ra_D and approximately the same number of cylinders in a horizontal row, heat transfer enhancement from the molten salt with higher Pr number, is in the same range compared to that of air with smaller Pr number, and the difference is less than 10%. Thus, correlations represented by Eqn. 5-1 and Eqn. 5-3 developed in this study for $\overline{Nu}_D$ for a horizontal row of circular cylinders immersed in a molten solar salt, can also be used for predicting heat transfer for a horizontal row of circular cylinders immersed in air, with the average relative error of less than 10%.

Also, as shown in Figure 5-11 due to the different flow behavior, HTE for a vertical column of horizontal cylinders and thus, the results obtained by Corcione [56] follow a completely different trend compared to the horizontal row of cylinders; i.e., HTE increases as cylinder spacing is increased, eventually reaching an asymptotic value. According to Corcione [56] this asymptotic value depends on the Ra_D number and the number of cylinders in the column. The analysis of heat transfer and fluid flow for a vertical column of cylinders and the associated results are presented in CHAPTER 6:.

In summary, correlations developed for different heat storage media and cylinder (tube) orientation in the heat exchanger cannot be used as a general solution without introducing considerable errors. Correlations represented by Eqn. 5-1 and Eqn. 5-3 were

developed in this study to provide accurate information on heat transfer and optimal cylinder (tube) spacing in a single row heat exchanger immersed in solar salt.

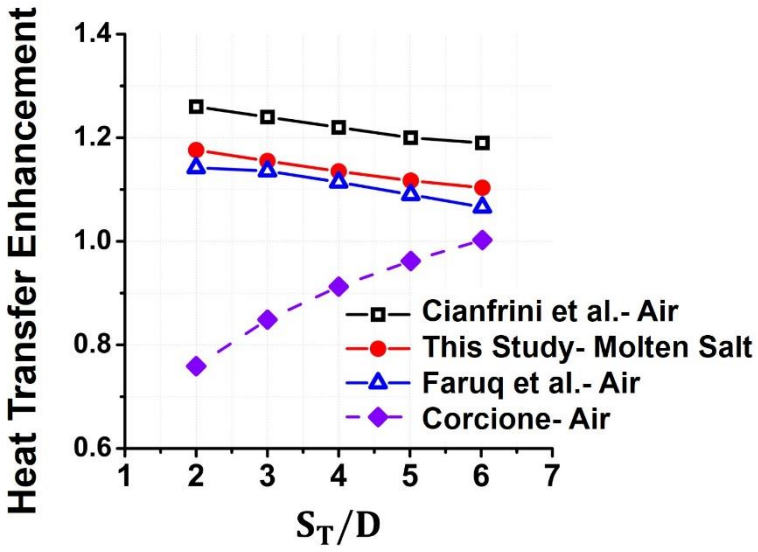

Figure 5-11 Comparison of HTE vs. S_T/D for a horizontal row of N cylinders and $Ra_D = 10^5$, between the Eqn. 5-1 from this study (N=9, Molten Salt), Cianfrini [75] (N=10, Air), Farouk et al. [74] (N=∞, Air) and the average HTE for a vertical column of nine cylinders from the correlation proposed by Corcione [56].

The literature review of the experimental and numerical studies concerning the steady-state natural convection heat transfer from a vertical column of horizontal cylinders, physical model, a detailed analysis of the temperature and velocity distributions around the cylinders, and statistical regression analysis of the numerical results are presented and discussed in the next chapter.

CHAPTER 6: ONE VERTICAL COLUMN OF HORIZONTAL CYLINDERS

6-1. Overview

Laminar natural convection from a vertical column of multiple horizontal cylinders has been investigated in studies [56, 77-81]. The results of these studies show that heat transfer from the bottom cylinder in the column is not affected by the presence of the downstream cylinders; its Nusselt number is identical to that for a single cylinder and is unaffected by the cylinder spacing. In contrast, the upper (downstream) cylinders in the column exhibit complex heat transfer behavior affected by the longitudinal cylinder spacing S_L, i.e., by dimensionless ratio S_L/D, with small spacing resulting in lower heat transfer and vice versa [56]. Most of the studies investigated heat transfer from the horizontal cylinders immersed in air or water.

Correlations, based on experimental results, concerning heat transfer from a vertical column of circular cylinders in air have been proposed by Ashjaee and Yousefi [81]. The correlations are given in terms of the Ra number, cylinder spacing, and number of cylinders in the column for the steady-state free laminar convection heat transfer. Tokura et al. [82] investigated free convection heat transfer from a vertical column of circular cylinders immersed in air in a free (unconfined) flow and flow confined between parallel walls. The study concluded that flow confinement has a significant effect on flow and heat transfer since for the confined column the average Nusselt number was 10 to 15% higher compared to the unconfined column. Also, in the confined flow, the heat transfer for the first (bottom) cylinder in the column was significantly higher compared to the unconfined column.

The effect of the number of the cylinders in a confined column of circular cylinders, cylinder spacing, distance between the walls, and Rayleigh number on heat transfer in air for the steady-state laminar flow was investigated by Hannani et al. [83]. They concluded that the average heat transfer from the vertical column reaches the maximum value at the optimal distance between the confining walls.

Kitamura et al. [60] performed experimental study of natural convection heat transfer from a column of ten horizontal cylinders in air. He compared both the laminar and turbulent transition flow behavior and proposed a number of correlations for heat transfer.

Numerical simulation of the steady-state laminar natural convection from a vertical column of horizontal circular cylinders was performed in this study to determine the effect of Ra number and dimensionless longitudinal cylinder spacing S_L/D on heat transfer and optimize column geometry. Optimization of geometry to maximize heat transfer from a vertical column of horizontal cylinders submerged in molten salt is time consuming and has not been adequately studied. The results were used to develop correlations for the average Nusselt number for the entire cylinder column and for the individual cylinders in the column in terms of the Rayleigh number Ra and dimensionless spacing S_L/D.

6-2. Physical Model

Figure 6-1 is the schematic of a single-tank thermal energy storage system proposed by Lu et al. [55] employing a number of vertically-aligned cylinders as a HXE. The computational domain (ABDC) is presented in Figure 6-2a. The HXE geometry analyzed in this study comprises one vertical column of two to ten circular cylinders immersed into

the thermal energy storage fluid (see Figure 6-2b). Due to the symmetry along the A-C line and to reduce computational effort, the analysis was performed for the right half of the domain.

Numerical simulations were performed for a range of the longitudinal cylinder spacings S_L/D and Rayleigh number Ra_D (based on the cylinder diameter) to determine their effect on heat transfer, average Nusselt $\overline{Nu}_{D,N}$ number for the entire column, and $\overline{Nu}_{D,i}$ for individual cylinders in the column. The predictions were obtained for the Rayleigh number range from 10^4 to 10^7. As discussed earlier, the flow regime is laminar for $Ra_D < 10^8$ [51].

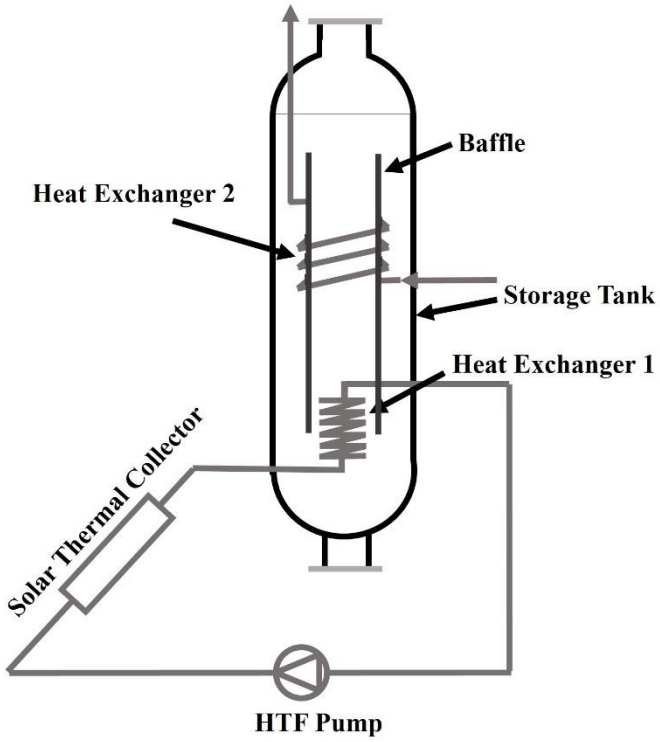

Figure 6-1 Schematic of the TES proposed by Lu et al. [55]

The distance from the right wall to the centerline of the cylinder column was set to 15D to provide a domain-independent solution based on the analysis proposed by Warrington [84].

The external boundaries of the computational domain in the y-direction were located at the distance of 15D for the inlet and 15D for the outlet from the bottom and top cylinder centers respectively, to provide a domain-independent solution. Warrington [84] provides a method for calculating this distance. However, inlet and outlet boundaries used in this study were placed further away than recommended by Warrington [84].

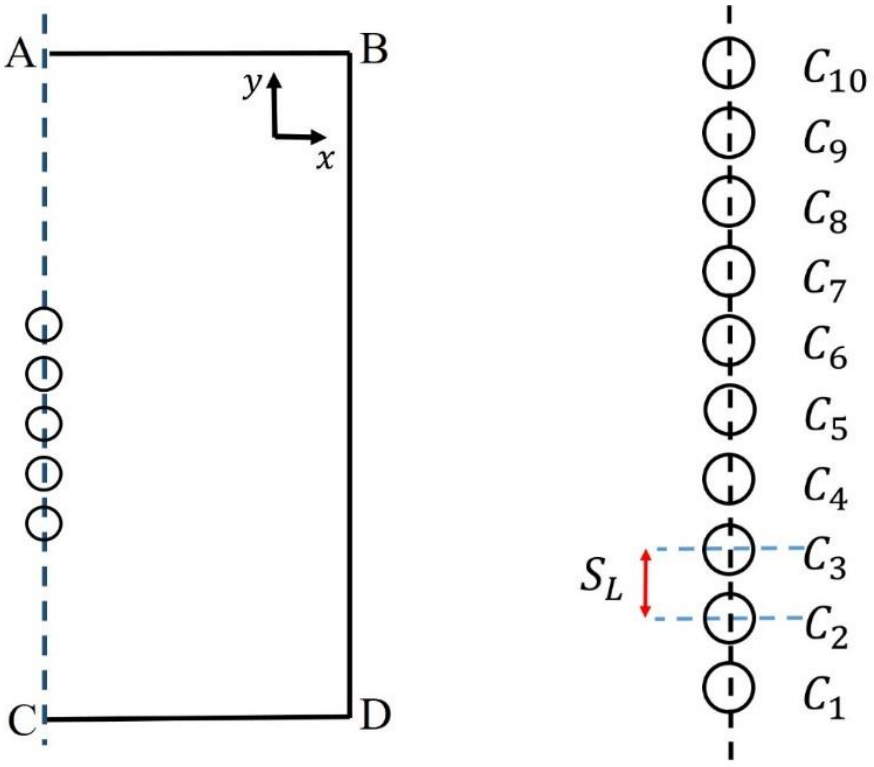

a) b)

Figure 6-2 a) Schematic of computational domain and cylinder arrangement. b) Schematic of the cylinder column with cylinder numbers specified.

6-3. Steady-State Temperature and Velocity Distribution Around Circular Cylinders

The results for the overall flow behavior obtained in this study are similar to the results presented in previous studies [55, 56, 60, 68, 74, 77-83, 85] concerning natural convection heat transfer to air, water and molten slat from a vertical column of a finite number of horizontal cylinders. In a vertical column of horizontal cylinders, presence of the upstream and downstream cylinders can either enhance or degrade heat transfer from the individual cylinder (i^{th} cylinder) relative to a single cylinder in a free flow [77]. The effect depends on flow interactions and temperature gradients in a column.

According to Chouikh et al. [77] for a vertical column of two cylinders in a free flow, the plume from the bottom (upstream) cylinder influences heat transfer from the top (downstream) cylinder in two different ways. First, the warm wake of the bottom cylinder acts as a forced convection field for the top cylinder; second, it lowers the temperature difference between the cylinder's surface and the adjacent fluid. The first effect tends to increase the heat transfer, while the second effect decreases the heat transfer from the downstream cylinder. For small cylinder spacing S_L/D, higher temperature of the wake plays a dominant role and reduces the heat transfer rate from the downstream cylinder(s). On the other hand, for large cylinder spacing S_L/D, the velocity effect becomes dominant and increases the heat transfer rate from the downstream cylinder(s). Therefore, the heat transfer in a column of N horizontal cylinders is influenced by two main factors, cylinder spacing S_L/D and Rayleigh number Ra_D, which is a function of fluid properties, fluid velocity and temperature difference.

The heat transfer enhancement HTE predicted in this study for the first cylinder in a column of ten horizontal cylinders is presented in Figure 6-3a as a function of the cylinder spacing and Rayleigh number. The heat transfer enhancement values of close to one show that heat transfer from the first cylinder in a vertical column of cylinders is virtually identical to that for a single cylinder. The predicted values of HTE are in agreement with the results from previous studies [55, 56, 74, 77, 80, 83] and show that, except for very small cylinder spacings ($S_L/D < 1.8$), the effect of the downstream cylinders on heat transfer from the first cylinder in a column is negligible. For very small cylinder spacings ($S_L/D < 1.8$) temperature gradient around the first cylinder is lowered and formation of a natural convection plume around the cylinder is suppressed, therefore the heat transfer rate from the first cylinder in a column is lower compared to that of a free single cylinder.

The values of the average Nusselt number for the i^{th} cylinder for five vertical columns comprising two, three, five, eight and ten horizontal cylinders and $Ra_D = 10^4$ presented in Figure 6-3b show that the heat transfer enhancement for the i^{th} cylinder is not affected by the number of cylinders in the column. The results obtained in this study are in agreement with the results from the previous studies conducted by Corcione [56] and Lu et al. [55], showing that for a vertical column of N number of cylinders in a free flow the heat transfer for the i^{th} cylinder is only affected by interactions with the upstream cylinders; the downstream cylinders have no effect on the i^{th} cylinder.

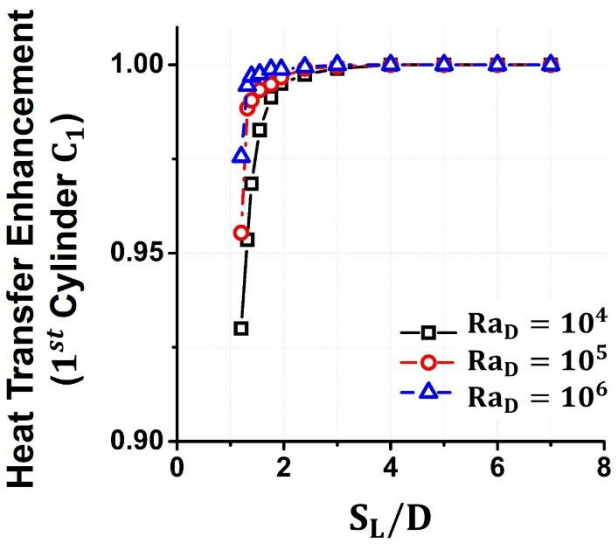

a)

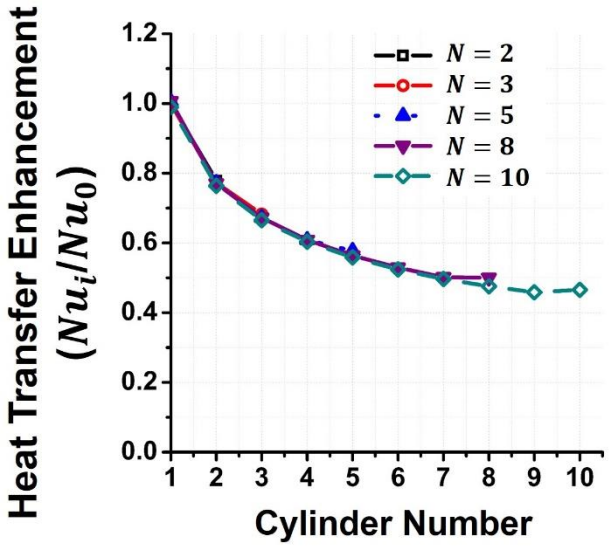

b)

Figure 6-3 a) Heat transfer enhancement for the first cylinder in a vertical column of ten horizontal cylinders vs. cylinder spacing S_L/D. b) Heat transfer enhancement for the i^{th} cylinder from five different geometries of one vertical column of N (N=2, 3, 5, 8, 10) horizontal cylinders for the cylinder spacing (S_L/D=2) and $Ra_D = 10^4$.

The velocity (buoyancy) effect on heat transfer from individual cylinders varies with the location of the cylinder in the column, i.e., the number of the upstream cylinders. As shown in Figure 6-4a, for a constant number of cylinders in the column, HTE for the

bottom (first cylinder) in the column is virtually unaffected by the cylinder spacing S_L/D, except for very small spacings. However, for the downstream cylinders HTE and the average Nusselt number $\overline{Nu}_D$ increase as S_L/D is increased, reaching highest values for the second cylinder before decreasing for the cylinders further downstream. The results indicate that for a large value of S_L/D, heat transfer enhancement for all cylinders is asymptotically approaching constant value, and also confirm existence of the critical spacing $(S_L/D)_{cr}$ where HTE = 1 suggested by Lu et al. [55]. The heat transfer rate from the vertical column decreases for the cylinder spacings S_L/D smaller than the critical spacing, while for the cylinder spacings larger than the critical value, heat transfer is higher compared to a single cylinder [56] and increases with the cylinder spacing.

The results presented in Figure 6-4b for the second cylinder in the column and low Ra_D number (10^4) show that the increase in heat transfer enhancement begins for $S_L/D \geq 4$ (i.e., $(S_L/D)_{cr} = 4$), while for the high Ra_D number (10^7), $(S_L/D)_{cr} = 2.7$, i.e., heat transfer enhancement begins at lower spacing, showing the critical spacing is a function of the Ra_D number. Also, for a constant spacing, an increase in the Ra_D number results in higher HTE and higher heat transfer due to stronger buoyancy force acting on the fluid and, consequently, higher flow velocities, thinner boundary layers, and reduced flow separation. However, as the Rayleigh number and buoyancy force increase, the effect of cylinder spacing diminishes [74].

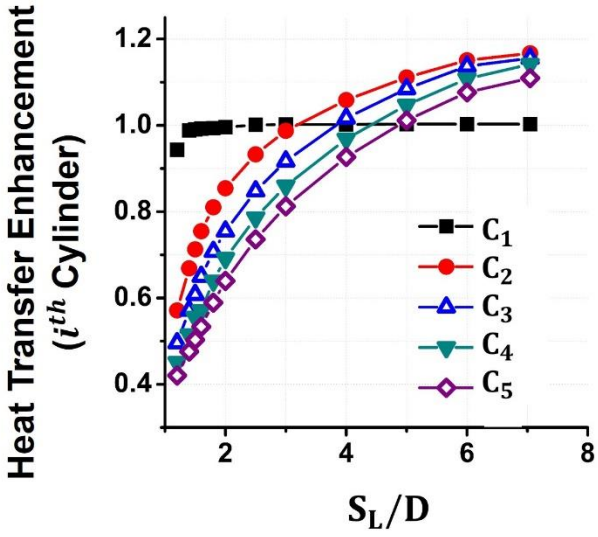

a)

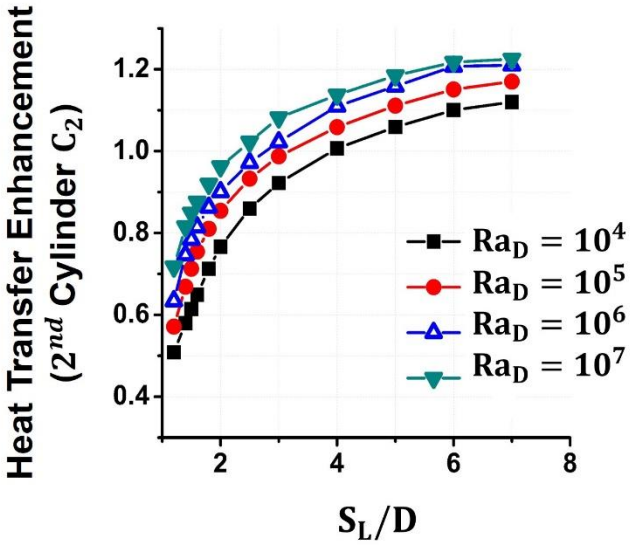

b)

Figure 6-4 Heat transfer enhancement vs. S_L/Da) The first and four downstream cylinders in a vertical column of five horizontal cylinders and $Ra_D = 10^5$. b) The second cylinder in a vertical column of horizontal cylinders for different Ra_D numbers.

The patterns of heat transfer enhancement or degradation for individual cylinders in a vertical column of ten horizontal cylinders are presented in Figure 6-5 as functions of cylinder spacing ($1.2 \leq S_L/D \leq 7$) and values of Rayleigh number Ra_D of 10^4 and 10^6. Similar to the five-cylinder column, the results for the ten-cylinder column show that heat

transfer from the downstream cylinders is highly sensitive to the cylinder spacing and less sensitive to the Ra_D number. For cylinder spacings $S_L/D \leq 3$ and $Ra_D = 10^4$ heat transfer is degraded (HTE < 1) compared to a single cylinder in a free flow. The value of HTE decreases for cylinders further downstream. For $S_L/D > 3$ HTE reaches maximum value for the 2nd cylinder, then continues to decrease monotonically for the cylinders further downstream.

The HTE trend with cylinder spacing and its position in the column remains virtually identical for higher Ra_D numbers as shown in Figure 6-5b for $Ra_D = 10^6$, except degradation in heat transfer enhancement occurs at smaller spacings ($S_L/D \leq 2$ for $Ra_D = 10^6$). For all Ra_D numbers heat transfer degradation is higher for cylinders located further downstream in the column. Also, for the small analyzed spacings ($S_L/D = 1.2$ and 1.6), heat transfer for the top cylinder in the column (cylinder 10) is higher compared to the three upstream cylinders. These trends can be explained by taking a closer look at the velocity and temperature contours presented in Figure 6-6.

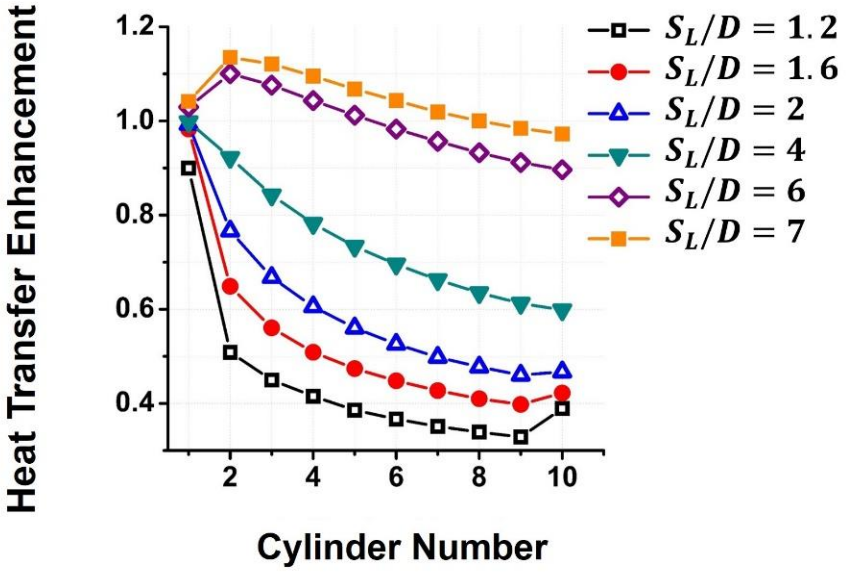

a) $Ra_D = 10^4$

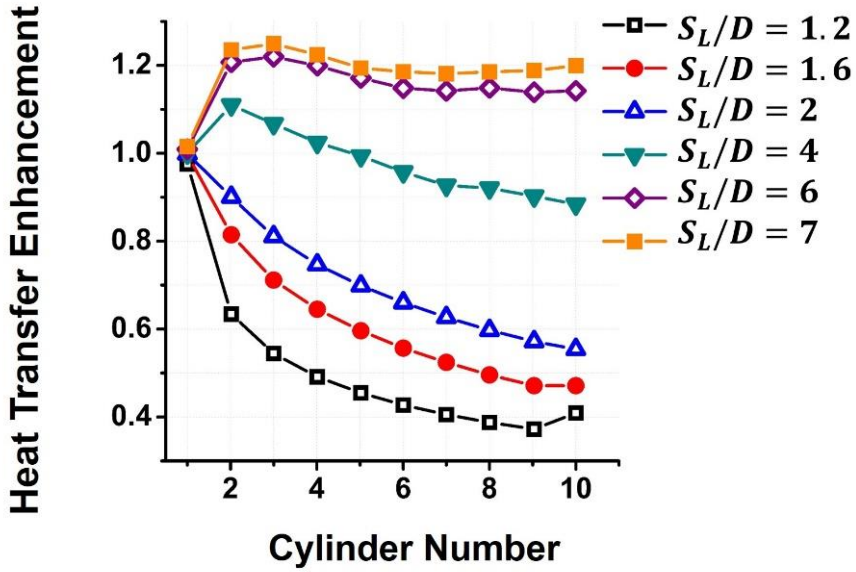

b) $Ra_D = 10^6$

Figure 6-5 Variation of the heat transfer enhancement HTE in a vertical column of ten horizontal cylinders vs. cylinder spacing S_L/D for a) $Ra_D = 10^4$, b) $Ra_D = 10^6$.

The velocity and dimensionless temperature contours presented in Figure 6-6 for cylinder spacings of S_L/D = 1.4 and 3 show that for small spacing between any two

downstream cylinders in the column, stagnation regions form between the cylinders since the flow passage between adjacent cylinders is too narrow for flow to fully penetrate the passage, as shown in Figure 6-6a.

The details concerning flow velocity and dimensionless temperature for the last two cylinders in the column are presented in Figure 6-6 and Figure 6-7 for cylinder spacings of S_L/D = 1.4 and 3. As shown in Figure 6-6a and Figure 6-7a, for small cylinder spacing (S_L/D = 1.4), temperature gradient between the cylinders is decreased due to interference of the thermal boundary layers and the bulk fluid flow, leading to a decrease in heat transfer. Also, as cylinders get closer, the presence of the top cylinder restricts development of the thermal boundary layer. Comparison of flow velocities between two cylinders for S_L/D = 1.4 and 3 given in Figure 6-6b and Figure 6-7b shows stagnation zone for S_L/D = 1.4 where flow velocity is zero. As explained earlier, this stagnation zone forms because the flow passage between adjacent cylinders is too narrow for flow to fully penetrate the passage.

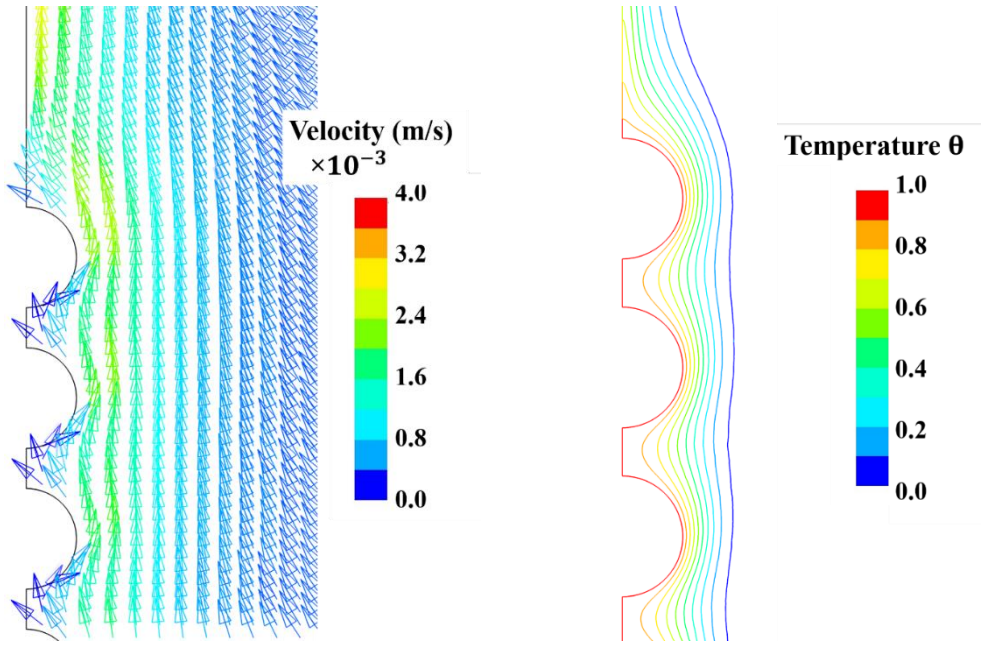

a) $S_L/D=2$

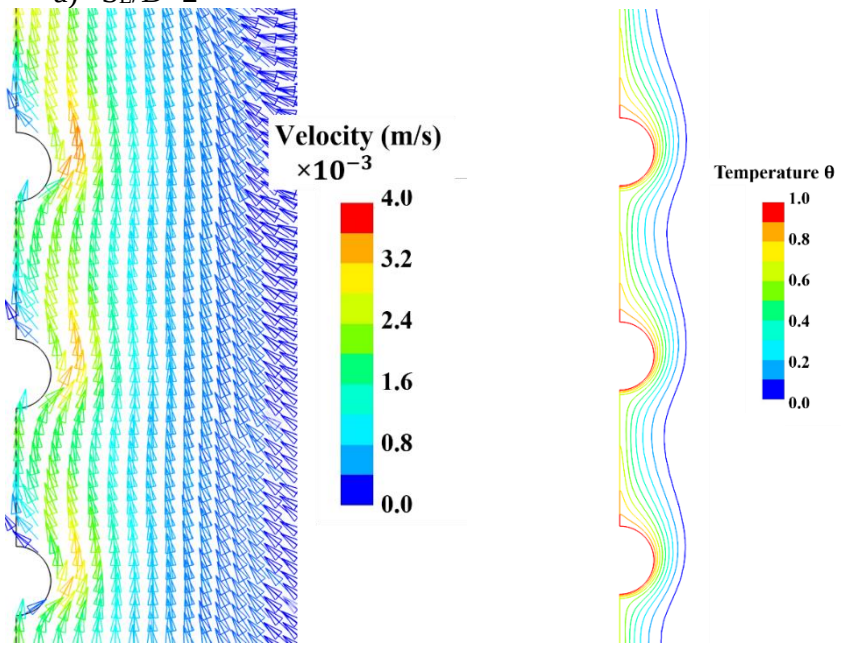

b) $S_L/D=3$

Figure 6-6 Velocity and dimensionless temperature contours for a vertical column of ten horizontal cylinders for $Ra_D = 10^4$ for two different cylinder spacings, S_L/D= 1.4 and 3.

For the top cylinder in the column due to the absence of the downstream cylinders or other flow obstacles, formation of a natural convection plume is unobstructed, increasing flow velocities at the top of the cylinder. Therefore, depending on the cylinder spacing and

Ra_D number, heat transfer from the top cylinder may increase compared to the last upstream cylinder as shown in Figure 6-5. However, as cylinder spacing S_L/D increases, the flow passage between the cylinders becomes wider establishing the full flow penetration (Figure 6-7b) and increasing temperature gradient between the cylinders as presented in Figure 6-7a, thus increasing heat transfer as shown in Figure 6-5.

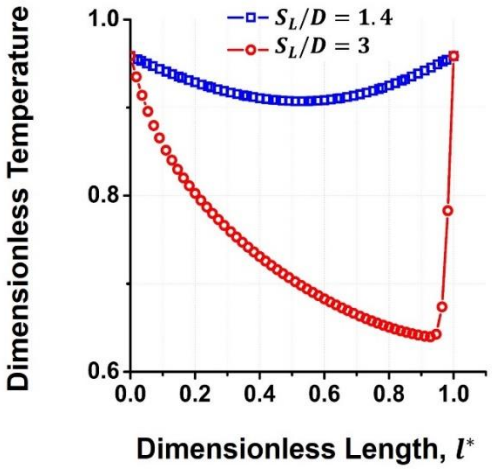

a)

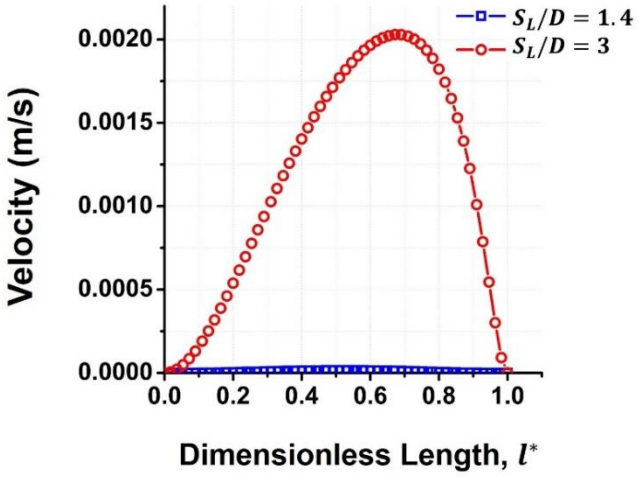

b)

Figure 6-7 a) Dimensionless temperature vs. dimensionless lengthl*. b) Velocity magnitude vs. dimensionless length l* between the last two cylinders in a vertical column of ten horizontal cylinders for $Ra_D = 10^4$ and cylinder spacing, S_T/D=1.4 and 3.

Variation of the heat transfer enhancement, HTE, and the average Nusselt number for a column of ten horizontal cylinders is shown in Figure 6-8 over a wide range of cylinder spacings ($1.2 \leq S_L/D \leq 7$)) and Rayleigh numbers ($10^4 \leq Ra_D \leq 10^7$). The results show that as the cylinder spacing increases the effect of temperature gradient decreases, thus heat transfer enhancement rate decreases and eventually approaches asymptotic value which varies with the Rayleigh number and the number of cylinders in a column. Also, as shown in Figure 6-8, the effect of the Rayleigh number on average Nusselt number and, thus on heat transfer enhancement is exponential.

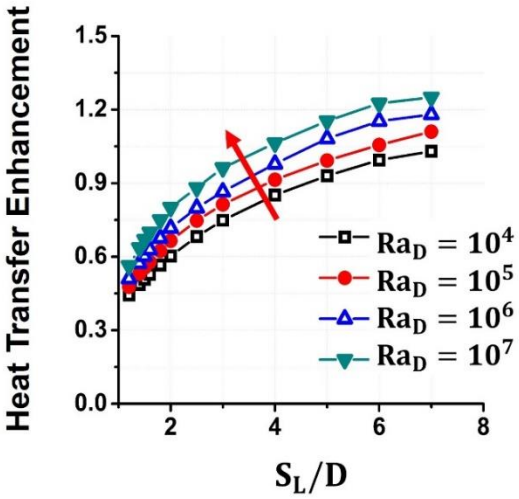

a)

Figure 6-8 Variation of the a) heat transfer enhancement vs. cylinder spacing(S_L/D) and b) Average Nusselt number vs. Rayleigh number (Ra_D) for one column of ten horizontal cylinders.

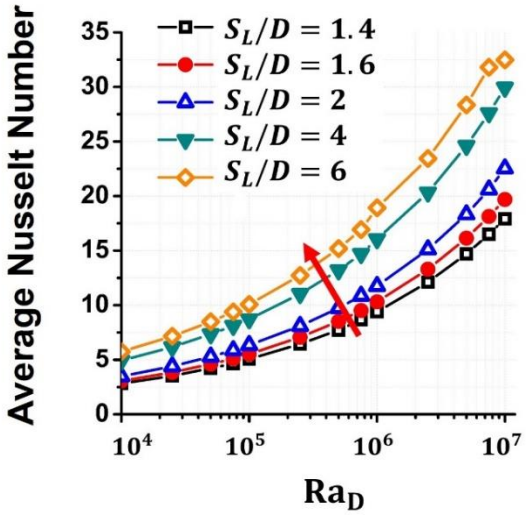

b)

Figure 6-8 cont.

6-4. Correlations for the Natural Convection Heat Transfer and Molten Salt

Numerical results obtained in this study show that the natural convection heat transfer for a vertical column of horizontal circular cylinders immersed in a molten solar salt depends on the Rayleigh number and cylinder-to-cylinder spacing S_L/D . The statistical regression analysis was used to correlate the average Nusselt number $\overline{Nu}_{D,N}$ for the entire column of N cylinders and the peripherally-averaged value of Nusselt number $\overline{Nu}_{D,i}$ for individual cylinders in the column as functions of the Rayleigh number Ra_D and cylinder spacing S_L/D over the range of Ra_D numbers from10^4 to 10^7 and the S_L/D range from 1.2 to 30.

The proposed form of the correlation for $\overline{Nu}_D$ for a vertical column of ten horizontal circular cylinders immersed in a molten solar salt is given by Eqn. 6-1 as a function of the Ra_D number and parameter A, where parameter A is a function of the cylinder spacing.

$$\overline{Nu}_{D,10} = A\, Ra_D^{0.267} \qquad \text{Eqn. 6-1}$$

Where:

$$A = 0.154 \times \ln\left(\frac{S_L}{D}\right) + 0.186 \qquad \text{Eqn. 6-1a}$$

Expressions given by Eqn. 6-1 and 6-1a are valid for $1.2 \leq S_L/D \leq 10$ and $10^4 \leq Ra_D \leq 10^7$.

The correlation shows there is an exponential variation of the average Nusselt number with the Rayleigh number while the variation with the cylinder spacing is logarithmic. The correlation given by Eqn. 6-1 is valid for a vertical column of ten circular cylinders. A more general form of Eqn. 6-1 valid for $2 \leq N \leq 10$ cylinders represented by Eqn. 6-2 was developed to provide predictions for $\overline{Nu}_{D,N}$ for columns with varying number of cylinders.

$$\overline{Nu}_{D,N} = A_N\, Ra_D^{0.26} \qquad \text{Eqn. 6-2}$$

$$A_N = 0.2 \times \ln\left[\left(\frac{S_L}{D}\right)^{0.7} \times (N - 0.96)^{-0.2}\right] + 0.32 \qquad \text{Eqn. 6-2a}$$

Eqn. 6-2 and 6-2a are valid over the same range of Ra_D numbers and cylinder spacings as Eqn. 6-1 and 6-1a. The average relative error is less than 4.0%.

Correlations represented by Eqn. 6-1 and 6-2 are valid for the average $\overline{Nu}_D$ number for the entire column of cylinders. A correlation for the peripherally-averaged value of the Nusselt number $\overline{Nu}_{D,i}$ for individual cylinders in the column was also developed. Correlation for the i^{th} cylinder in the column is given by Eqn. 6-3 in terms of the Rayleigh number, cylinder spacing (S_L/D) and cylinder number N_i.

$$\overline{Nu}_{D,i} = C_i \, Ra_D^{0.26} \qquad \text{Eqn. 6-3}$$

$$C_i = 0.24 \times \ln[(\frac{S_T}{D})^{0.75} \times (0.9 \times N_i)^{-0.32}] + 0.3 \qquad \text{Eqn. 6-3a}$$

The expressions given by Eqn. 6-3 and Eqn. 6-3a are valid for $1.2 \leq S_L/D \leq 10$, $2 \leq N \leq 10$, and $10^4 \leq Ra_D \leq 10^7$. The average relative error between the proposed correlation and the numerical results is less than 5.0%.

To increase prediction accuracy, an alternate form of the correlation was developed for individual cylinders in the column where the average Nusselt number for the i^{th} cylinder was correlated as a function of the Rayleigh number Ra_D and cylinder spacing S_L/D (Eqn. 6-4). However, instead of using a single correlation (such as Eqn. 6-3a) to determine values of parameters A_i and B_i appearing in Eqn. 6-4, these parameters were determined from two correlations represented by Eqn. 6-4a and Eqn. 6-4b where parameter A_i is a logarithmic function of the cylinder spacing (S_L/D) and parameter B_i is a power function of the spacing.

The values of constants, C_i, D_i, E_i and F_i appearing in expressions for parameters A_i and B_i were determined for individual cylinders in the column and tabulated in Table 6-1. As the results show, except for cylinder 3, the alternate approach significantly improves prediction accuracy for individual cylinders. The downside of the alternate approach is the increase in computational effort needed to determine values of parameters A_i and B_i for individual cylinders.

$$\overline{Nu}_{D,i} = A_i \, Ra_D^{B_i} \qquad \text{Eqn. 6-4}$$

$$A_i = C_i \ln (S_L/D) + D_i \qquad \text{Eqn. 6-4a}$$

$$B_i = E_i (S_L/D)^{F_i} \qquad \text{Eqn. 6-4b}$$

Equations Eqn. 6-4, Eqn. 6-4a and b are valid for $1.2 \leq S_L/D \leq 10$, $2 \leq i \leq 10$ and $10^4 \leq Ra_D \leq 10^7$.

Table 6-1 Parameters C_i to F_i and the average relative error for individual i^{th} cylinder in the vertical column of ten cylinders.

Cylinder number i	C_i	D_i	E_i	F_i	Relative Error %
2	0.2744	0.1844	0.2836	-0.084	1.9
3	0.2709	0.1305	0.2866	-0.074	4.4
4	0.2571	0.1062	0.2874	-0.07	0.92
5	0.2416	0.0931	0.2877	-0.062	1.16
6	0.2149	0.0926	0.2851	-0.044	1.22
7	0.1872	0.0972	0.2823	-0.022	1.27
8	0.1781	0.0902	0.281	-0.012	1.43
9	0.168	0.09	0.28	0	1.66
10	0.1096	0.1489	0.2604	0.055	1.54

Figure 6-9a shows an excellent agreement between the results for the total average Nusselt number for a vertical column of ten cylinders obtained by the numerical analysis and correlation given by Eqn. 6-1.

Figure 6-9b shows variation of the correlation parameter A for the total average Nusselt number for a vertical column of ten cylinders (Eqn. 6-1a) and parameter A_i (Eqn. 6-4a) for two randomly selected cylinders (C_2 and C_6) with cylinder spacing (S_L/D). The results show that the parameter A_i monotonically increases asymptotically approaching a constant value as cylinder spacing is increased and cylinders move further away from each other.

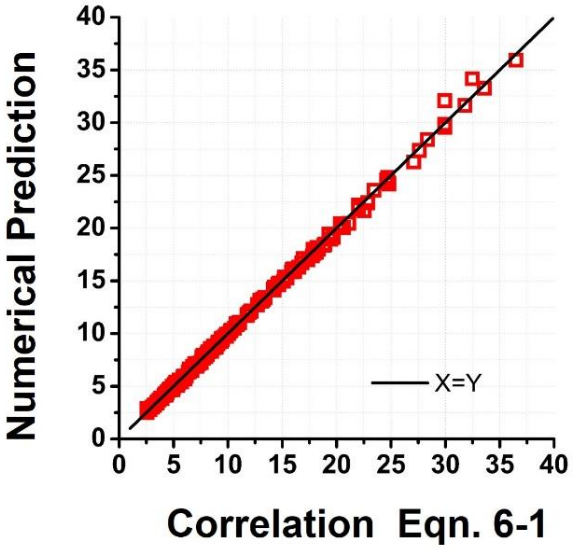

a)

Figure 6-9 a) Predicted values of average Nusselt number vs. values obtained from correlation represented by Eqn. 6-1, b) Variation of the parameter A (Eqn. 6-1a) and parameter A_i (Eqn. 6-4a) vs. cylinder spacing (S_L/D).

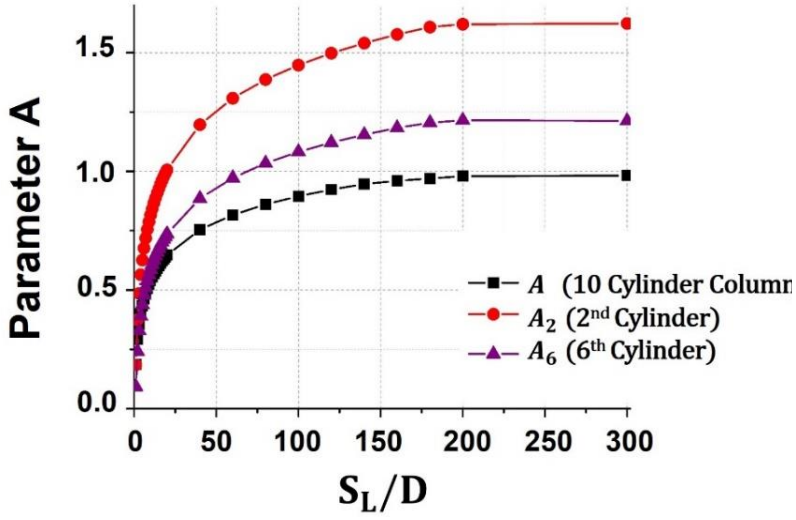

b)

Figure 6-9 cont.

A number of numerical and experimental studies of natural convection heat transfer and fluid flow in a vertical column of N horizontal cylinders have been performed [55, 56, 60, 64, 77, 78, 80, 81, 83, 85] by other authors. The majority of these studies were focused on heat transfer in air and water. However, molten salt, one of the most popular fluids for heat storage systems has not been adequately studied. The Nusselt number predictions obtained by the correlations developed in this work (Eqn. 6-2 and Eqn. 6-3) for molten salt, were compared to the predictions obtained from the experimentally developed correlations proposed by Corcione [56], Lu et al. [55] and Kitamura et al. [60] (Eqn. 3-27 to Eqn. 3-30) for a vertical column of N=2 to 10 cylinders immersed in air.

The results for the first, second, and sixth cylinder in the column are compared in Figure 6-10 and Figure 6-11a. Figure 6-10a shows that the values of $\overline{\mathrm{Nu}}_{\mathrm{D},1}$ obtained numerically in this study for the first cylinder in a column of ten circular cylinders

immersed in molten solar salt are in the excellent agreement with the results obtained from Eqn. 3-28 proposed by Lu [55]; the average relative error is 1.2%.

The results for the second cylinder in a column of N circular cylinders immersed in molten salt obtained in this study (Eqn. 6-3) and reported by Lu et al. [55] and Corcione [56] are presented in Figure 6-10b. As discussed in Section 4-4, the average difference of 10% between the results obtained in this study and those reported by Lu et al. [55] may be explained by the difference in values of Pr number used in the analysis and uncertainty of ±5% associated with Lu's correlation. Figure 6-10b also shows that correlation proposed by Corcione [56] given by Eqn. 3-27 under-predicts the average value of Nusselt number for the second cylinder in the column by 20 to 40%.

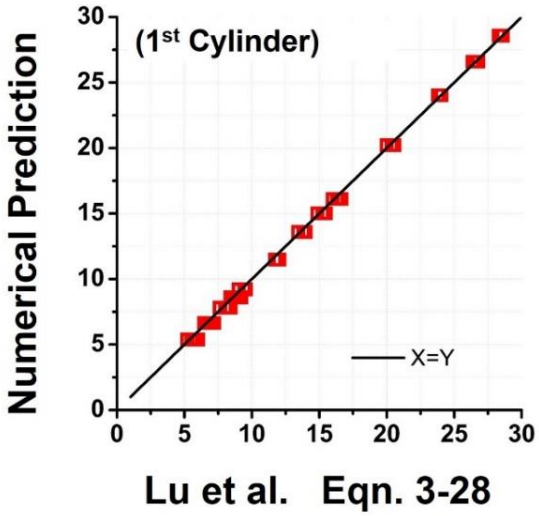

a)

Figure 6-10 a) Nusselt number (for the first horizontal cylinder of the column $\overline{Nu}_{D,1}$) comparison: numerical predictions vs. correlation (Eqn. 3-28) proposed by Lu et al. [55] for molten salt. b) Comparison of the predicted peripherally-averaged $\overline{Nu}_{D,2}$ values for the second horizontal cylinder of the column from this study, correlation Eqn. 3-29 proposed by Lu et al. [55] for molten salt, and correlation Eqn. 3-27 proposed by Corcione [56] for air.

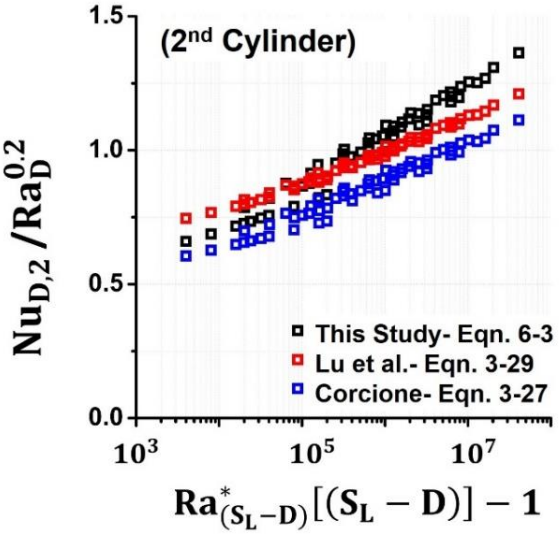

b)

Figure 6-10 cont.

Comparison of the results for the 6th cylinder in the column obtained in this study and determined from correlations proposed by Corcione [56] and Kitamura et al [60] (Eqn. 3-27 and Eqn. 3-30) is presented in Figure 6-11, where the average Nusselt number for the sixth cylinder based on the cylinder spacing $Nu_{(S_L-D),6}$ is plotted versus the modified Rayleigh number based on the cylinder spacing $Ra_{(S_L-D)}{}^{*} \times ({}^{S_L}/_{D} - 1)$. The results show a considerable difference in heat transfer, with correlation by Kitamura under-predicting heat tranfer by almost an order of magnitude.

Figure 6-11b shows the comparison of the total average Nusselt number for a vertical column of cylinders in molten salt obtained from Eqn. 3-26 proposed by Corcione [56] for air and Eqn. 6-2 from this study for molten salt. The results show that Eqn. 3-26 developed for air underpredicts values of the total average Nusselt number for molten salt, which may lead to considerable errors in heat exchager design.

Thus, it may be concluded that heat transfer correlations developed for different storage media, cannot be used as a general solution for all cases and illustrates the importance of the heat transfer correlations developed in this study for molten salt.

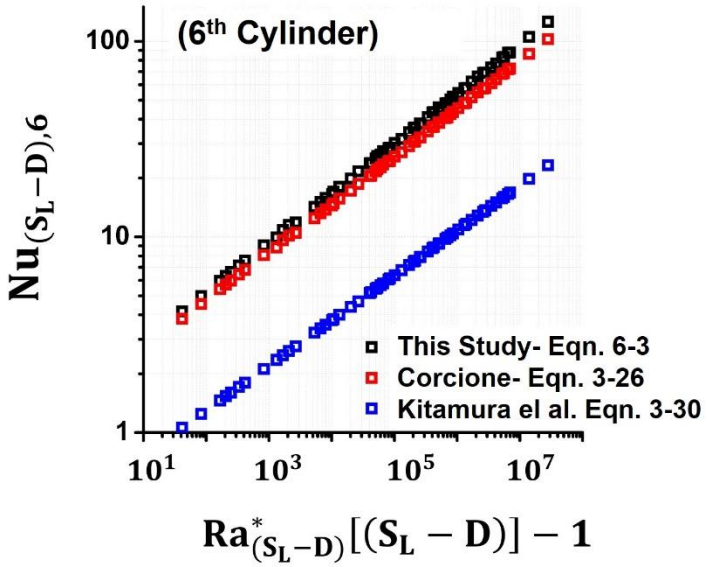

a)

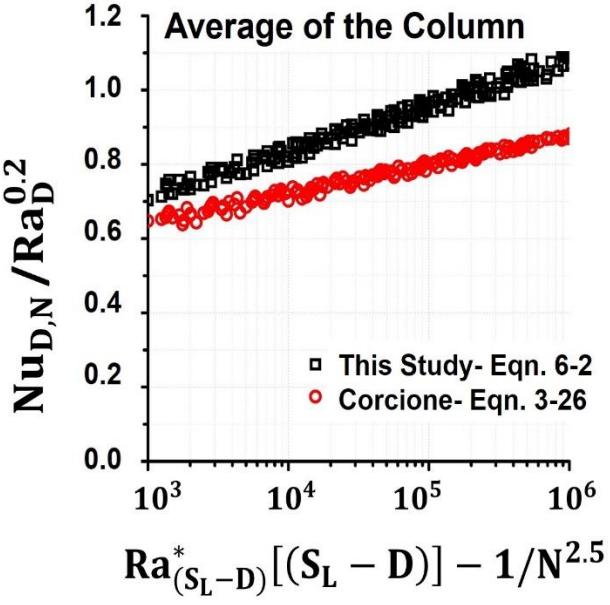

b)

Figure 6-11 a) Comparison of the predicted average Nusselt number based on the cylinder spacing $\overline{Nu}_{(SL-D),6}$ for the sixth horizontal cylinder in the column from this

study with the correlation Eqn. 3-30 proposed by Kitamura et al. [60], and the correlation Eqn. 3-26 proposed by Corcione [56] b) Comparison of the predicted average Nusselt number for a column of cylinders based on the cylinder diameter from Eqn. 6-2 from this study with the correlation Eqn. 3-26 proposed by Corcione [56]

The literature review of the experimental and numerical studies concerning the natural convection heat transfer from the in-line and staggered bundle of 9×5 horizontal cylinders, physical model, a detailed analysis of the steady-state temperature and velocity distributions around the cylinders, and statistical analysis of the numerical results are presented and discussed in the next chapter.

CHAPTER 7: TUBE BUNDLE

7-1. Overview

A two-dimensional steady-state natural convection heat transfer from a bundle of closely spaced isothermally heated horizontal cylinders in the in-line and staggered arrangements immersed in molten solar salt was investigated for a laminar flow regime. The flow and temperature fields and heat transfer from the bundle of 9×5 cylinders (nine columns and five rows) were predicted as functions of tube bundle geometry (tube spacing and arrangement) and flow conditions (Rayleigh number). The physical model and the results of numerical analysis for the in-line and staggered arrangements are presented and compared in this chapter.

Studies of the forced convection heat transfer from isothermal, bundle of cylinders immersed in the crossflow [86-93] and natural convection heat transfer from the vertical and horizontal arrays of horizontal cylinders [56, 59, 60, 74, 75, 77, 78, 80-83] show that the cylinder-to-cylinder spacing plays an important role on both the forced and natural convection heat transfer. However, the buoyancy-induced flow and heat transfer for a bundle of horizontal cylinders has received inadequate attention [57, 76, 79, 94-96].

The experimental study by Tillman [94] concerning natural convection heat transfer from a bundle of horizontal cylinders to air with the in-line and staggered arrangement showed that the transverse and longitudinal cylinder-to-cylinder spacing S_T/D and S_L/D, and the Rayleigh number Ra are important parameters having a significant effect on natural convection heat transfer from the cylinders. Furthermore, they concluded that the arrangement of the cylinders has smaller impact on the average heat transfer rate of the

bundle compared to the cylinder-to-cylinder spacing S_T/D and S_L/D and the Rayleigh number. Tillman [94] proposed two correlations for the average heat transfer rate from a bundle of horizontal cylinders in the in-line and staggered arrangements as functions of the Rayleigh number but has neglected the effect of the transverse and longitudinal cylinder-to-cylinder spacing S_T/D and S_L/D. Another experimental study by Keyhani and Dalton [95] proposed correlations for the natural convection heat transfer from an in-line bundle of N×N (3-5 and 7) cylinders with a constant heat flux dissipation inside a cavity.

Bejan et al. [79] proposed two correlations based on numerical and experimental studies for the natural convection heat transfer from a tube bundle immersed in air for selection of the optimal spacing between the cylinders in a staggered bundle of horizontal cylinders. The optimal cylinder spacing was determined applying the criterion of maximum thermal conductance between the tube bundle and surrounding air. Warrington and Crupper [76] performed experimental analysis of natural convection heat transfer from a 2×2 bundle of isothermally heated horizontal cylinders placed inside an isothermal colder enclosure. They proposed a correlation based on the experimental data for the heat transfer rate from a bundle of horizontal cylinders to the enclosure as a function of a modified Rayleigh number, but have neglected the effect of the cylinder-to-cylinder spacing on heat transfer.

Hata et al. [96] performed numerical analysis of the natural convection heat transfer from a bundle of N×N (5 and 9) horizontal cylinders with the constant heat flux in the in-line and staggered arrangements immersed in liquid sodium. They proposed three correlations for the average natural convection heat transfer rate expressed in

dimensionless form as Nu_{av} from the entire bundle for three cylinder arrangements, eight relatively low Rayleigh numbers ranging from 5.98×10 to 6.17×10^4, and a narrow range of dimensionless longitudinal and transverse cylinder spacings from 1.6 to 2.5.

Ivanov et al. [57] studied numerically temperature and flow fields and the effects of the transverse and longitudinal cylinder-to-cylinder spacings on the heat transfer rate from a staggered bundle of horizontal cylinders immersed in water. They reported that the results of numerical analysis for natural convection from a staggered bundle of horizontal cylinders are in a good agreement with the empirical correlation proposed by Zukauskas et. al. [97] for the Nusselt number from a forced convection heat transfer, except the case of tube banks with a jet-like inter-tube flow.

The previous studies published in the literature employed air, water, or liquid sodium as the heat storage medium and studied natural convection heat transfer between the heat exchanger and surrounding colder medium. Despite the increasingly wide engineering applications of molten salt, very few studies were conducted concerning natural convection heat transfer from circular cylinders immersed in molten solar salt [26, 55, 68]. Natural convection heat transfer from a bundle of horizontal cylinders immersed in molten solar salt has not been studied in the past.

In summary, a relatively small number of experimental and numerical investigations have been conducted concerning natural convection from tube bundles. The previous studies were performed for a range of relatively small Rayleigh numbers and many have neglected the effect of cylinder spacing on the heat transfer rate to the surrounding medium (air or water). A small number of studies considered heat transfer

from a tube bundle to a liquid sodium, while heat transfer from a tube bundle immersed in molten salt has not been studied at all.

To close this knowledge gap, natural convection heat transfer from a TES system comprising a (9×5) bundle of circular cylinders, representing a heat exchanger immersed in a heat storage medium, was investigated in this study to determine heat transfer characteristics of a realistic heat exchanger used in TES application for the improved utilization of solar energy. The main objective of this study was to investigate and determine the effect of transverse and longitudinal cylinder-to-cylinder spacing S_T/D and S_L/D on heat transfer and determine the optimum geometry of the tube bundle resulting in the maximum volumetric heat transfer rate. The optimal geometry and volumetric heat transfer were determined as functions of the Rayleigh number.

7-2. In-line Arrangement

A heat exchanger comprising an in-line bundle of (9×5) circular cylinders immersed in a tank of the TES fluid (molten solar salt) was analyzed to determine the effect of the tube arrangement and tube spacing (lateral and longitudinal) on heat transfer.

7-2-1. Physical Model

The heat exchanger geometry analyzed in this study comprises an in-line bundle of circular cylinders immersed into the molten solar salt representing an indirect TES system. The analyzed heat exchanger geometry involving an in-line bundle of 9×5 circular cylinders of diameter D, height H, and width W presented is in Figure 7-1a. The tube bundle and computational domain (ABCD) used in the numerical analysis are presented in

Figure 7-1b. Due to the symmetry along the A-C line, the analysis was performed for the right half of the domain.

Numerical simulations were performed for a range of dimensionless transverse and longitudinal cylinder-to-cylinder spacings S_T/D and S_L/D and Rayleigh number Ra_D to determine their effect on heat transfer and heat transfer volumetric density for the entire tube bundle. Nine values of the longitudinal cylinder-to-cylinder spacing ratio S_L/D and eighteen values of the transverse cylinder-to-cylinder spacing ratio S_T/D were selected for parametric computations. For each value of S_L/D the transverse cylinder-to-cylinder spacing ratio S_T/D was varied. Predictions were obtained for the Rayleigh number range of 10^4 to 10^6 and Pr number range of 6.7 to 10. The regime is laminar for $Ra_D < 10^7$[51]. The matrix of computational cases is summarized in Table 7-1. The Nusselt number Nu in this case is a function of the Rayleigh number and dimensionless spacings S_T/D and S_L/D.

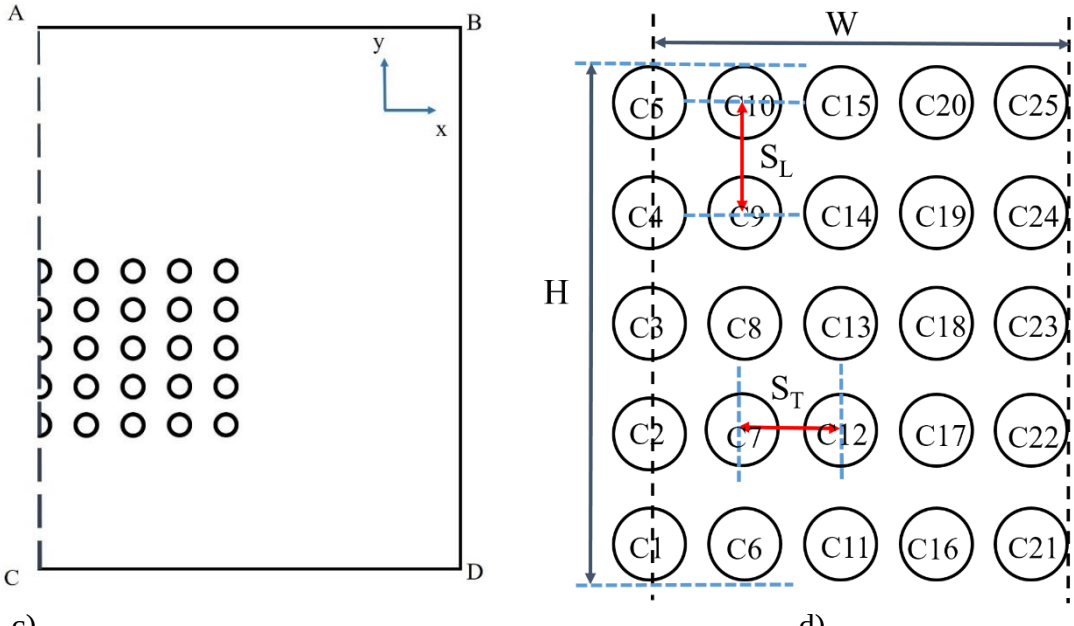

c) d)

Figure 7-1 a) Computational domain and the in-line tube bundle, (b) Geometry of the analyzed in-line bundle of 9×5 circular cylinders with cylinder numbers specified.

Table 7-1 Matrix of the computed cases.

Ra	S_L/D	S_T/D
10^4, 5×10^4, 10^5, 5×10^5, 10^6	1.2-1.4-1.6-1.8-2-4-6-8-10	1.1-1.2-1.3-1.4-1.5-1.6-1.7-1.8-1.9-2-3-4-5-6-7-8-9-10

Based on the analysis proposed by Warrington [76], the distance from the side walls, pressure outlet and pressure inlet of the domain to the center of the closet cylinder in the row (for example, cylinder C_{25} in Figure 7-1) was set to 15D for the very small cylinder spacing to provide a domain-independent solution. This value was increased for larger cylinder spacing.

7-2-2. Steady-State Temperature and Velocity Distribution Around Circular Cylinders

Temperature contours and flow fields predicted for an in-line bundle of (9×5) horizontal cylinders for two transverse spacings S_T/D=1.2 and 1.6, constant longitudinal spacing S_L/D=1.2, and $Ra_D = 10^4$ are shown in Figure 7-2 and 7-3. For the smallest transverse and longitudinal spacings of $S_T/D = S_L/D$=1.2, due to the small temperature gradient between the cylinders conduction is the dominant mode of heat transfer for the cylinders located inside the bundle. In this case natural convection occurs only on the surface of the cylinders located at the bottom and top rows where temperature gradient is larger. As the transverse cylinder spacing increases, temperature gradient between the cylinder columns increases and induces low-velocity fluid flow between the columns, resulting in natural convection heat transfer on the surface of the cylinders located within the bundle.

As transverse spacing increases, the buoyancy-induced flow forms distinct plumes between cylinder columns attached to the cylinder surface. Individual plumes interact and

merge into a single plume above the top row of cylinders in the bundle. Therefore, the bottom row of cylinders in the bundle has a lower average temperature and the highest temperature gradient between the cylinder surface and the storage medium, leading to the highest Nusselt number values. The average temperature increases as the fluid flows upwards to the top row of the bundle where the average temperature is the highest and temperature gradient between the cylinder surface and the storage medium is the lowest, resulting in the lowest Nusselt number values. The Nusselt number values for individual cylinders in the bundle are presented in Figure 7-2 and 7-3.

The fluid flows inwards from the outer columns of the computational domain and for small transverse spacings ($S_T/D \leq 4$) the flow moves towards the center column, turns upwards and becomes vertical at the center cylinder. This results in a higher temperature gradient and higher Nusselt number values for the cylinders located in the semi-confined outer column. The temperature gradient decreases for the inner columns in the bundle with the center column having the lowest temperature gradient and, therefore, the lowest Nusselt number. As the transverse cylinder spacing is increased, interactions between individual columns in the bundle diminish and the bundle behaves as a set of independent columns.

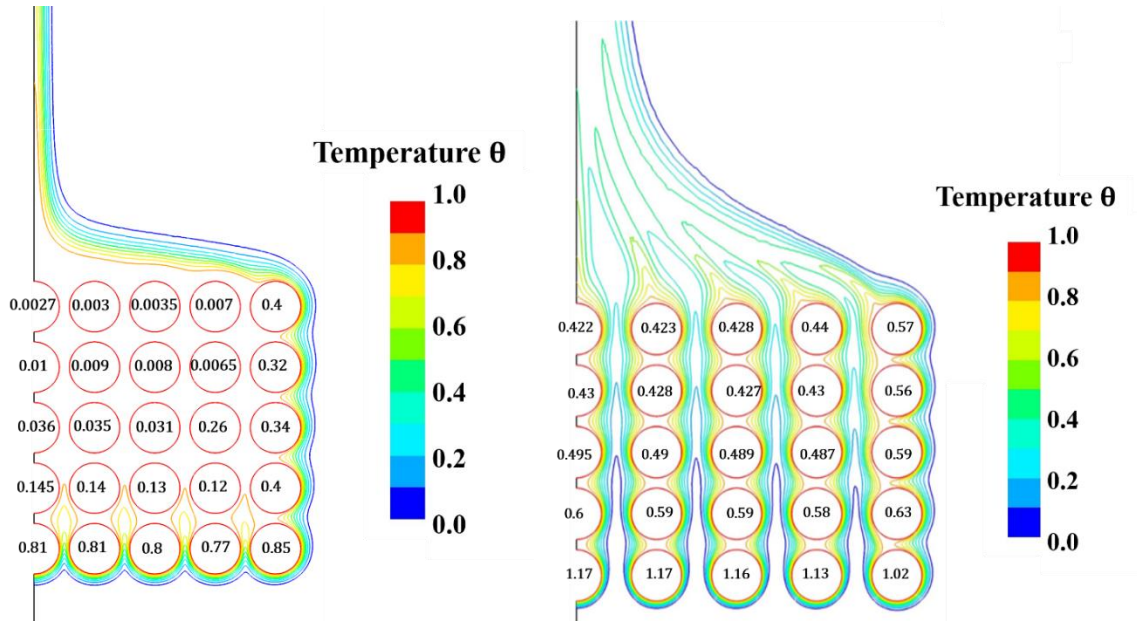

a) $S_T/D=1.2$ b) $S_T/D=1.6$

Figure 7-2 Dimensionless temperature contours and HTE values for constant longitudinal spacing $S_L/D=1.2$, $Ra_D=10^4$ and two values of transverse spacings $S_T/D=1.2$ and 1.6.

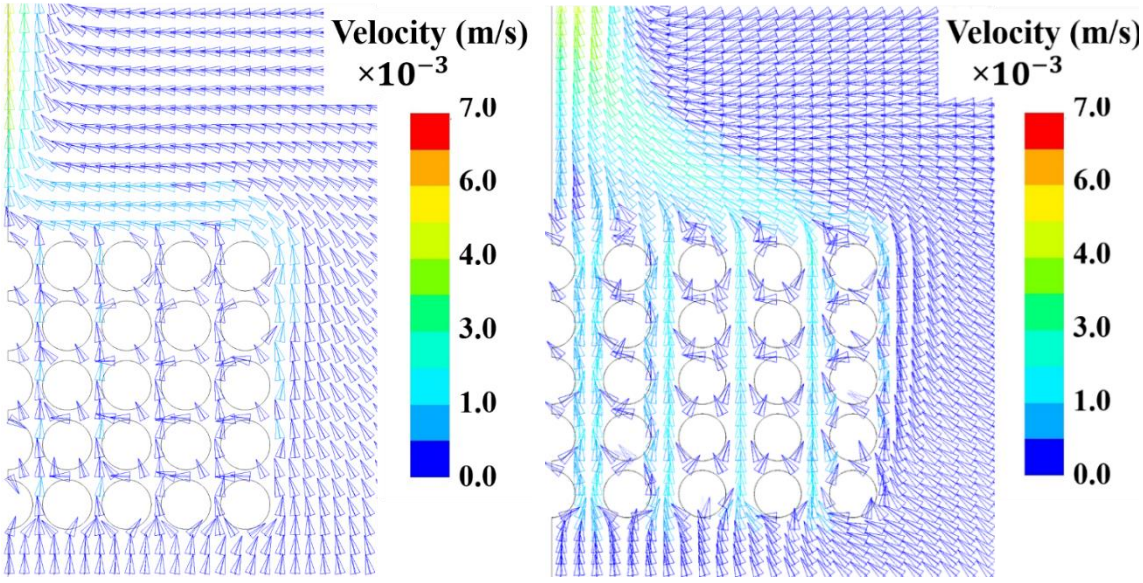

a) $S_T/D=1.2$ b) $S_T/D=1.6$

Figure 7-3 Velocity vectors for constant longitudinal spacing $S_L/D=1.2$, $Ra_D=10^4$ and two values of transverse spacings $S_T/D=1.2$ and 1.6.

Figure 7-4 compares temperature contours for two longitudinal spacings S_L/D=1.2 and 6, and constant transverse spacing S_T/D=1.6 for $Ra_D = 10^4$. As longitudinal spacing increases, the buoyancy-induced flow forms distinct plumes around individual cylinders attached to the cylinder surface. Individual plumes interact and eventually merge into a single plume. The temperature gradient between the cylinders in the top row of the bundle and the storage medium increases and Nusselt number increases.

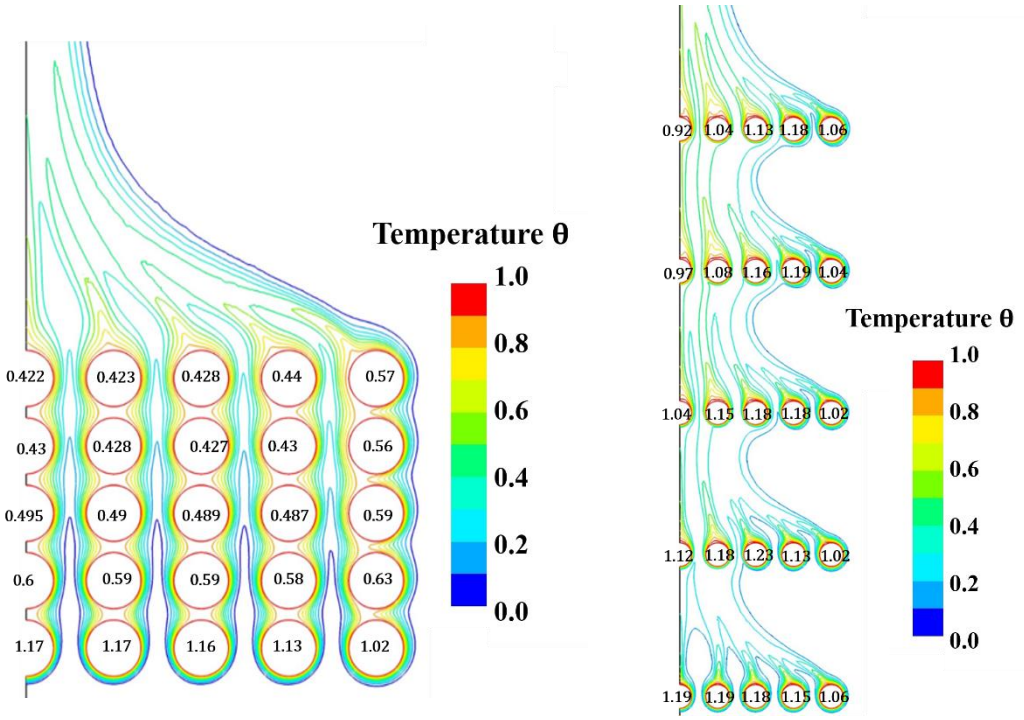

a) S_L/D=1.2 b) S_L/D=6

Figure 7-4 Dimensionless temperature contours for transverse cylinder S_T/D =1.6, Ra_D =10^4 and longitudinal spacings S_L/D=1.2 and 6.

Variation of the total average heat transfer enhancement $\overline{Nu}_D/\overline{Nu}_0$ (HTE) values for the Rayleigh number of Ra_D =10^4 with transverse and longitudinal cylinder spacings S_T/D and S_L/D in a tube bundle is presented in Figure 7-5a.

HTE increases as the transverse cylinder spacing S_T/D increases. For longitudinal spacings $1.2 < S_L/D < 6$, HTE reaches maximum value at S_T/D = 2 to 4 and decreases as

transverse spacing is further increased. This trend can be explained by the variation of HTE for a horizontal row of circular cylinders discussed in [98]. For the transverse cylinder spacings smaller than the thickness of the velocity boundary layer, interference of the boundary layers and fluid flow between the adjacent cylinders reduces thermal gradient and heat transfer. However, this effect diminishes as transverse spacing is increased and heat transfer enhancement reaches its maximum value as the transverse cylinder spacing is increased to values close to the thickness of the velocity boundary layer. For transverse spacings larger than the velocity boundary layer thickness, the effect of the adjacent cylinders diminishes, and heat transfer enhancement is decreased. For small longitudinal spacings there is no maximum in HTE since heat transfer is dominated by the conduction, while for $S_L/D > 6$, cylinder rows are far apart, and their interaction is weak. This is same trend as for the total average heat transfer enhancement $\overline{Nu}_D/\overline{Nu}_0$ from one horizontal row of cylinders [99] .

Variation of the total average heat transfer enhancement $\overline{Nu}_D/\overline{Nu}_0$ (HTE) for $Ra_D = 10^4$ with longitudinal and transverse cylinder spacings S_L/D and S_T/D in a tube bundle is presented in Figure 7-5b. HTE increases monotonically as longitudinal spacing S_L/D is increased for all values of the transverse spacing S_T/D. Heat transfer enhancement is the smallest for the lowest analyzed value of longitudinal spacing S_L/D and increases as S_T/D is increased. This is same trend as for a vertical column of horizontal cylinders [99] .

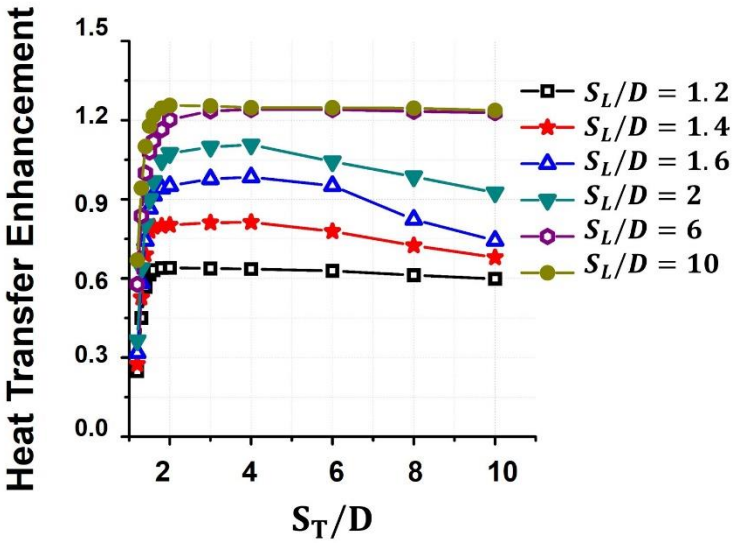

a)

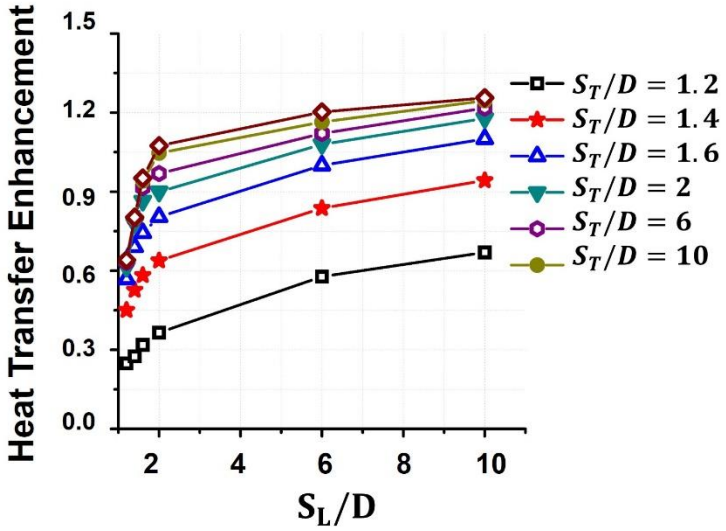

b)

Figure 7-5 Total heat transfer enhancement vs a) Transverse spacing and b) Longitudinal spacing for Rayleigh number of $Ra_D = 10^4$.

As the Rayleigh number increases, longitudinal and transverse cylinder spacings S_L/D and S_T/D have a more complex effect on the flow and, therefore, on the total average heat transfer enhancement $\overline{Nu}_D/\overline{Nu}_0$.

Values of the total average heat transfer enhancement $\overline{Nu}_D/\overline{Nu}_0$ (HTE) are plotted as functions of transverse and longitudinal spacings S_T/D and S_L/D are presented in Figure 7-6 in form of contour diagrams (performance maps) for three Rayleigh numbers. The HTE contours show that for the range of Rayleigh numbers between $10^4 \leq Ra_D \leq 10^6$ the total average heat transfer enhancement $\overline{Nu}_D/\overline{Nu}_0$ (HTE) follows the same trend as for $Ra_D=10^4$. HTE monotonically increases as the longitudinal spacing S_L/D is increased. The transverse spacing, however, has a more complex effect: HTE increases as the transverse spacing S_T/D is increased, reaches maximum value, and decreases as spacing is further increased.

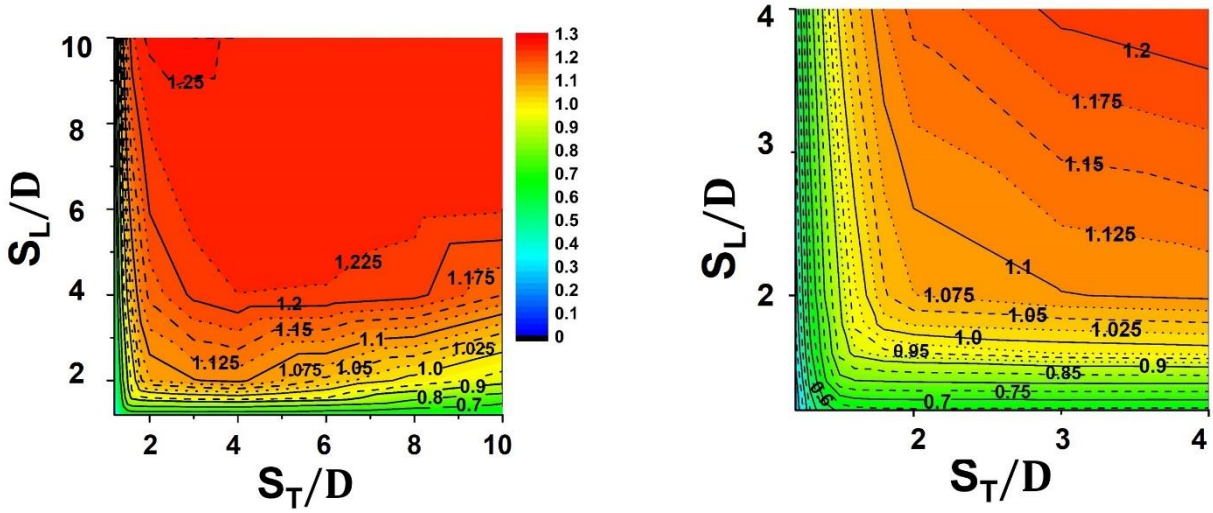

a) $Ra_D = 10^4$

Figure 7-6 (Left) Contour diagrams presenting heat transfer enhancement vs transverse and longitudinal spacings for three values of Rayleigh number Ra_D (Right) Contour diagrams presenting heat transfer enhancement for a smaller range of transverse and longitudinal spacings.

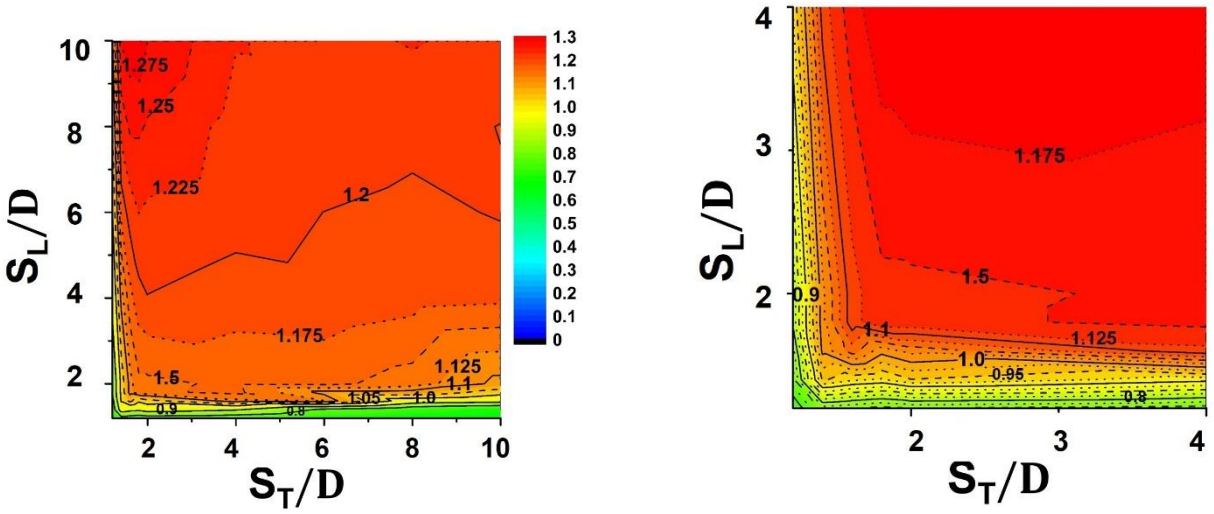

b) $Ra_D = 10^5$

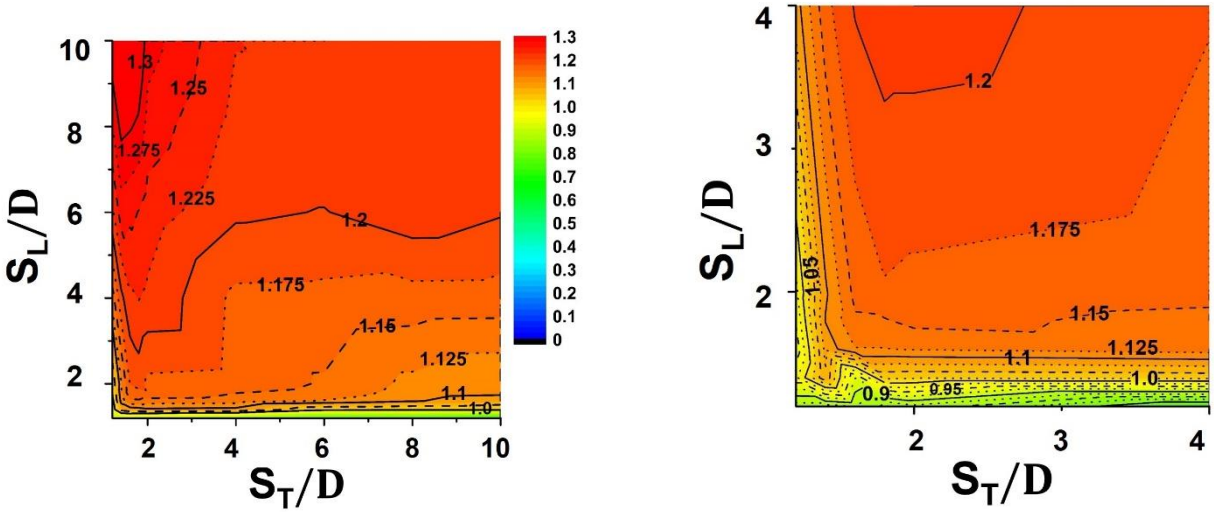

c) $Ra_D = 10^6$

Figure 7-6 cont.

Although Figure 7-5 and the HTE contours presented in Figure 7-6 show there is a set of optimal longitudinal and transverse cylinder spacings $(S_L/D, S_T/D)_{opt,HTE}$ resulting in the maximum heat transfer enhancement HTE_{max}, the objective of the heat exchanger optimization performed in this study was to determine the optimal set of the cylinder spacings $(S_L/D, S_T/D)_{opt}$ resulting in the maximum volumetric heat transfer rate and, thus minimize the size and cost of a heat exchanger. Eqn. 3-16 proposed by Bejan et al. [79]

was used to calculate the dimensionless heat transfer volumetric density $\tilde{q}$ and determine the optimal set of transverse and longitudinal tube spacings in a bundle.

Values of the dimensionless heat transfer volumetric density $\tilde{q}$ are plotted as functions of the transverse and longitudinal spacings S_T/D and S_L/D are presented in Figure 7-7 in form of the contour diagrams (performance maps) for three Ra numbers; 10^4, 10^5, and 10^6. The results show there is optimal set of transverse and longitudinal spacings at which dimensionless heat transfer volumetric density $\tilde{q}$ reaches its maximum value $\tilde{q}_{max}$. For the range of the investigated Rayleigh numbers, the maximum dimensionless heat transfer volumetric density is achieved for small values of cylinder spacings. This is because although increasing cylinder spacing increases the total heat transfer rate from the bundle, this increase is smaller compared to the increase of the bundle volume HWL, thus resulting in the optimal spacing. The optimal spacing decreases as Rayleigh number is increased, and the value of $\tilde{q}_{max}$ increases with the Rayleigh number as the overall heat transfer in the bundle is increased.

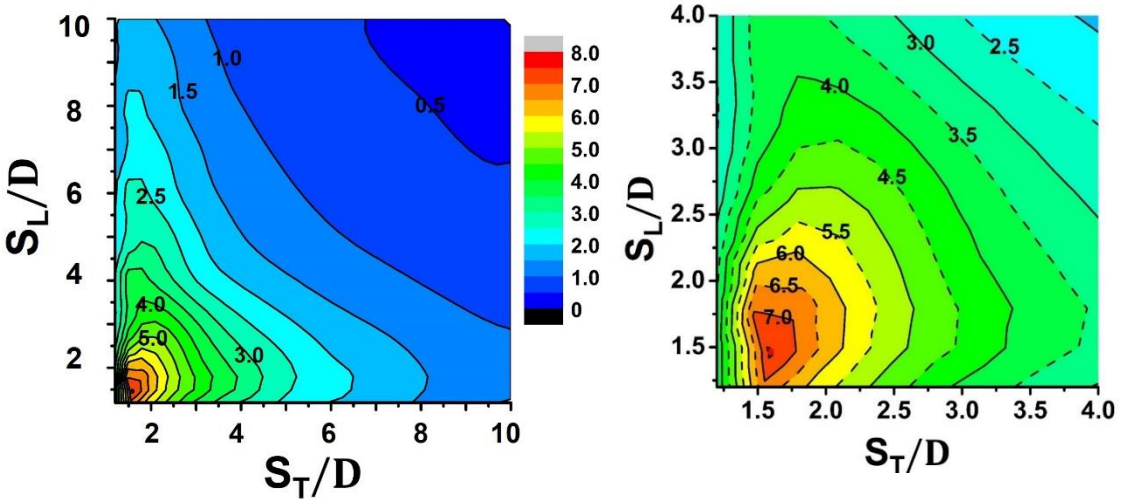

a) $Ra_D = 10^4$

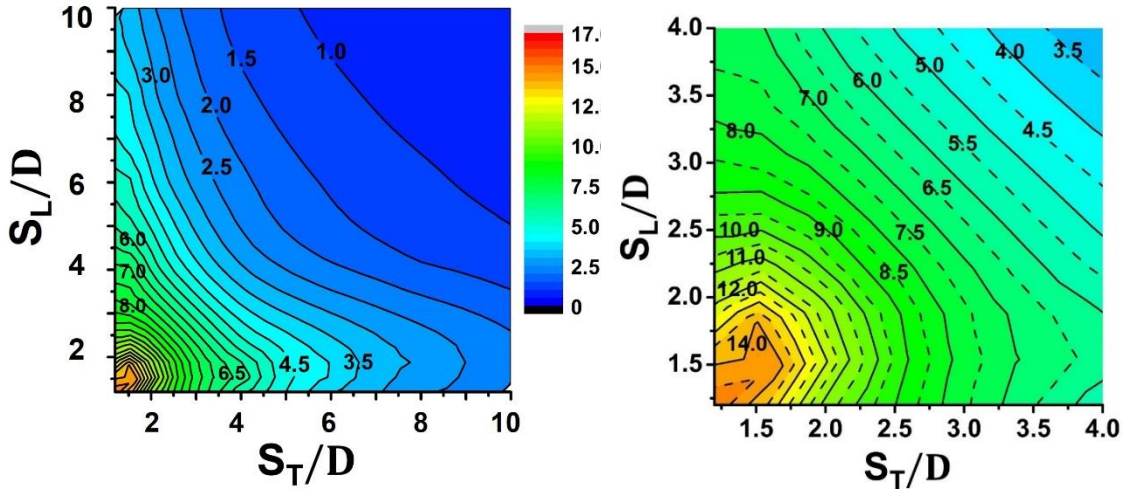

b) $Ra_D = 10^5$

Figure 7-7 Contour diagrams presenting dimensionless heat transfer volumetric density$\tilde{q}$ vs transverse and longitudinal spacing for the 9×5 in-line bundle and three values of Rayleigh number. (Right) Contour diagrams presenting $\tilde{q}$ for a smaller range of spacings.

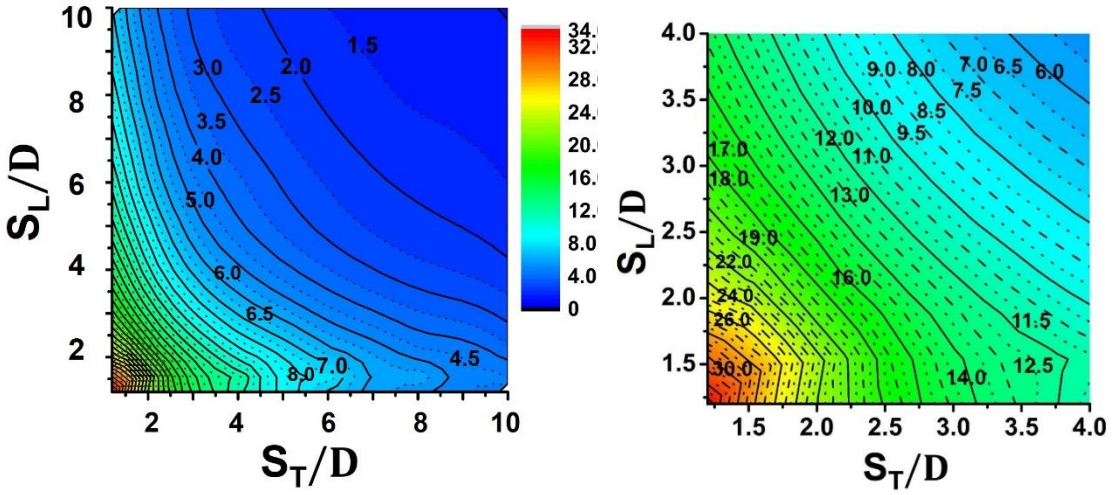

c) $Ra_D = 10^6$

Figure 7-7cont.

There are no correlations or performance maps published in the open literature for the dimensionless heat transfer volumetric density q̃ for the in-line bundle of horizontal cylinders immersed in molten solar salt. A few available correlations are either limited to a specific geometry of a bundle and specific storage medium or neglect the effect of the longitudinal and transverse spacings on the heat transfer rate and, therefore, on dimensionless heat transfer volumetric density. Thus, using correlations from the literature could result in large errors in predicting the average Nusselt number $\overline{Nu}_D$ and dimensionless heat transfer volumetric density q̃ for an in-line bundle. To improve design of the heat exchangers used in TES and thermal systems for solar and other applications, correlations were developed in this study for the dimensionless heat transfer volumetric density q̃ for an in-line bundle of horizontal cylinders immersed in molten solar salt.

Numerical results obtained in this study and statistical regression analysis were used to develop correlation for the dimensionless heat transfer volumetric density q̃ for an

in-line bundle of 9×5 horizontal cylinders as a function of the Rayleigh number Ra_D and longitudinal and transverse cylinder spacing S_L/D and S_T/D,

The proposed form of the correlation for dimensionless heat transfer volumetric density $\tilde{q}$, for an in-line bundle of 9×5 horizontal cylinders immersed in a molten solar salt is given by Eqn. 7-1 as a function of the Ra_D number and the height and width of the bundle (shown in Figure 7-1b).

$$\tilde{q} = 8.0 \times \left(\frac{H}{D}\right)^{-0.75} \times \left(\frac{W}{D}\right)^{-0.95} \times Ra_D{}^{0.32} \quad \text{Eqn. 7-1}$$

$$\frac{H}{D} = \left(M_y - 1\right) \times \left({}^{S_L}/_{D}\right) + 1 \quad \text{Eqn. 7-1a}$$

$$\frac{W}{D} = \left(N_x - 1\right) \times \left({}^{S_T}/_{D}\right) + 1 \quad \text{Eqn. 7-1b}$$

Eqn. 7-1 shows exponential variation of the dimensionless heat transfer volumetric density $\tilde{q}$ with Ra_D number and longitudinal and transverse cylinder spacing S_L/D and S_T/D, and is valid for $1.2 \leq (S_L/D, S_T/D) \leq 10$ and $10^4 \leq Ra_D \leq 10^6$.

The average relative error between the proposed correlation and the numerical results is less than 20.0%.

As the results presented in Figure 7-8 show, there is a good agreement between values of the Nusselt number obtained from numerical predictions and correlation Eqn. 7-1; the maximum difference is less than 30%. The difference is the largest for the lowest analyzed Rayleigh number ($Ra_D = 10^4$) and for cylinder spacing $S_T/D \leq 2$. This is because for small Ra_D number and small cylinder spacing conduction is a dominant mode of heat transfer between the cylinders. As Ra_D number and cylinder spacing increase, convection heat transfer becomes dominant.

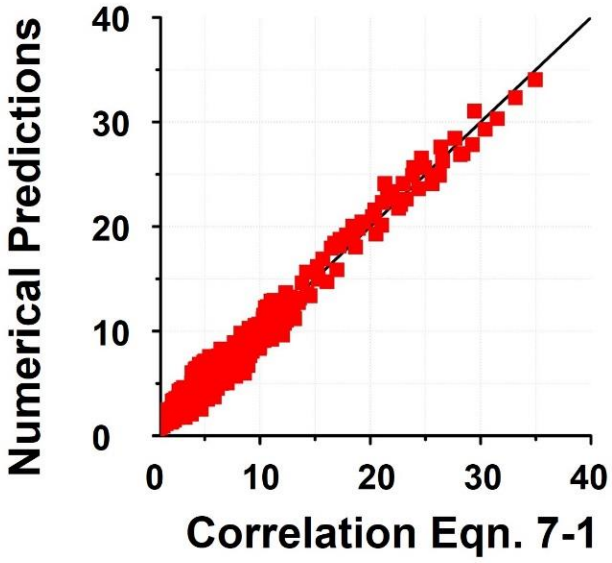

Figure 7-8 Dimensionless heat transfer volumetric density$\tilde{q}$ comparison: numerical predictions vs. correlation Eqn. 7-1.

Variation of the maximum dimensionless heat transfer volumetric density $\tilde{q}_{max}$ with longitudinal and transverse cylinder spacings S_L/D and S_T/D for five values of Rayleigh number is presented in Figure 7-9. The figure shows that for $Ra < 5\times10^5$ $\tilde{q}_{max}$ reaches maximum value called here the optimal dimensionless heat transfer volumetric density $\widetilde{q_{opt}}$. The location of $\widetilde{q_{opt}}$ is defined by the optimal cylinder spacings $S_{L,opt}/D$ and $S_{T,opt}/D$. For $Ra > 5\times10^5$ there is no optimum because $\tilde{q}_{max}$ monotonically increases as spacing is reduced. In this case the value and location of $\widetilde{q_{opt}}$ correspond to the maximum value of $\tilde{q}_{max}$ determined at the smallest analyzed cylinder spacing.

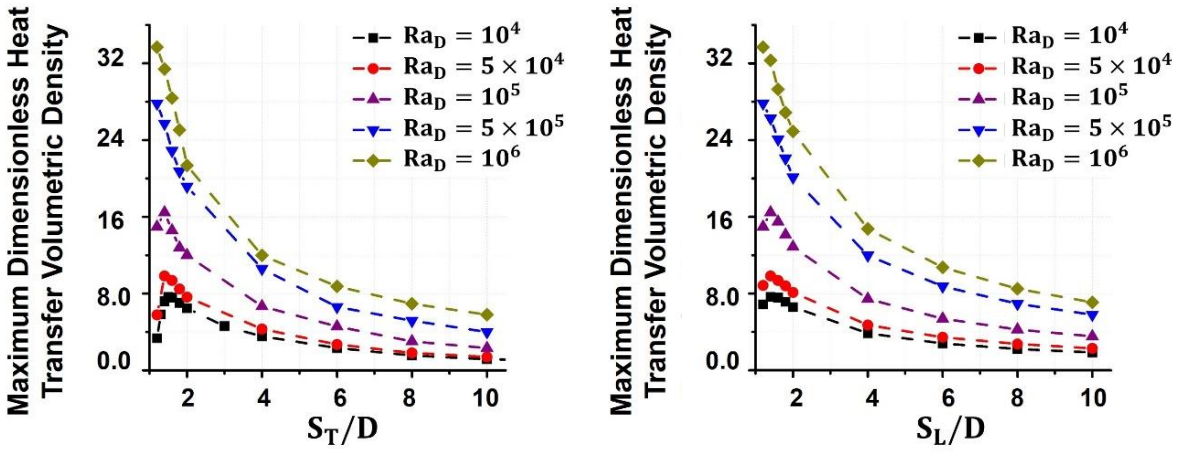

a) b)

Figure 7-9 Maximum dimensionless heat transfer volumetric density$\tilde{q}_{max}$ for an in-line bundle of 9×5 horizontal cylinders vs dimensionless cylinder spacing (a)Transverse spacing (b)Longitudinal spacing.

The maximum dimensionless heat transfer volumetric density $\tilde{q}_{max}$ for an in-line bundle of 9×5 horizontal cylinders is plotted in Figure 7-11a as a function of dimensionless parameter $(H/D \times W/D)^{0.6} Ra_D^{-0.25}$. The exponent -0.25 originates from the dimensional analysis by Bejan et. al. [79]. Although they [79] used the exponent 0.3 for the height of the bundle, due to the difference in optimization objectives between this study and the study by Bejan et. al. [79], the value of 0.6 used in this study provides better fit to the data. The results show that $\tilde{q}_{max}$ is an exponential function of the bundle height H and width W, and the Rayleigh number. For the Ra_D number in the $10^4 \leq Ra_D \leq 10^6$ range and $1.2 \leq (S_{L,opt}/D, S_{T,opt}/D) \leq 10$ the value of $\tilde{q}_{max}$ for an in-line bundle of 9×5 horizontal cylinders immersed in molten solar salt is given by Eqn. 7-2 as a function of the Ra_D number and the corresponding optimal height H_{opt} and width W_{opt} of the bundle.

$$\tilde{q}_{max} = 6.65 \times \left(\frac{H_{opt}}{D} \times \frac{W_{opt}}{D}\right)^{-0.7} \times Ra_D^{0.29} \qquad \text{Eqn. 7-2}$$

Quantities H_{opt} and W_{opt} can be determined from the contour diagrams presented in Figure 7-7. For example, from Figure 7-10 for $Ra_D = 10^4$ and S_L /D =1.5 the maximum value of $\tilde{q}_{max} = 7$ occurs at $S_{T,opt}$/D =1.5. Substituting $S_L/D = S_{T,opt}/D = 1.5$ into Eqn. 7-1a and 7-1b gives H_{opt}/D =7 and W_{opt}/D = 6.5 for the 9×5 bundle. The value of $\tilde{q}_{max}$ calculated from Eqn. 7-2 is 6.8 , which compares well with the value from Figure 7-10.

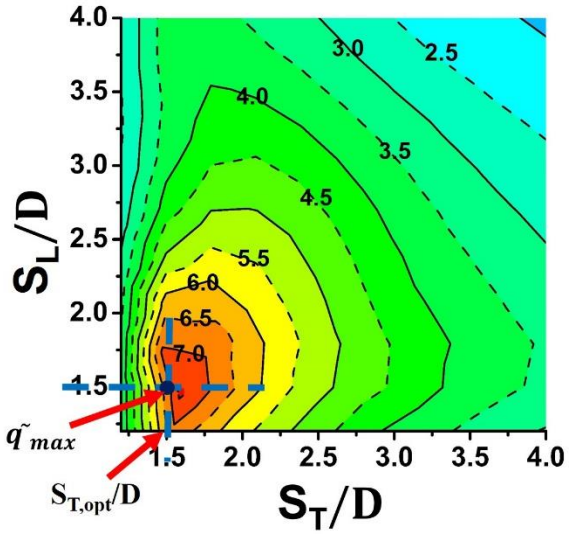

Figure 7-10 Contour diagrams presenting dimensionless heat transfer volumetric density $\tilde{q}$ vs transverse and longitudinal spacing for $Ra_D = 10^4$.

A comparison between numerical predictions and correlation represented by Eqn. 7-2 presented in Figure 7-11b shows a good agreement between the numerical results and correlation with the average relative error of 10.0%.

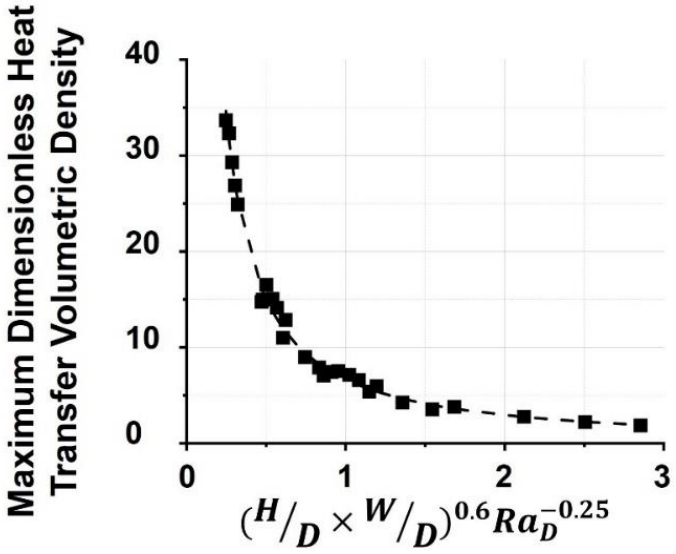

a)

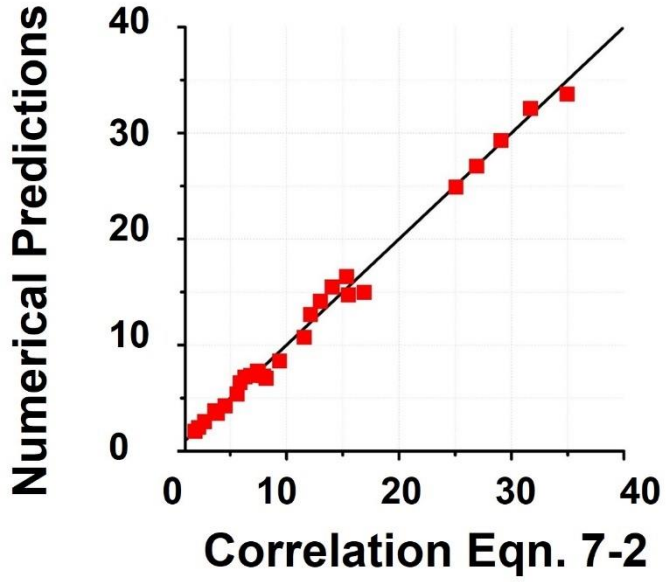

b)

Figure 7-11 a) Maximum dimensionless heat transfer volumetric density $\tilde{q}_{max}$ for a 9×5 in-line bundle of horizontal cylinders vs corresponding height and width of the bundle. b) Maximum dimensionless heat transfer volumetric density $\tilde{q}_{max}$ comparison: numerical predictions vs. correlation (Eqn. 7-2)

The presented results are strictly valid for the 9×5 in-line bundle. If used for a bundle of different size, the predicted values of the optimal heat transfer volumetric density

and spacing will not be correct. In an attempt to estimate these errors, it was assumed that the "generalized" form of the results applicable to an in-line bundle of the infinite number of cylinders may obtained by omitting cylinders from the top row and the outer semi-confined column of the 9×5 bundle from the data analysis, and the resulting difference with respect to the full 9×5 bundle would be indicative of the error. Figure 7-12 and Table 7-2 compare the results for the maximum dimensionless heat transfer volumetric density $\tilde{q}_{max,(9\times5)}$ for the in-line bundle of 9×5 horizontal cylinders and for the infinite number of horizontal cylinders $\tilde{q}_{max,Infinite}$. For an in-line bundle of the infinite number of cylinders, variation of the maximum dimensionless heat transfer volumetric density $\tilde{q}_{max}$ with S_L/D and the location of $\widetilde{q_{opt}}$ are the same as for the 9×5 in-line bundle. As the results presented in Figure 7-12a show, for low Rayleigh numbers, such as Ra = 10^4 $\tilde{q}_{max}$ reaches its optimal value $\widetilde{q_{opt}}$ at $S_L/D \approx 1.75$. However, as presented in Figure 15b and discussed earlier, for high Rayleigh numbers such as Ra = 10^6 the value of $\tilde{q}_{max}$ increases monotonically as spacing is reduced, and the value and the location of $\widetilde{q_{opt}}$ correspond to the smallest analyzed cylinder spacing.

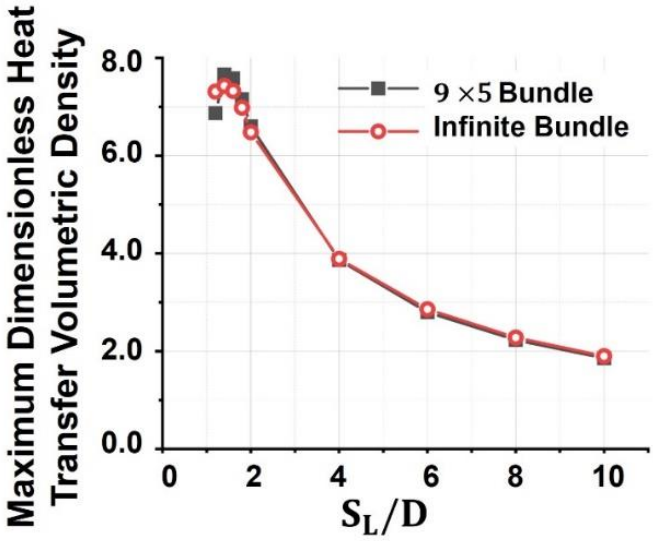

a) $Ra_D = 10^4$

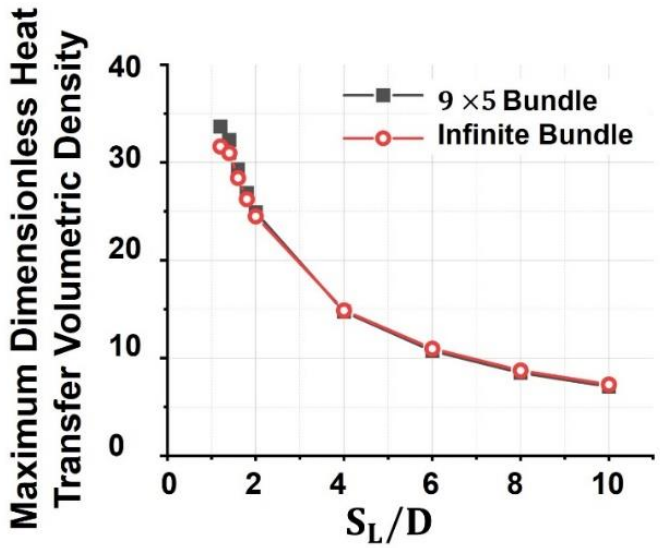

b) $Ra_D = 10^6$

Figure 7-12 Maximum dimensionless heat transfer volumetric density $\tilde{q}_{max}$ vs longitudinal spacing for two Rayleigh numbers Ra_D.

Table 7-2 Maximum dimensionless heat transfer volumetric density for five Rayleigh numbers.

Ra_D	$S_{T,\,opt}/D$	$S_{L,\,opt}/D$	$\tilde{q}_{max,\,(9\times5)}$	$\tilde{q}_{max,Infinite}$	Difference Percentage %
10^4	1.5	1.4	7.66	7.43	1.4
5×10^4	1.4	1.4	9.84	9.45	3.9
10^5	1.4	1.4	16.45	15.73	4.4
5×10^5	1.2	1.2	27.82	26.23	5.7
10^6	1.2	1.2	33.68	31.64	6.0

The optimal dimensionless heat transfer volumetric density $\widetilde{q_{opt}}$ is plotted as a function of the Rayleigh number in Figure 7-13 for the finite and infinite number of tubes in the bundle. As the results presented in Figure 7-9 and 7-13 show $\widetilde{q_{opt,9\times5}}$ increases as the Rayleigh number increases. The relationship between the optimal dimensionless heat transfer volumetric density $\tilde{q}_{opt,(9\times5)}$ for the 9×5 in-line bundle and infinite number of cylinders $\tilde{q}_{opt,Infinite}$ and Rayleigh number can be expressed by the Eqn. 7-3 and Eqn. 7-4, respectively.

$$\tilde{q}_{opt,\,(9\times5)} = 0.2919\ Ra_D^{0.3441} \qquad \text{Eqn. 7-3}$$

$$\tilde{q}_{opt,Infinite} = 0.312\ Ra_D^{0.3344} \qquad \text{Eqn. 7-4}$$

The expressions given by Eqn. 7-3 and Eqn. 7-4 are valid for $10^4 \leq Ra_D \leq 10^6$. The average relative error between the proposed correlations and numerical results is less than 5.0%.

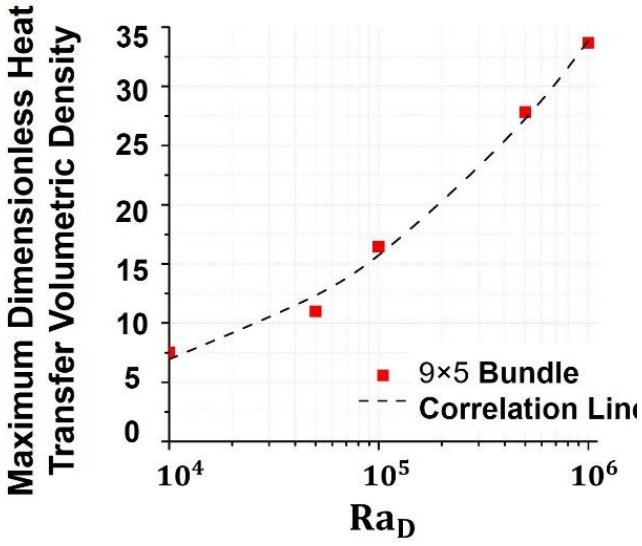

a) (9×5) Bundle

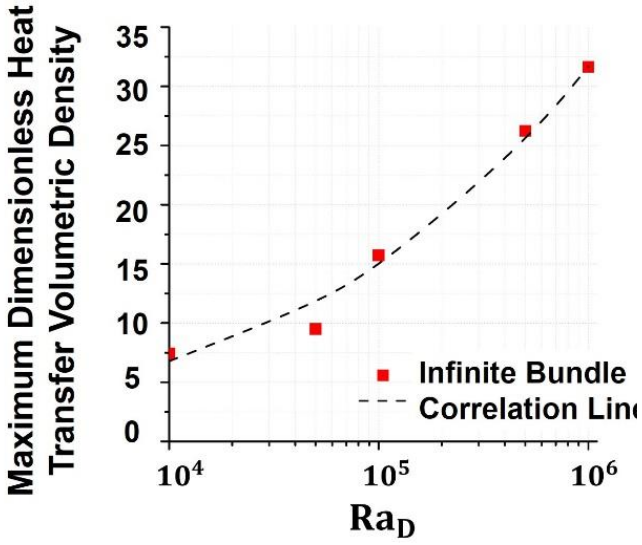

b) Infinite Bundle

Figure 7-13 Optimal dimensionless heat transfer volumetric density$\widetilde{q_{opt}}$ vs Rayleigh number for an in-line of (9×5) horizontal cylinders and an in-line bundle of infinite number of horizontal cylinders.

7-3. Staggered Tube Arrangement

An HXE comprising a staggered bundle of (9×5) circular cylinders, immersed in a tank of the TES fluid was analyzed to determine the effect of the tube arrangement and tube spacing (lateral and longitudinal) on heat transfer. The temperature and fluid flow,

and their effects on heat transfer from the bundle to the surrounding fluid (molten solar salt) are compared for the in-line and staggered bundle arrangements.

7-3-1. Physical Model

The analyzed heat exchanger geometry comprises a staggered bundle of 9×5 circular cylinders immersed into the molten solar salt representing an indirect TES system. The staggered bundle of 9×5 circular cylinders of diameter D, height H, and width W is presented in Figure 7-14a. The bundle and computational domain (ABCD) used in the numerical analysis are presented in Figure 7-14b. Due to the symmetry along the A-C line, the analysis was performed for the right half of the domain. Numerical simulations were performed for a range of transverse and longitudinal cylinder-to-cylinder spacings S_T/D and S_L/D and Rayleigh number Ra_D (based on the cylinder diameter) to determine their effect on heat transfer and the heat transfer volumetric density for the entire bundle. Nine values of the longitudinal cylinder-to-cylinder spacing ratio S_L/D and sixteen values of the transverse cylinder-to-cylinder spacing ratio S_T/D were selected for parametric computations for a total of 432 cases. For each value of S_L/D the transverse cylinder-to-cylinder spacing ratio S_T/D was varied. The computational matrix is shown in Table 7-3. The Nusselt number Nu in this case is a function of the Rayleigh number and dimensionless transverse and longitudinal spacings S_T/D and S_L/D. Numerical predictions were obtained for the Rayleigh number range of 10^4 to 10^6 and Pr number range of 6.7 to 10. The regime is laminar when $Ra_D < 10^7$ [51].

Based on the analysis proposed by Warrington [76], the distance from the side walls, pressure outlet and pressure inlet of the domain to the center of the closet cylinder

in the row (for example, cylinder C_{23} in Figure 7-14b) was set to 15D for very small cylinder spacing and Rayleigh number to provide a domain-independent solution. This value was increased for larger cylinder spacing.

Table 7-3 Matrix of the computed cases.

Ra	S_L/D	S_T/D
10^4, 10^5,10^6	1.2-1.4-1.6-1.8-2-4-6-8-10	1.1-1.2-1.3-1.4-1.5-1.6-1.7-1.8-1.9-2-3-4-5-6-8-10

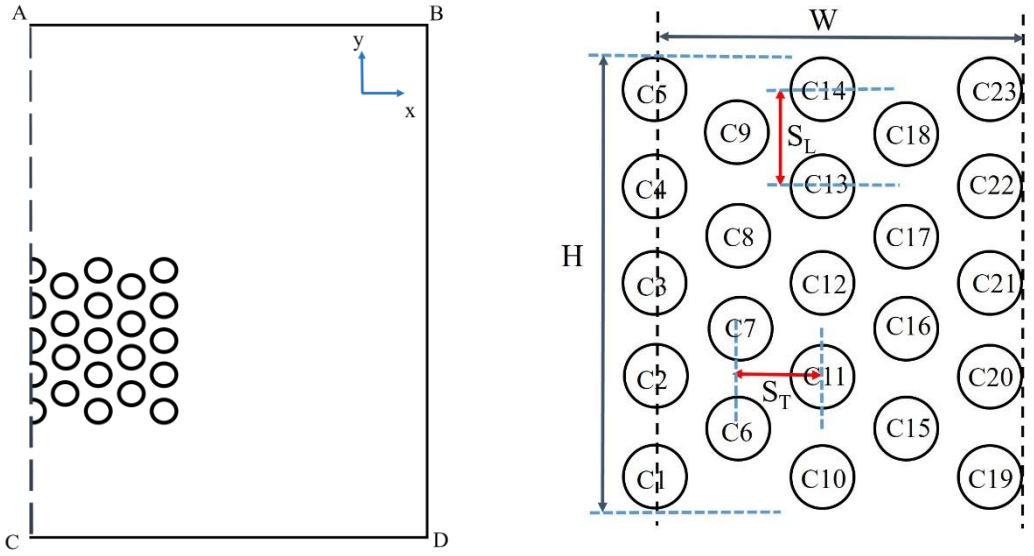

a) b)

Figure 7-14 a) Schematic of the control volume and a staggered bundle of circular cylinders, (b) geometry of the analyzed staggered bundle of 9×5 circular cylinders with cylinder numbers specified.

7-3-2. Steady-state Temperature and Velocity Distribution Around Circular Cylinders

Temperature contours for the staggered and in-line bundles of 5×9 cylinders are presented in Figure 7-15 for the two transverses spacings of S_T/D=1.2 and S_T/D=1.6, longitudinal spacing S_L/D=1.2, and $Ra_D = 10^4$. Numerical values of Nu number for individual cylinders are also given. As the results presented in Figure 7-15 show, for the

in-line arrangement and small transverse and longitudinal spacings of $S_T/D = S_L/D = 1.2$, due to the small temperature gradient between the cylinders conduction is the dominant mode of heat transfer between the cylinders located inside the bundle. In this case natural convection occurs only on the surface of the cylinders located at the bottom row and the outer semi-confined column where temperature gradient is larger. However, for the staggered arrangement, due to the larger space between the cylinders, temperature gradient between the cylinders is higher and natural convection is the dominant mode of heat transfer in the bundle including the inner cylinders. Thus, for small cylinder spacings heat transfer in a staggered bundle is higher compared to the in-line bundle. For a staggered arrangement with larger transverse spacings (i.e., $S_T/D=1.6$), the transverse spacing is comparable to or exceeds the velocity boundary layer thickness resulting in decreased through-flow resistance and, thus higher heat transfer rate compared to the in-line arrangement as shown in Figure 7-15c and d.

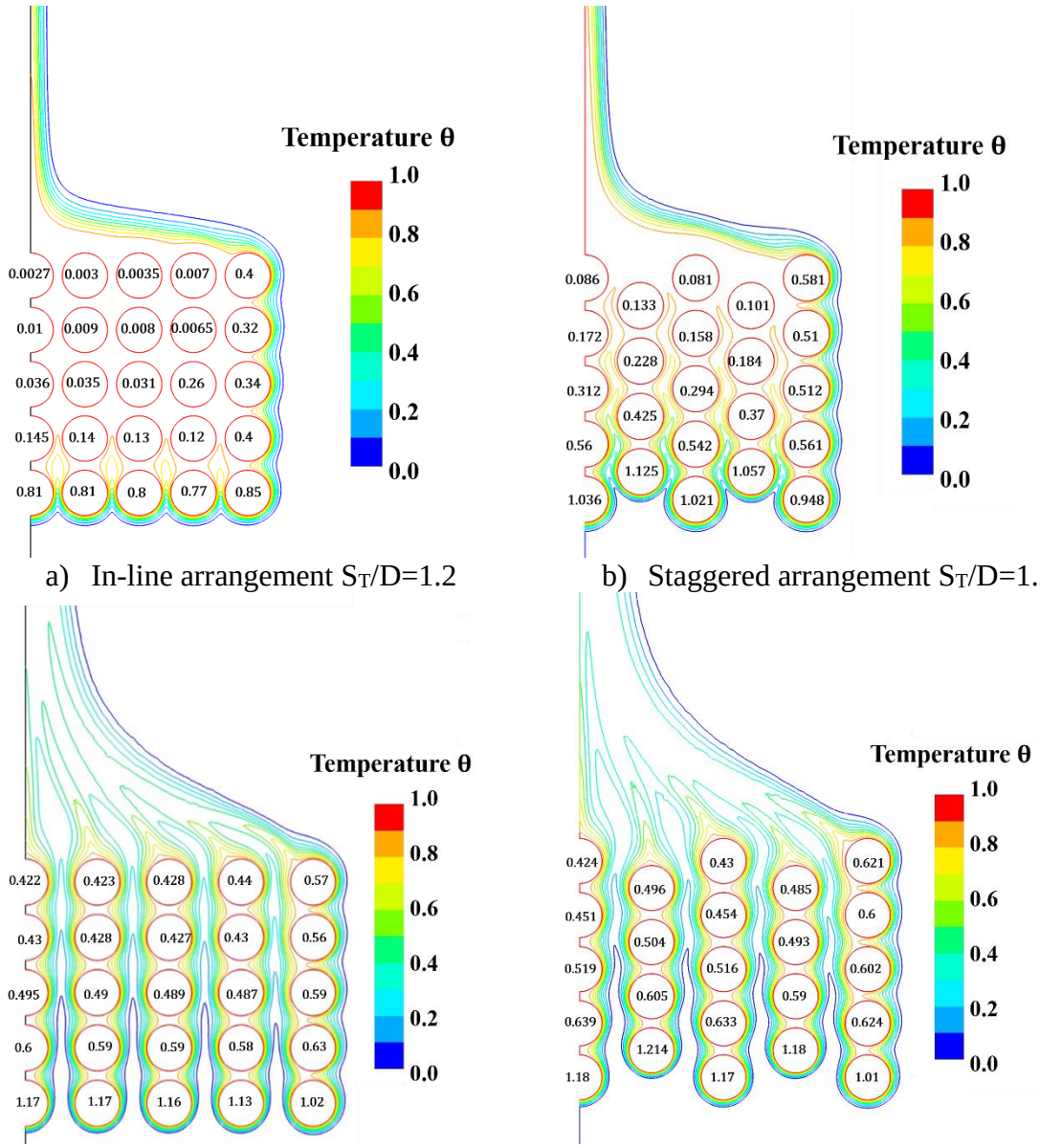

a) In-line arrangement $S_T/D=1.2$ b) Staggered arrangement $S_T/D=1.2$

c) In-line arrangement $S_T/D=1.6$ d) Staggered arrangement $S_T/D=1.6$

Figure 7-15 Dimensionless temperature contours from the in-line and staggered bundles of 5×9 cylinders for two transverse spacings of $S_T/D=1.2$ and $S_T/D=1.6$, $S_L/D=1.2$, and $Ra_D = 10^4$.

Velocity vectors presented in Figure 7-16 show that the general fluid flow behavior in the staggered bundle follows the same trend as for the in-line arrangement. For small transverse spacing of $S_T/D =1.2$, there is virtually no through flow through the bundle. The fluid flows inwards from the outer columns towards the center and becomes vertical as it

approaches the center column. For larger transverse spacing of $S_T/D = 1.6$, there is a well-established trough flow through the bundle, especially for the staggered arrangement as presented in Figure 7-16c and d.

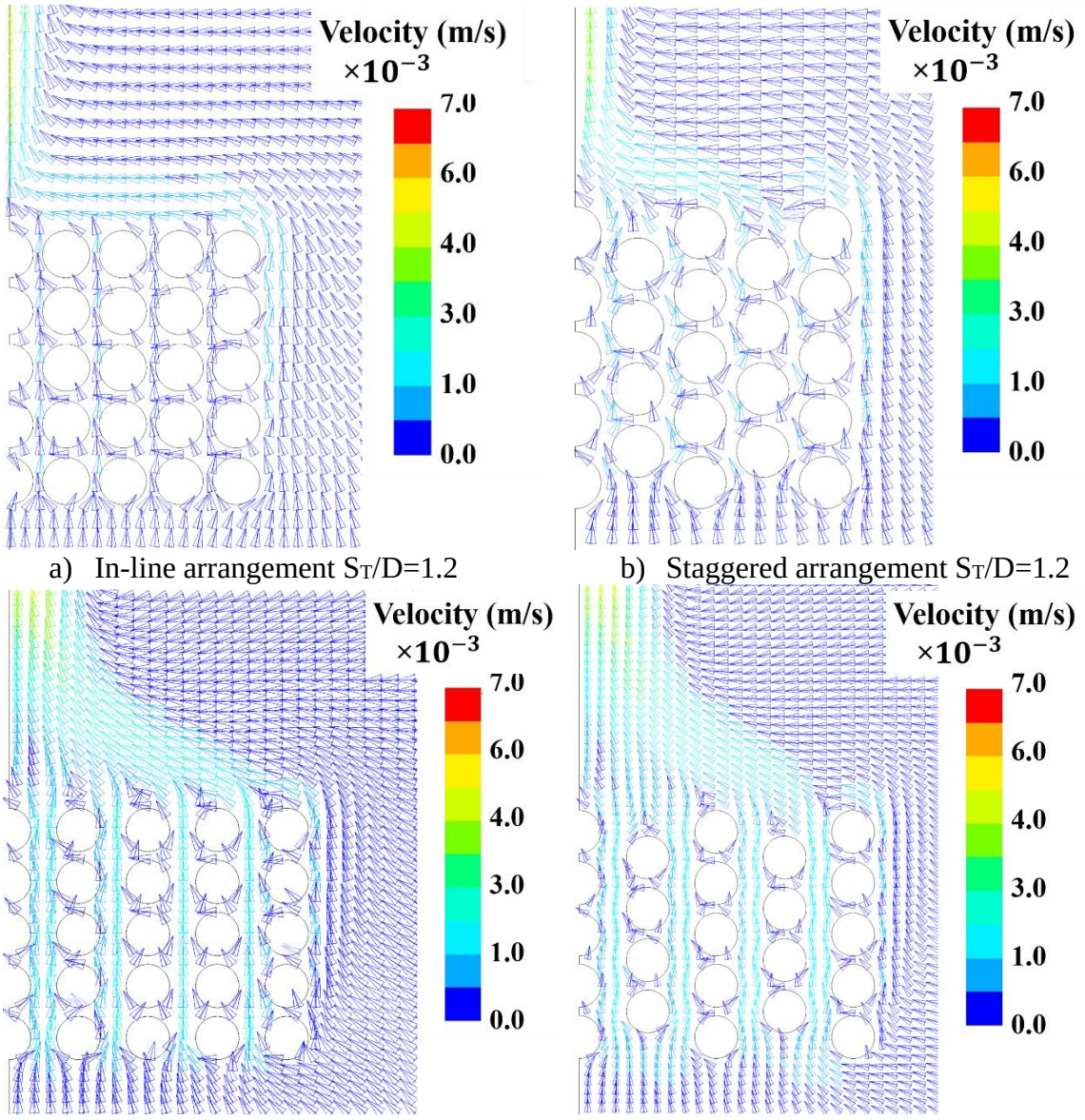

a) In-line arrangement $S_T/D=1.2$ b) Staggered arrangement $S_T/D=1.2$

c) In-line arrangement $S_T/D=1.6$ d) Staggered arrangement $S_T/D=1.6$

Figure 7-16 Velocity vectors for constant longitudinal spacing $S_L/D = 1.2$, $Ra_D = 10^4$ and two values of transverse spacings $S_T/D=1.2$ and 1.6 for the in-line and staggered arrangements.

Figure 7-17 a to d, compare temperature contours for two longitudinal spacings S_L/D=1.2 and 6, and constant transverse spacing S_T/D=1.6 for $Ra_D = 10^4$. For the in-line arrangement, as longitudinal spacing increases, distinct plumes forming around individual cylinders are interacting and eventually merging into a single plume as shown in Figure 7-17a and b. For the staggered arrangement increasing the longitudinal spacing leads to formation of distinct plumes around individual cylinders attached to the cylinder surface as shown in Figure 7-17b and c. The plumes rising from the upstream cylinders merge with the plumes from the downstream cylinders forming a cascade of plumes.

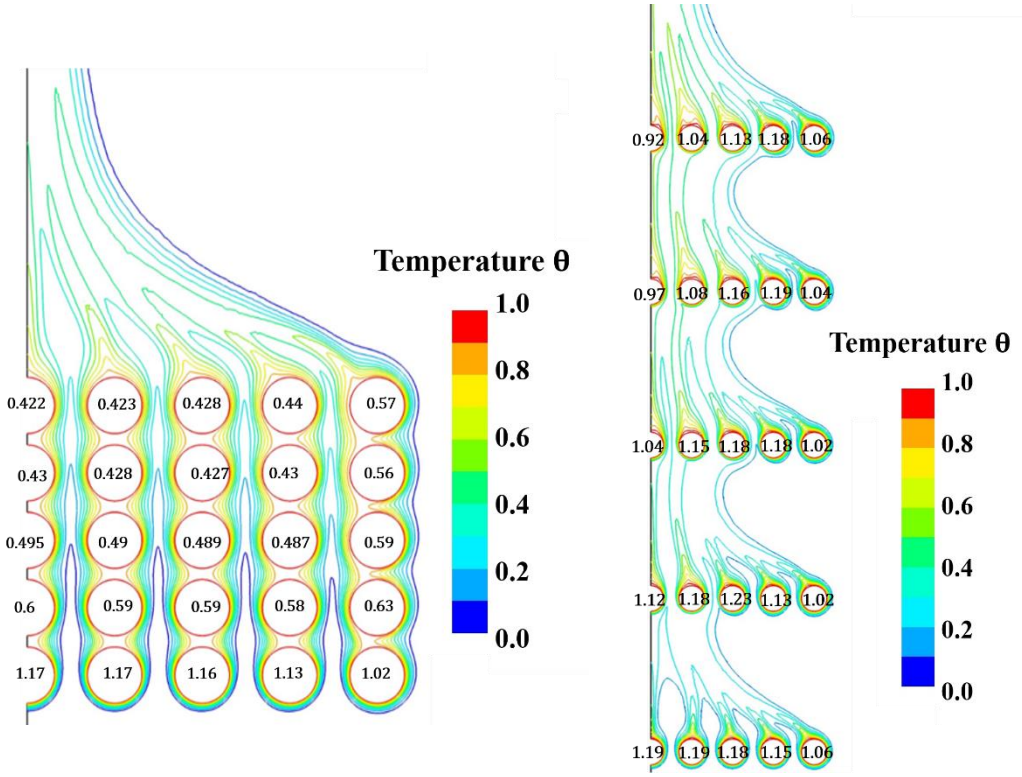

a) In-line arrangement S_L/D=1.2 b) Staggered arrangement S_L/D=6

Figure 7-17 Dimensionless temperature contours for transverse cylinder spacing S_T/D =1.6, Ra_D =10^4 and longitudinal spacings S_L/D=1.2 and 6 for the in-line and staggered 9×5 bundle.

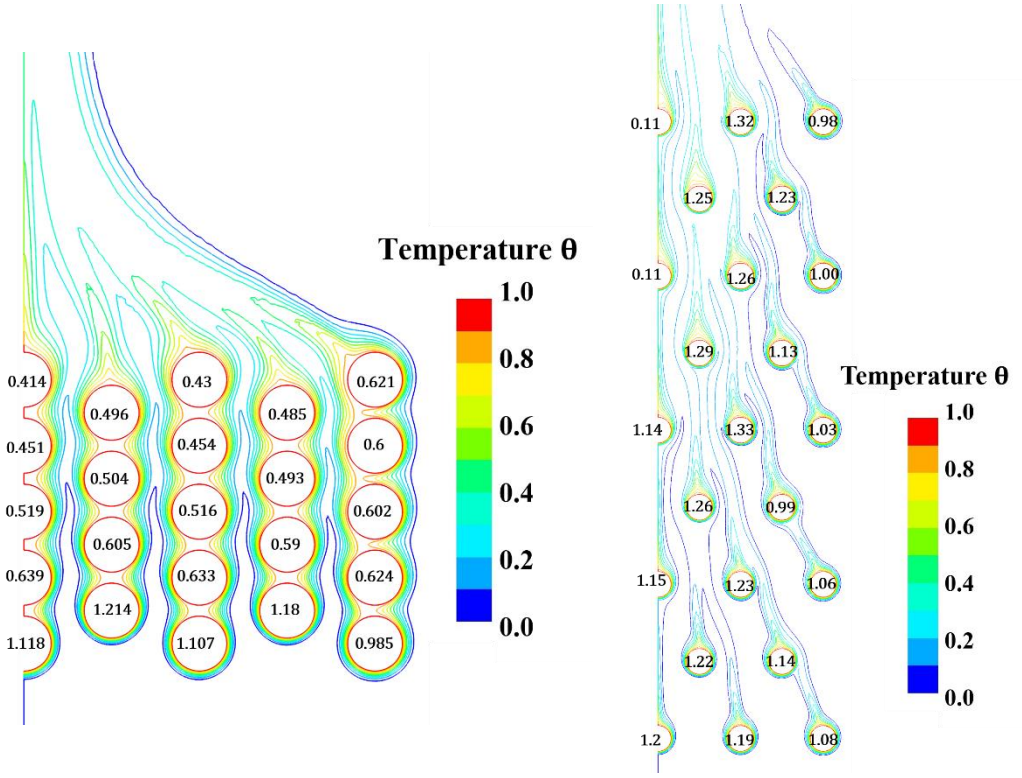

c) In-line arrangement $S_L/D=1.2$ d) Staggered arrangement $S_L/D=6$

Figure 7-17 cont.

Variation of the total average heat transfer enhancement $\overline{Nu}_D/\overline{Nu}_0$ (HTE) values for the Rayleigh number of $Ra_D = 10^4$ with transverse and longitudinal cylinder spacings in a staggered tube bundle is presented in Figure 7-18a and c. The results for the in-line bundle are shown for comparison in Figure 7-18b and d. As the results presented in Figure 7-18a and b show, variation of HTE with transverse spacing for the staggered and in-line bundles is virtually identical. However, as shown in Figure 7-18c and d, variation of HTE with longitudinal spacing for the staggered and in-line bundle geometries although having similar trend is not the same.

Similar to the in-line bundle, HTE in the staggered bundle increases as the transverse cylinder spacing S_T/D increases as shown in Figure 7-18a. For longitudinal

spacings $1.2 < S_L/D < 6$, HTE reaches maximum value in the $S_T/D = 2$ to 4 range and decreases as transverse spacing is further increased. This trend can be explained by the variation of HTE in a horizontal row of circular cylinders discussed in [98]. For the transverse spacings smaller than thickness of the velocity boundary layer, interference of the boundary layers and fluid flow between the adjacent cylinders reduces thermal gradient and heat transfer. However, this effect diminishes as transverse cylinder spacing is increased and HTE reaches its maximum value as the transverse cylinder spacing is increased to values close to the thickness of the velocity boundary layer. For transverse spacings larger than the velocity boundary layer thickness, the effect of the adjacent cylinders diminishes, and heat transfer enhancement is decreased. For small longitudinal spacings there is no maximum in HTE since heat transfer is dominated by conduction, while for $S_L/D > 6$, cylinder rows are far apart, and their interaction is weak.

Variation of the total average heat transfer enhancement HTE for $Ra_D = 10^4$ with longitudinal and transverse cylinder spacings S_L/D and S_T/D in the staggered and in-line tube bundles is presented in Figure 7-18c and d. For both geometries HTE increases monotonically as longitudinal spacing S_L/D is increased for all values of the transverse spacing S_T/D. Heat transfer enhancement is the smallest for the lowest analyzed value of longitudinal spacing S_L/D and increases as S_T/D is increased. This is same trend as for a vertical column of horizontal cylinders [99]. However, as presented in Figure 7-18c, for the staggered arrangement transverse cylinder spacing has smaller effect on the heat transfer enhancement compared to the in-line tube arrangement.

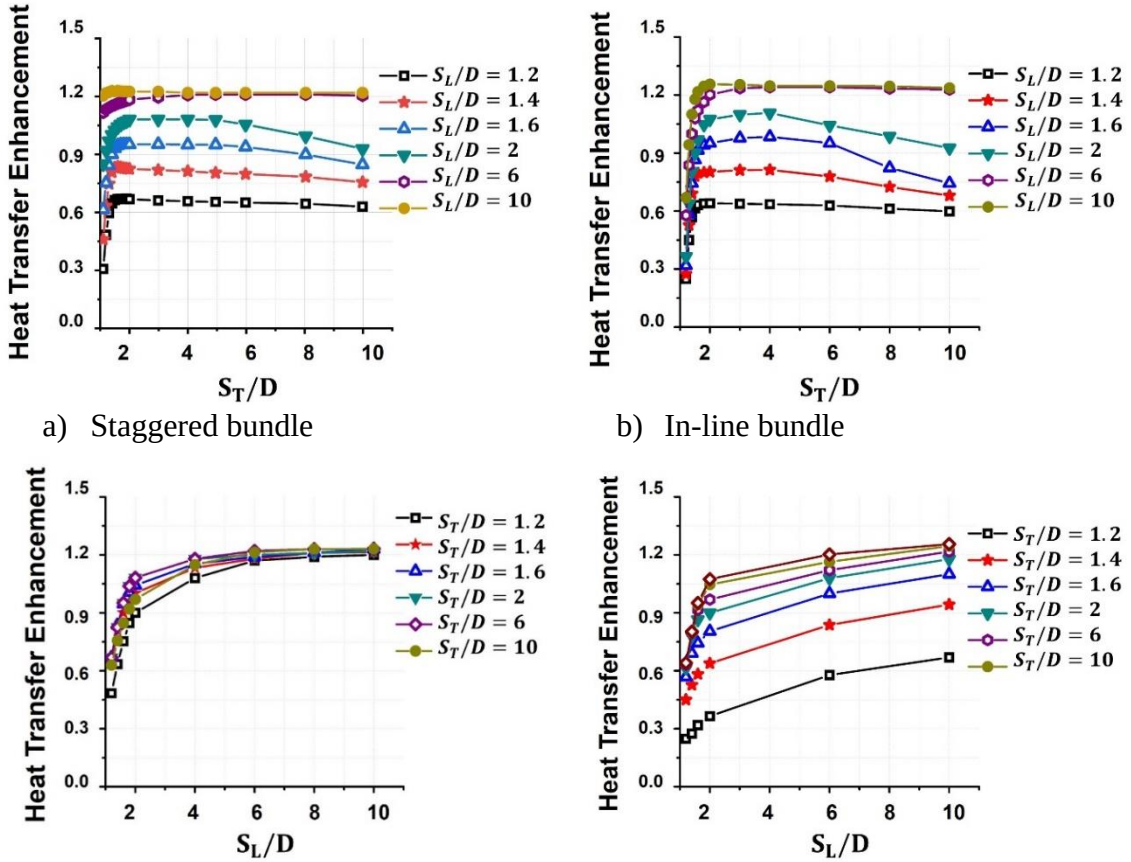

a) Staggered bundle b) In-line bundle

c) Staggered bundle d) In-line bundle

Figure 7-18 Total heat transfer enhancement vs transverse and longitudinal spacing for staggered and in-line 9×5 bundles and Rayleigh number $Ra_D = 10^4$.

As the Rayleigh number increases, longitudinal and transverse cylinder spacings S_L/D and S_T/D have a more complex effect on the flow and, therefore, on the total average heat transfer enhancement $\overline{Nu}_D/\overline{Nu}_0$.

Values of the total average heat transfer enhancement $\overline{Nu}_D/\overline{Nu}_0$ (HTE) are plotted as functions of transverse and longitudinal spacings S_T/D and S_L/D and are presented in Figure 7-19 in form of the contour diagrams (performance maps) for three Rayleigh numbers. The HTE contours show that for the range of Rayleigh numbers between $10^4 \leq Ra_D \leq 10^6$ the heat transfer enhancement follows the same trend as for $Ra_D=10^4$; HTE

monotonically increases as the longitudinal spacing S_L/D is increased. The transverse spacing, however, has a more complex effect: HTE increases as the transverse spacing S_T/D is increased, reaches a maximum value, and decreases as spacing is further increased. These trends are very similar to the variation of HTE with S_L/D, S_T/D, and Ra_D determined for the in-line arrangement [96].

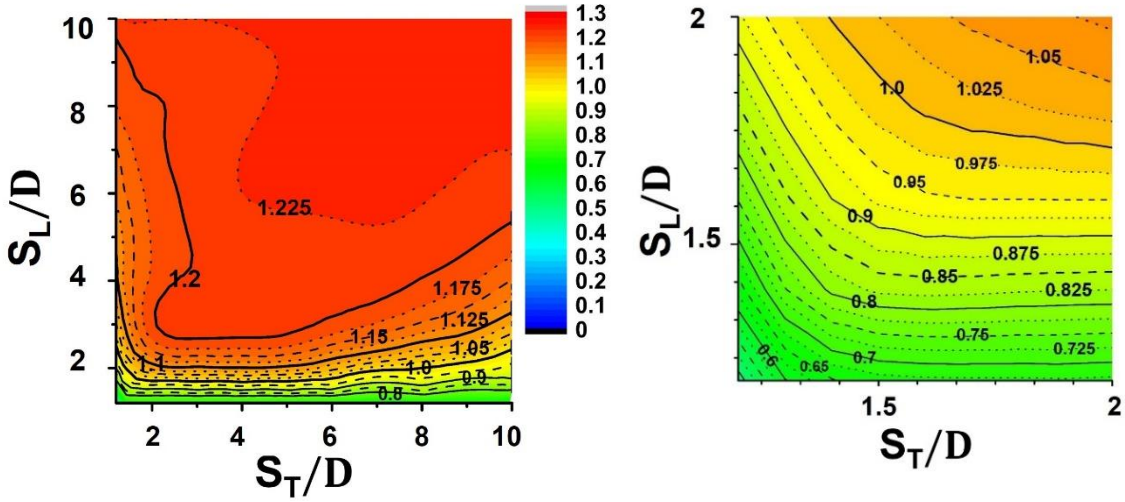

a) $Ra_D = 10^4$

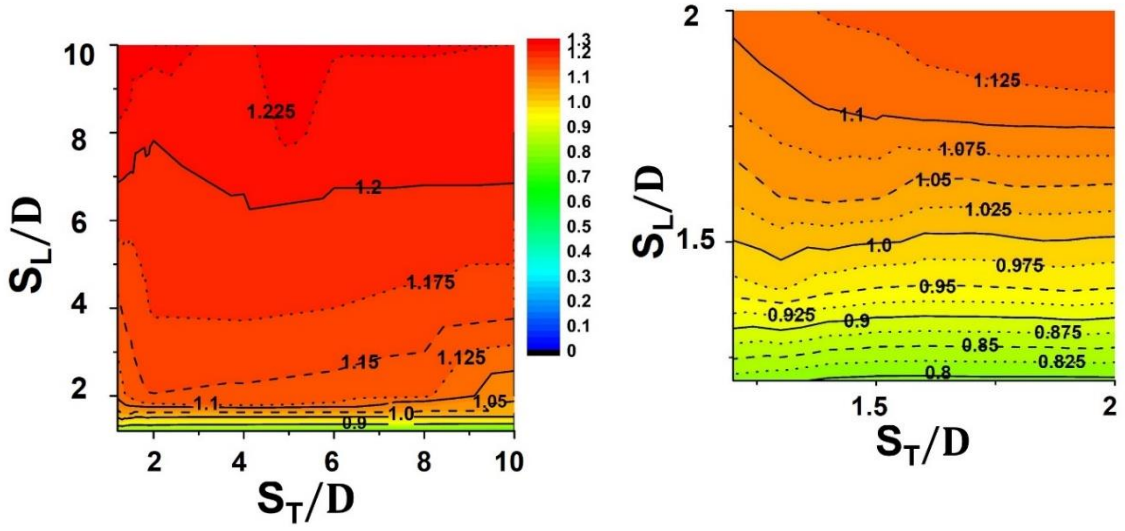

c) $Ra_D = 10^5$

Figure 7-19 Contour diagrams presenting heat transfer enhancement vs transverse and longitudinal spacing for three values of Rayleigh number and staggered arrangement.

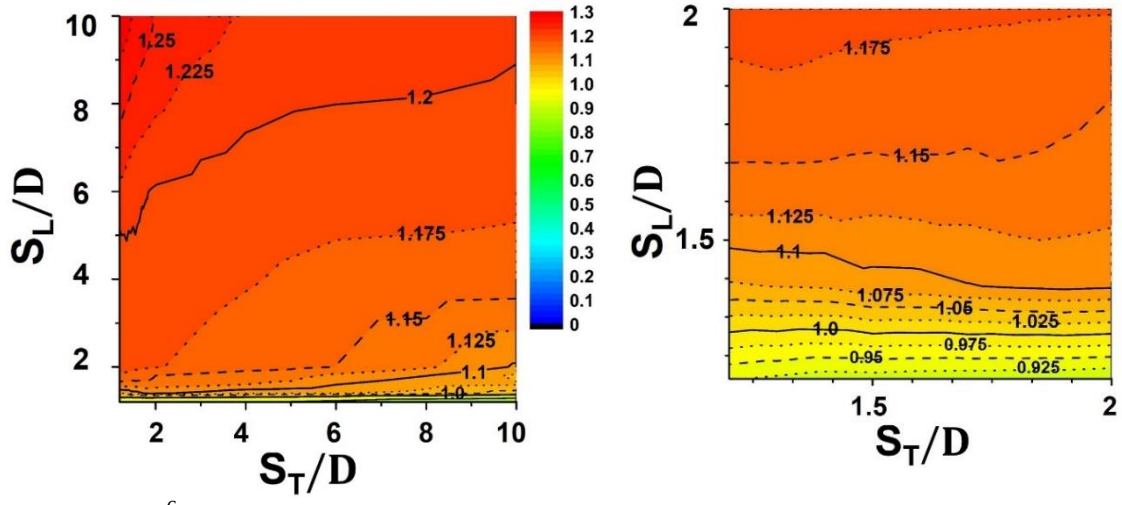

b) $Ra_D = 10^6$

Figure 7-19 cont.

Although Figure 7-18 and HTE contours presented in Figure 7-19 show there is a set of optimal longitudinal and transverse cylinder spacings $(S_L/D, S_T/D)_{opt,HTE}$ resulting in the maximum heat transfer enhancement, as discussed earlier, the objective of the heat exchanger optimization performed in this study is to determine the optimal set of the cylinder spacings $(S_L/D, S_T/D)_{opt}$ resulting in the maximum volumetric heat transfer rate and, thus minimize the size and cost of a heat exchanger. Eqn. 3-16 proposed by Bejan et al. [79] was used to calculate the dimensionless heat transfer volumetric density $\tilde{q}$ and determine the optimal set of transverse and longitudinal tube spacings in a bundle.

Values of the dimensionless heat transfer volumetric density $\tilde{q}$ are plotted as functions of the transverse and longitudinal spacings S_T/D and S_L/D and presented in Figure 7-20 in form of the contour diagrams (performance maps) for three Ra numbers; 10^4, 10^5, and 10^6. The results show there is optimal set of transverse and longitudinal spacings at which dimensionless heat transfer volumetric density $\tilde{q}$ reaches its maximum

value $\tilde{q}_{max}$. For the range of the investigated Rayleigh numbers, similar to the in-line bundle, the maximum dimensionless heat transfer volumetric density is achieved for small values of cylinder spacings. This is because although increasing cylinder spacing increases the total heat transfer rate from the bundle, this increase is smaller compared to the increase of the bundle volume HWL, thus resulting in the optimal spacing. The optimal spacing decreases as Rayleigh number is increased, and the value of $\tilde{q}_{max}$ increases with the Rayleigh number as the overall heat transfer in the bundle is increased. The results obtained for the staggered bundle are similar to the in-line bundle. However, values of $\tilde{q}_{max}$ are higher for the staggered bundle due to higher heat transfer compared to the in-line arrangement.

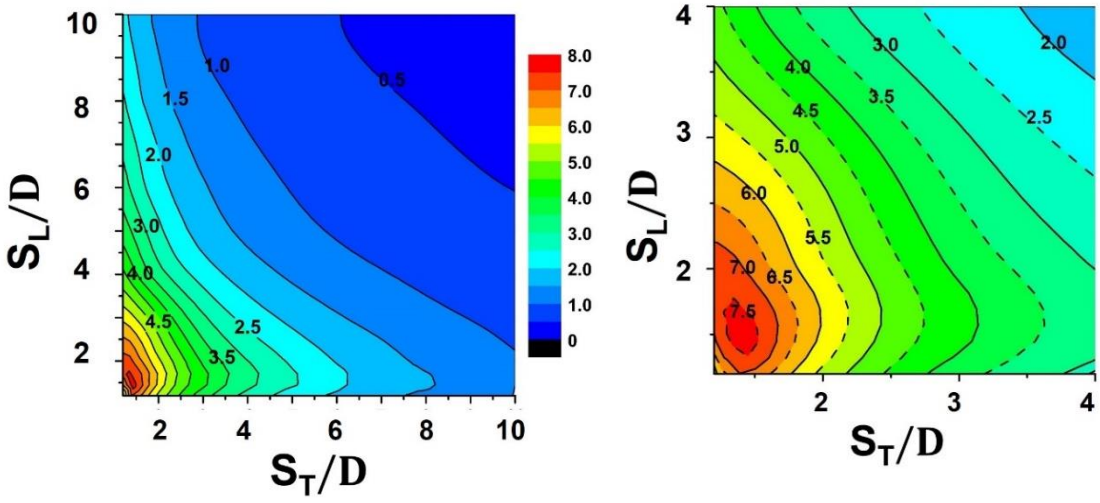

a) $Ra_D = 10^4$

Figure 7-20 Contour diagrams presenting dimensionless heat transfer volumetric density$\tilde{q}$ vs transverse and longitudinal spacing for the 9×5 staggered bundle and three Rayleigh values of number. (Right) Contour diagrams presenting $\tilde{q}$ for a smaller range of spacings.

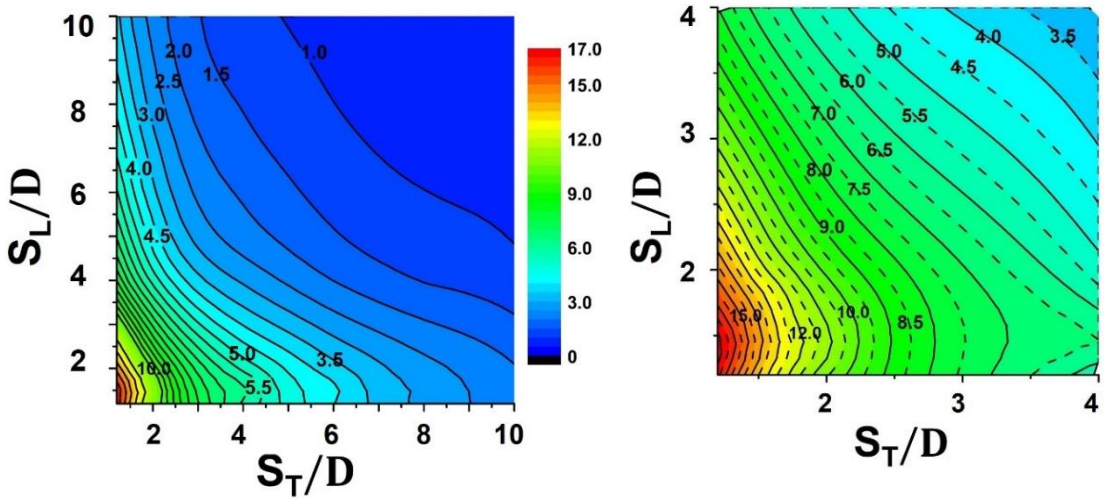

a) $Ra_D = 10^5$

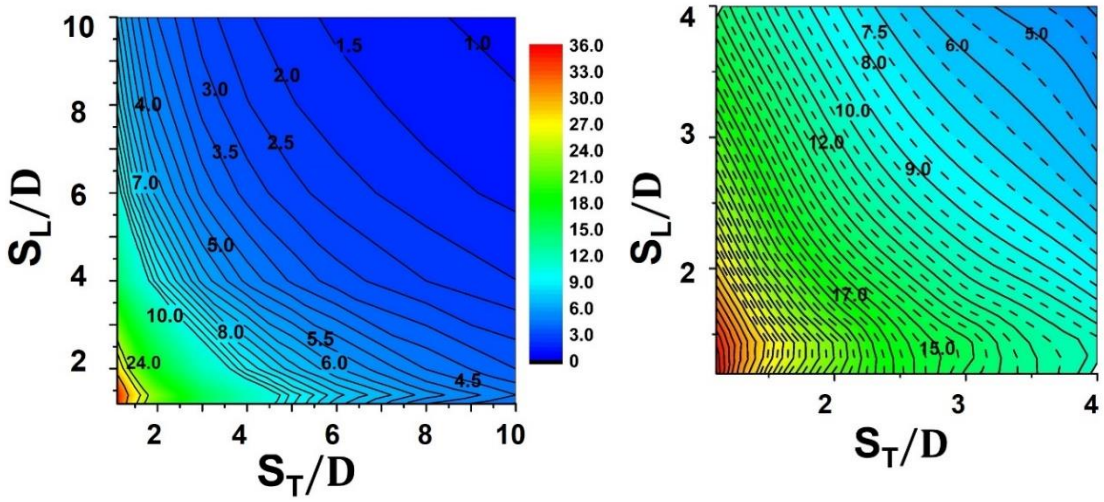

b) $Ra_D = 10^6$

Figure 7-20 cont.

Similar to the in-line bundle geometry, there are no correlations or performance maps published in the open literature for the dimensionless heat transfer volumetric density q̃ for the staggered bundle of horizontal cylinders immersed in molten solar salt. A few available correlations are either limited to a specific geometry of a bundle and specific storage medium or neglect the effect of the longitudinal and transverse spacings on heat transfer rate and, therefore, on q̃. Thus, using correlations from the literature could result

in large errors in predicting the average Nusselt number $\overline{Nu}_D$ or dimensionless heat transfer volumetric density $\tilde{q}$ for a staggered bundle. To improve design of heat exchangers used in TES and thermal systems for solar and other applications, correlations were developed in this study for the dimensionless heat transfer volumetric density $\tilde{q}$ for the 9×5 staggered bundle of horizontal cylinders immersed in molten solar salt.

Numerical results obtained in this study and statistical regression analysis were used to develop correlation for the dimensionless heat transfer volumetric density $\tilde{q}$ for the 9×5 staggered bundle of horizontal cylinders as a function of the Rayleigh number Ra_D and longitudinal and transverse cylinder spacings S_L/D and S_T/D.

The proposed form of the correlation for dimensionless heat transfer volumetric density $\tilde{q}$ for the staggered bundle of 9×5 horizontal cylinders immersed in a molten solar salt is given by Eqn. 7-5 as a function of the Ra_D number and the height and width of the bundle (shown in Figure 7-14b).

$$\tilde{q} = 20 \times \left(\frac{H}{D}\right)^{-0.77} \times \left(\frac{W}{D}\right)^{-1} \times Ra_D{}^{0.26} \qquad \text{Eqn. 7-5}$$

$$\frac{H}{D} = \left(M_y - 1\right) \times \left({}^{S_L}/_{D}\right) + 1 \qquad \text{Eqn. 7-5a}$$

$$\frac{W}{D} = \left(N_x - 1\right) \times \left({}^{S_T}/_{D}\right) + 1 \qquad \text{Eqn. 7-5b}$$

Eqn. 7-5 shows exponential variation of the dimensionless heat transfer volumetric density $\tilde{q}$ with Ra_D number and longitudinal and transverse cylinder spacing S_L/D and S_T/D and is valid for $1.2 \leq (S_L/D,\ S_T/D) \leq 10$ and $10^4 \leq Ra_D \leq 10^6$.

For comparison, the expression given by Eqn. 7-1 for $\tilde{q}$ developed in part 7-2-2 of this chapter, for the in-line bundle is:

$$\tilde{q} = 8.0 \times \left(\frac{H}{D}\right)^{-0.75} \times \left(\frac{W}{D}\right)^{-0.95} \times Ra_D{}^{0.32} \qquad \text{Eqn. 7-1}$$

Eqn. 7-5 and Eqn. 7-1 are similar, the main differences are the values of the leading constant and exponent for the Rayleigh number. The average relative error between the correlation (Eqn. 7-5) and the numerical results is less than 10.0 %.

As the results presented in Figure 7-21 show, there is a very good agreement between values of the Nusselt number obtained from numerical predictions and correlation represented by Eqn. 7-5; the maximum difference is less than 16%. The difference is the largest for the lowest analyzed Rayleigh number ($Ra_D = 10^4$) and for cylinder spacing $S_T/D \leq 2$. This is because for small Ra_D number and small cylinder spacing conduction is dominant mode of heat transfer between the cylinders. As Ra_D number and cylinder spacing increase, convection heat transfer becomes dominant.

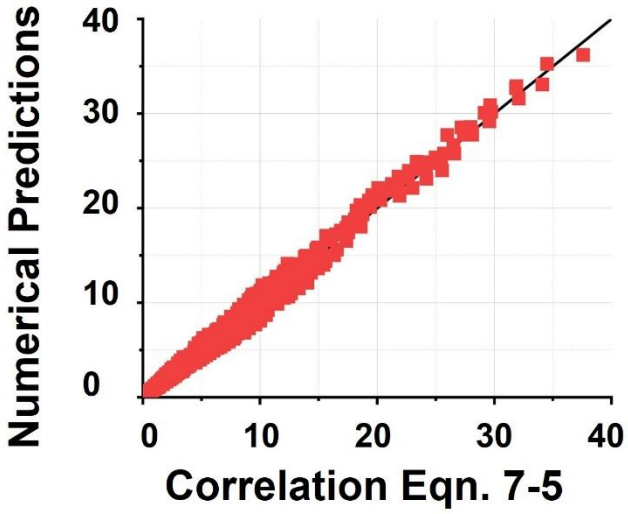

Figure 7-21 Dimensionless heat transfer volumetric density $\tilde{q}$ comparison numerical predictions vs. correlation (Eqn. 7-5).

Variation of the maximum dimensionless heat transfer volumetric density $\tilde{q}_{max}$ with transverse and longitudinal cylinder spacings S_L/D and S_T/D for three values of Rayleigh number is presented in Figure 7-22a and b. The results for the staggered bundle presented in Figure 7-22a show that for $Ra = 10^4$, $\tilde{q}_{max}$ reaches maximum value, referred to the optimal dimensionless heat transfer volumetric density $\widetilde{\mathbf{q}_{opt}}$, at the optimal transverse spacing $S_{T,opt}/D \approx 1$. For $Ra > 10^4$ there is no optimum because $\tilde{q}_{max}$ increases monotonically

as transverse spacing is reduced. In this case the value and the location of $\widetilde{q_{opt}}$ correspond to the maximum value of $\tilde{q}_{max}$ determined at the smallest analyzed transverse cylinder spacing.

Variation of $\tilde{q}_{max}$ with longitudinal spacing S_L/D presented in Figure 7-22b for the in-line and staggered arrangements shows that for $Ra < 10^6$, $\tilde{q}_{max}$ reaches maximum value for $S_{L,opt}/D \approx 1$. There is no optimum for $Ra = 10^6$, and the value and the location of $\widetilde{q_{opt}}$ correspond to the maximum value of $\tilde{q}_{max}$ determined at the smallest analyzed longitudinal cylinder spacing. Also, variation of $\tilde{q}_{max}$ with S_L/D for the staggered and in-line arrangements for the investigated Ra number range is very similar, with values of $\tilde{q}_{max}$ determined for the staggered arrangement being somewhat higher due to higher heat transfer in the staggered arrangement as discussed earlier.

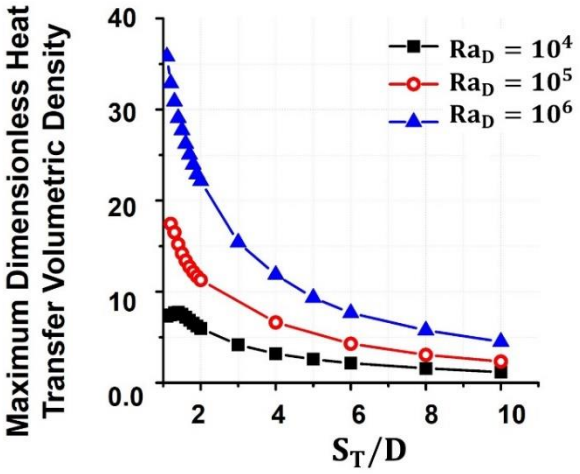

a)

Figure 7-22 Maximum dimensionless heat transfer volumetric density$\tilde{q}_{max}$ for a staggered 9×5 bundle of horizontal cylinders vs dimensionless cylinder spacing (a)Transverse spacing, (b) Longitudinal spacing.

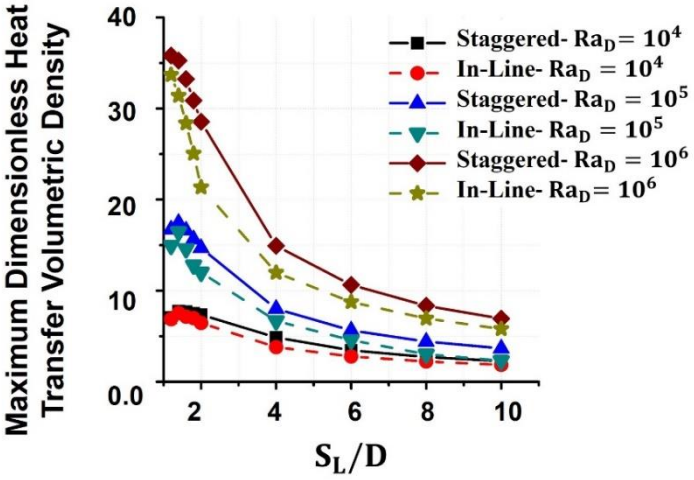

b)

Figure 7-22 cont.

The maximum dimensionless heat transfer volumetric density $\tilde{q}_{max}$ for the staggered bundle of 9×5 horizontal cylinders is plotted in Figure 7-11a as a function of dimensionless parameter $(H/D \times W/D)^{0.65} Ra_D^{-0.22}$. The value of the exponent for the Rayleigh number of -0.22 is close to -0.25 which originates from the dimensional analysis by Bejan et. al. [79]. Although they [79] used the exponent 0.3 for the height of the bundle, due to the difference in optimization objectives between this study and the study by Bejan et. al. [79], the value of 0.65 used in this study provides better fit to the data. The results presented in Figure 7-11a show that $\tilde{q}_{max}$ is an exponential function of the bundle height H and width W, and the Rayleigh number. For the Ra_D number in the $10^4 \leq Ra_D \leq 10^6$ range and $1.2 \leq (S_{L,opt}/D, S_{T,opt}/D) \leq 10$ the value of $\tilde{q}_{max}$ for the staggered bundle of 9×5 horizontal cylinders immersed in molten solar salt is given by Eqn. 7-6 as a function of the Ra_D number and the corresponding optimal height H_{opt} and width W_{opt} of the bundle. Quantities H_{opt} and W_{opt} can be determined from the contour diagrams presented in Figure 7-20.

$$\tilde{q}_{max} = 13 \times \left(\frac{H_{opt}}{D} \times \frac{W_{opt}}{D}\right)^{-0.8} \times Ra_D^{\,0.27} \qquad \text{Eqn. 7-6}$$

For example, from Figure 7-23 for $Ra_D = 10^4$ and $S_L/D = 1.5$ the maximum value of $\tilde{q}_{max} = 7.5$ occurs at $S_{T,opt}/D = 1.2$. For the 9×5 bundle substituting $S_{T,opt}/D = 1.2$ into

Eqn. 7-5a and Eqn. 7-5b gives $H_{opt}/D = 7.0$ and $W_{opt}/D = 5.3$. The value of $\tilde{q}_{max}$ calculated from Eqn. 7-6 is 7.24, which compares well with the value from Figure 7-23.

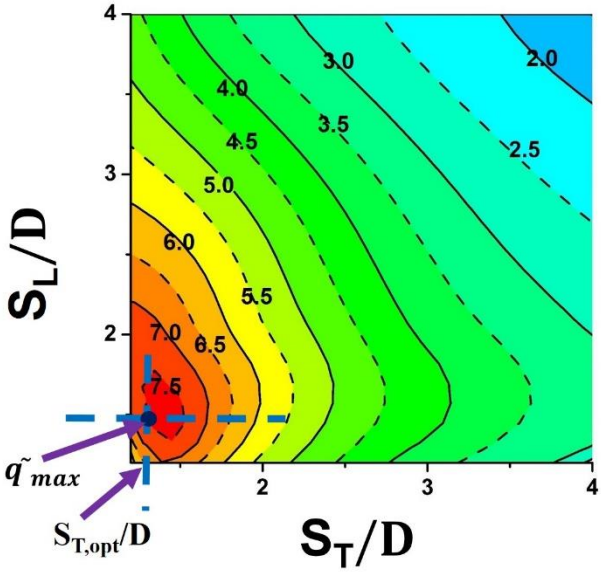

Figure 7-23 Contour diagrams presenting dimensionless heat transfer volumetric density $\tilde{q}$ vs transverse and longitudinal spacing for $Ra_D = 10^4$.

A comparison between numerical predictions and correlation represented by Eqn. 7-6 presented in Figure 7-11b shows a very good agreement between the numerical results and correlation with the average relative error of 7%.

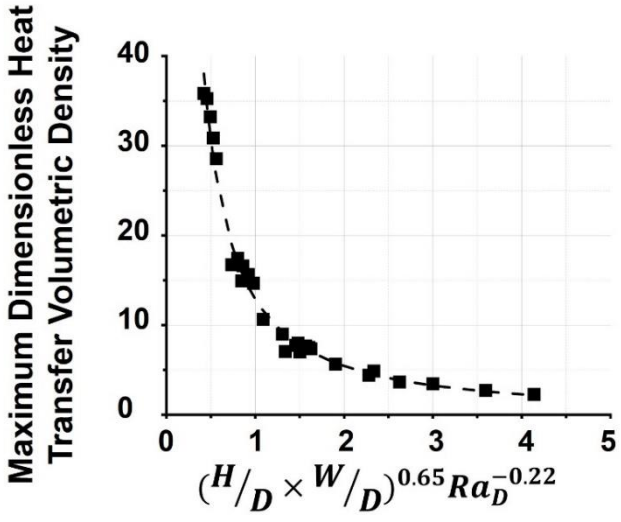

a)

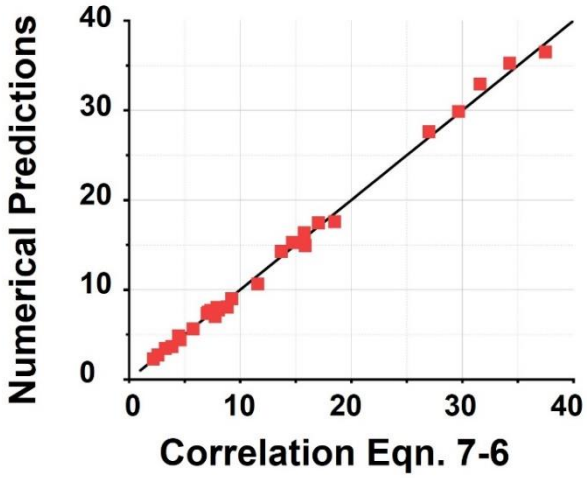

b)

Figure 7-24 a) Maximum dimensionless heat transfer volumetric density for a 9×5 staggered bundle of horizontal cylinders vs corresponding height and width of the bundle. b) Dimensionless heat transfer volumetric density $\tilde{q}$ comparison: numerical predictions vs. correlation (Eqn. 7-6).

Figure 7-22 and 7-25 show that the optimum dimensionless heat transfer volumetric density $\widetilde{q_{opt}}$ increases as the Rayleigh number increases. The relationship between the optimum dimensionless heat transfer volumetric density for a staggered bundle of horizontal cylinders and the Rayleigh number can be expressed by the Eqn. 7-7

$\tilde{q}_{opt} = 0.367\ Ra_D^{0.3327}$ Eqn. 7-7

The expression given by Eqn. 7-7 is valid for $10^4 \leq Ra_D \leq 10^6$. The average relative error between the proposed correlation and the numerical results is less than 0.05%.

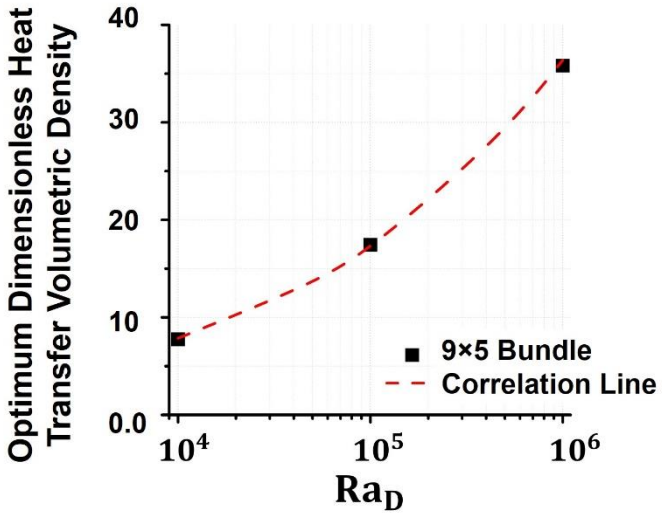

Figure 7-25 Optimum dimensionless heat transfer volumetric density $\widetilde{q_{opt}}$ vs Rayleigh number for a staggered bundle of 9 x 5 horizontal cylinders.

The presented results are strictly valid for the 9×5 staggered bundle. If used for a bundle of different size, the predicted values of the optimal heat transfer volumetric density and spacing will not be correct. Similar to the in-line bundle to estimate these errors, it was assumed that the "generalized" form of the results applicable to a staggered bundle of the infinite number of cylinders may obtained by omitting cylinders from the top row and the outer column of the 9×5 bundle from the analysis, and the resulting difference with respect to the full 9×5 bundle would be indicative of the error. Three possibilities (scenarios) in data analysis were considered: (1) the top row and outer semi-confined column were omitted, (2) the top row was omitted, and (3) the outer semi-confined column

was omitted. The results for the maximum dimensionless heat transfer volumetric density and optimal spacing for a staggered 9×5 bundle obtained for these three scenarios are compared in Figure 7-26 and Table 7-4. The results presented in Figure 7-26 show relatively small differences between the value of $\widetilde{q_{max}}$ obtained for the 9×5 bundle and values for the infinite bundle obtained for scenarios 1, 2, and 3. Also, although the location of the optimal dimensionless heat transfer volumetric density $\widetilde{q_{opt}}$ varies between the three considered scenarios, the difference is relatively small.

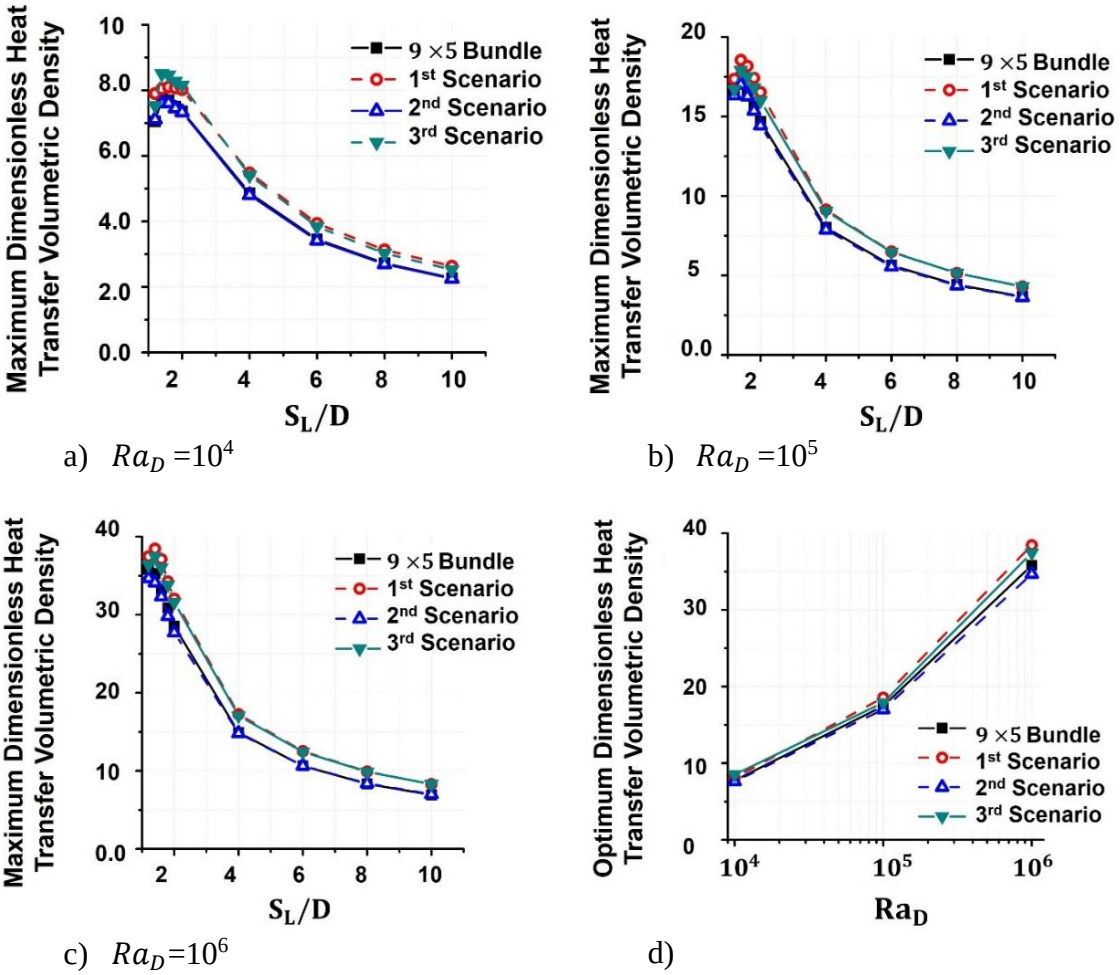

a) Ra_D =10^4 b) Ra_D =10^5

c) Ra_D=10^6 d)

Figure 7-26 Maximum dimensionless heat transfer volumetric density for a (9×5) bundle of staggered tubes and three data analysis scenarios vs longitudinal spacing for three Rayleigh numbers (a) Ra_D =10^4, (b) Ra_D=10^5, and (c) Ra_D =10^6. (d) Optimal

dimensionless heat transfer volumetric density vs Rayleigh number for a 9×5 staggered bundle and three scenarios.

Values of the optimal dimensionless heat transfer volumetric density and optimal spacing obtained for a (9×5) staggered bundle and three considered data analysis scenarios, and associated errors (differences with respect to the 9×5 bundle) are compared in Table 7-4. The results show that considering the optimal value $\widetilde{q_{opt}}$ and optimal spacing, the third scenario where the outer semi-confined column is omitted from data analysis gives the closest estimation to the values of $\widetilde{q_{opt}}$ from the 9×5 bundle, while the second scenario where the top row is omitted from data analysis gives the closest estimation for the location of the optimal spacing.

Table 7-4 Optimal dimensionless heat transfer volumetric density and optimal spacing for a (9×5) staggered bundle and three data analysis scenarios: 1st (top row and outer column omitted), 2nd (top row omitted), and 3rd (outer column omitted)

$Ra_D = 10^4$	(9×5) Bundle	1st scenario	% Difference	2nd scenario	% Difference	3rd scenario	% Difference
S_L/D_{opt}	1.4	1.6	14.3	1.6	14.3	1.4	0.0
S_T/D_{opt}	1.4	1.4	0.0	1.3	-7.14	1.4	0.0
$\widetilde{q_{opt}}$	7.74	8.1	**4.65**	7.618	**-1.6**	8.51	**9.92**
Ra_D=10^5	(9×5) Bundle	1st scenario	% Difference	2nd scenario	% Difference	3rd scenario	% Difference
S_L/D_{opt}	1.4	1.4	0.0	1.4	0.0	1.4	0.0
S_T/D_{opt}	1.2	1.2	0.0	1.2	0.0	1.2	0.0
$\widetilde{q_{opt}}$	17.45	18.56	**-6.36**	17.01	**-2.52**	17.91	**2.64**
Ra_D=10^6	(9×5) Bundle	1st scenario	% Difference	2nd scenario	% Difference	3rd scenario	% Difference
S_L/D_{opt}	1.2	1.4	16.67	1.2	0.0	1.4	16.67
S_T/D_{opt}	1.1	1.1	0.0	1.1	0.0	1.1	0.0
$\widetilde{q_{opt}}$	35.82	38.42	**-7.34**	34.67	**-3.21**	37.44	**4.52**

Contributions of this study to the relevant body of literature, summary of the main results, and conclusions are presented in the next chapter.

CHAPTER 8: SUMMARY AND CONCLUSIONS

8.1. Overview

This chapter discusses contributions of this study to the relevant body of literature, summarizes the main results, and provides recommendations for future work.

8.2. Contributions

The main contributions of this research work are the following:

8.2.1. Evaluation of the Basic Physics Associated with the Buoyancy-Induced Flow Around Different Arrangements of Heated Horizontal Cylinders.

Steady-state buoyancy-induced flow and temperature fields around isothermally heated horizontal circular cylinders with different arrangements immersed in the molten solar salt were studied to determine relevant design parameters affecting heat transfer and thermal energy storage in a TES system.

The results obtained in this study show that regardless of the arrangement of the cylinders studied in this work, Rayleigh number and dimensionless cylinder-to-cylinder spacing S/D are the main design parameters affecting heat transfer to the surrounding fluid.

An increase in the Rayleigh number results in an increase in the average Nusselt number.

The dimensionless longitudinal and transverse cylinder spacings S_L/D and S_T/D have a complex effect on the flow and heat transfer and, therefore, on the total average heat transfer enhancement $\overline{Nu}_D/\overline{Nu}_0$ (HTE). HTE monotonically increases as the longitudinal cylinder spacing S_L/D is increased. By increasing the longitudinal cylinder spacing S_L/D,

the effect of the temperature gradient between the cylinders decreases, therefore the heat transfer rate from the cylinders is increased.

Depending on the Ra number, transverse cylinder spacing S_T/D may either enhance or degrade HTE. There is an optimum value of transverse cylinder spacing $(S_T/D)_{opt}$ that is a weak function of the Ra_D number at which the average Nusselt number and HTE reach maximum values.

8.2.2. Heat transfer correlations for the analyzed cylinder arrangements.

Statistical regression analysis was performed using the results obtained in this study to develop correlations for the average $\overline{Nu}_D$ and optimum $\overline{Nu}_{D,opt}$ numbers for horizontal cylinders arranged in a single horizontal row, a single vertical column, an in-line tube bundle, and a staggered tube bundle as functions of the Rayleigh number Ra_D and dimensionless cylinder-to-cylinder spacing S/D.

Regression analysis was also used to develop correlations for the dimensionless volumetric heat transfer density $\tilde{q}$ and the maximum dimensionless volumetric heat transfer density $\tilde{q}_{max}$ as functions of the Ra_D number and cylinder-to-cylinder spacings The developed heat transfer correlations will be used for design of a more efficient heat exchanger in a TES system.

8.3. Summary of the Research

This study focused on a single-tank sensible thermal energy system integrated with a power cycle. The predicted temperature and flow fields, heat transfer enhancement, and heat transfer volumetric density were analyzed with the objective to reduce size and cost of a heat exchanger.

8.3.1. Single Row of Horizontal Cylinders

The laminar natural convection from a single row of heated horizontal circular cylinders immersed in the molten solar salt was studied to improve knowledge of heat transfer for this geometry in a TES system using molten salt as the heat storage medium and develop heat transfer correlations needed for design of a more efficient TES system.

There were no correlations found in the literature for the average Nusselt number $\overline{Nu}_D$ for a single row of horizontal cylinders. Using the existing correlations developed for natural convection heat transfer from a single cylinder would result in large errors in the average Nusselt number $\overline{Nu}_D$ for a single row of the horizontal cylinders.

The heat transfer correlations having the average error of less than 4% were developed for the $\overline{Nu}_D$ number for a single row of five and nine, and infinite number of horizontal circular cylinders immersed in molten salt as functions of the Ra_D number and dimensionless cylinder spacing S_T/D.

The developed correlation for the Nusselt number includes the power function of the Ra_D number and a natural logarithmic function of the cylinder spacing that decays to a constant value as the cylinder spacing is increased. This is because, as the distance between individual cylinders increases, they affect each other less, and eventually behave as isolated cylinders in a free flow. Correlations for the optimal cylinder spacing and heat transfer at the optimal cylinder spacing were also developed in terms of the Ra_D number.

8.3.2. One Vertical Column of Horizontal Cylinders

The laminar natural convection from a single column of heated vertical circular cylinders immersed in the molten solar salt was studied to determine heat transfer

characteristics for this geometry and develop heat transfer correlations needed for design of a more efficient heat exchanger used in a TES system.

The results show that the Rayleigh number plays a dominant role on heat transfer. An increase in the cylinder spacing increases the average heat transfer from the column, which approaches an asymptotic value for large spacings, and is a function of the Rayleigh number and the number of cylinders in a column. The results obtained in this study agree with the results from the previous studies that show that the heat transfer from the i^{th} cylinder in a vertical column of cylinders is affected only by the interactions with the upstream cylinders, and the downstream cylinders have no effect on the i^{th} cylinder.

The heat transfer correlations were developed for the average $\overline{Nu}_D$ number for a vertical column of 2 to 10 cylinders immersed in a molten solar salt, as well as for individual cylinders in the column. Nusselt number was correlated in terms of the Rayleigh number and dimensionless longitudinal cylinder-to-cylinder spacing S_L/D as an exponential function of the Rayleigh number and logarithmic function of spacing. The correlations are valid over the range of Ra_D numbers from 10^4 to 10^7 and the S_L/D range from 1.2 to 30. The average relative error of the correlation developed for the average Nusselt number for the entire column is less than 1.5%, while the relative error for individual cylinders in the column is in the 1.16 to 4.4% range depending on the cylinder location in the column.

8.3.3. Tube Bundle

The laminar natural convection from a tube bundle of 9×5 horizontal cylinders immersed in the molten solar salt was studied to determine heat transfer characteristics of

a realistic heat exchanger geometry (quantify the effect of tube arrangement and spacing) and develop heat transfer correlations needed for optimal design of a heat exchanger used in a TES system.

Numerical results obtained for both the in-line and staggered tube arrangements show that the heat transfer is a power function of the Rayleigh number and increases as the Rayleigh number increases. The longitudinal and transverse cylinder spacings S_L/D and S_T/D, however, have a complex effect on the flow and heat transfer and, thus on the total average heat transfer enhancement $\overline{Nu}_D/\overline{Nu}_0$(HTE).

HTE increases monotonically as the longitudinal cylinder spacing S_L/D is increased, which is the same behavior as for the natural convection heat transfer from a vertical column of horizontal cylinders [99]. The transverse cylinder spacing has a more complex effect on heat transfer; as the transverse cylinder spacing S_T/D is increased HTE increases reaching a maximum value. This is the same behavior as the natural convection heat transfer from a horizontal row of circular cylinders [98]. A further increase in S_T/D results in a decrease in HTE.

For the staggered arrangement, due to the larger space between the cylinders, higher temperature gradient between the cylinders and lower through-flow resistance between the cylinders, lead to higher heat transfer rate compared to the in-line arrangement.

The variation of the heat transfer enhancement for both tube arrangements shows that there is an optimal transverse cylinder spacing resulting in the highest heat transfer enhancement. The performance maps in form of contour diagrams were developed for the total average heat transfer enhancement $\overline{Nu}_D/\overline{Nu}_0$ and dimensionless heat transfer

volumetric density $\tilde{q}$ as functions of the transverse and longitudinal spacings S_T/D and S_L/D for three values of Rayleigh numbers Ra_D.

The heat transfer enhancement increases as Rayleigh number is increased; therefore, the dimensionless heat transfer volumetric density reaches maximum value at smaller values of transverse and longitudinal spacing.

Correlations for $\tilde{q}$ for both tube arrangements were developed as functions of the Rayleigh number and longitudinal and transverse cylinder spacings. The heat transfer enhancement increases as the Rayleigh number is increased; therefore, the dimensionless heat transfer volumetric density reaches maximum value at smaller values of transverse and longitudinal spacing.

The heat exchanger geometry was optimized by determining the optimal set of the tube (cylinder) spacings S_L/D and S_T/D in the tube bundle resulting in the maximum volumetric heat transfer rate, smallest size, and lowest cost of a heat exchanger. A set of correlations was also developed for the maximum and optimum dimensionless heat transfer volumetric densities as functions of the Rayleigh number Ra_D.

The generalized form of the results applicable to the in-line bundle of the infinite number of cylinders was obtained by omitting the top and semi-confined edge cylinders from the dimensionless heat transfer volumetric density analysis. The value of the maximum dimensionless heat transfer volumetric density and optimal spacing are the same for the 9×5 tube bundle and tube bundle comprising the infinite number of tubes.

Also, the generalized form of the results applicable to a staggered bundle of the infinite number of cylinders was obtained by omitting the semi-confined top and edge

cylinders from the analysis. The results show that omitting the outer semi-confined column from data the analysis gives the closest estimation to the values of $\widetilde{q_{opt}}$ from the 9×5 bundle, while omitting the top row from the data analysis gives the closest estimation for the location of the optimal spacing.

8.4. Recommendations for Future Research

This study focused on numerical analysis of a steady-state 2D sensible thermal energy storage system comprising a heat exchanger with different cylinder configurations and laminar regime of flow. It is recommended that future computational efforts extend the analysis to evaluating the natural convection heat transfer at conditions more akin to those present in sensible thermal energy storage systems.

Turbulent flow and wider range of Ra_D, higher operational temperatures, and different numbers of cylinders are the examples of the possible future studies. This would make it possible to verify computational investigations against experimental or industrial data.

Another recommendation is to perform the analysis for the candidate heat storage fluids and to evaluate other commercially available TES fluids to determine the effect of their thermo-physical properties on TES performance. The results from the sensitivity analysis can be used to determine thermo-physical properties of an ideal energy storage fluid suitable for high-temperature TES systems.

REFERENCES

1. Inc., A., ANSYS Workbench 17.0.
2. Adapco, C., StarCCM+.
3. Zhang, H., et al., Concentrated solar power plants: Review and design methodology. Renewable and sustainable energy reviews, 2013. **22**: p. 466-481.
4. Ali, T., et al., Study on thermal-fluid effect of thermal energy storage tank design in solar energy applications. Energy Procedia, 2015. **68**: p. 3-11.
5. Kalaiselvam, S. and R. Parameshwaran, Thermal Energy Storage Technologies for Sustainability: Systems Design, Assessment and Applications. 2014: Elsevier.
6. Irena, I., Renewable energy technologies: Cost analysis series. Concentrating solar power, 2012.
7. Machinda, G., et al. Concentrating solar thermal power technologies: a review. in India Conference (INDICON), 2011 Annual IEEE. 2011. IEEE.
8. AndrewBuck, B.
9. Ravaghi-Ardebilli, Z., et al., Study of direct thermal energy storage technologies for effectiveness of concentrating solar power plants. The Italian Association of Chemical Engineering (AIDIC), 2013. **32**.
10. Gil, A., et al., State of the art on high temperature thermal energy storage for power generation. Part 1—Concepts, materials and modellization. Renewable and Sustainable Energy Reviews, 2010. **14**(1): p. 31-55.
11. Kuravi, S., et al., Thermal energy storage technologies and systems for concentrating solar power plants. Progress in Energy and Combustion Science, 2013. **39**(4): p. 285-319.
12. Mouawad, J., The newest hybrid model. The New York Times, 2010. **4**.
13. Nallusamy, N. and R. Velraj, Numerical and experimental investigation on a combined sensible and latent heat storage unit integrated with solar water heating system. Journal of solar energy engineering, 2009. **131**(4): p. 041002.
14. Herrmann, U. and D.W. Kearney, Survey of thermal energy storage for parabolic trough power plants. TRANSACTIONS-AMERICAN SOCIETY OF MECHANICAL ENGINEERS JOURNAL OF SOLAR ENERGY ENGINEERING, 2002. **124**(2): p. 145-152.
15. Zheng, Y., Thermal Energy Storage with Encapsulated Phase Change Materials for High Temperature Applications. 2015.
16. Goswami, D.Y., F. Kreith, and J.F. Kreider, Principles of solar engineering. 2000: CRC Press.
17. Tamme, R., et al., Thermal Energy Storage thermal energy storage, in Encyclopedia of Sustainability Science and Technology, R.A. Meyers, Editor. 2012, Springer New York: New York, NY. p. 10551-10577.
18. Cabeza, L.F., Thermal energy storage. Comprehensive renewable energy, 2012. **3**: p. 211-253.
19. Timilsina, G.R., L. Kurdgelashvili, and P.A. Narbel, A review of solar energy: markets, economics and policies. 2011.

20. Vaivudh, S., W. Rakwichian, and S. Chindaruksa, Heat transfer of high thermal energy storage with heat exchanger for solar trough power plant. Energy conversion and management, 2008. **49**(11): p. 3311-3317.
21. Kang, Y., et al., A general model for analyzing the thermal characteristics of a class of latent heat thermal energy storage system. Journal of Solar Energy Engineering-Transactions of the ASME, 1999. **121**(4): p. 185-193.
22. Stine, W.B., Power from the sun: principles of high temperature solar thermal technology. 1987, Solar Energy Research Inst., Golden, CO (USA).
23. Steinmetz, G.
24. NREL. Available from: https://www.nrel.gov/csp/solarpaces/.
25. ANGELINI, G., Numerical modelling of molten salt thermocline storage systems: feasibility and criteria for performance improvement. 2013.
26. Brosseau, D., et al. Testing of thermocline filler materials and molten-salt heat transfer fluids for thermal energy storage systems in parabolic trough power plants. in ASME 2004 International Solar Energy Conference. 2004. American Society of Mechanical Engineers.
27. Levine, J.G., Large energy storage systems handbook. 2011: CRC press.
28. Bai, F. and C. Xu, Performance analysis of a two-stage thermal energy storage system using concrete and steam accumulator. Applied Thermal Engineering, 2011. **31**(14): p. 2764-2771.
29. Buschle, J., W.-D. Steinmann, and R. Tamme. Analysis of steam storage systems using Modelica. in Proceedings 5th Modelica Conference 2006. 2006.
30. Beasley, D.E. and J.A. Clark, Transient response of a packed bed for thermal energy storage. International Journal of Heat and Mass Transfer, 1984. **27**(9): p. 1659-1669.
31. Dincer, I., S. Dost, and X. Li, Performance analyses of sensible heat storage systems for thermal applications. International Journal of Energy Research, 1997. **21**(12): p. 1157-1171.
32. Collares-Pereira, M., et al., Design and optimization of solar industrial hot water systems with storage. Solar Energy, 1984. **32**(1): p. 121-133.
33. Sodha, M., et al., EXPERIMENTAL PERFORMANCE OF BUILT-IN-STORAGE SOLAR WATER HEATING SYSTEMS IN LABORATORY AND FIELD CONDITIONS. International journal of energy research, 1997. **21**(3): p. 275-287.
34. Reddy, K., et al., Phosphorus retention in streams and wetlands: a review. Critical reviews in environmental science and technology, 1999. **29**(1): p. 83-146.
35. Menghare, Y.M. and Y. Jibhakate. Review on Sensible Heat Storage System Principle, Performance and Analysis. in International Journal of Engineering Research and Technology. 2013. IJERT.
36. Domański, R. and G. Fellah, Thermoeconomic analysis of sensible heat, thermal energy storage systems. Applied thermal engineering, 1998. **18**(8): p. 693-704.
37. Badar, M.A., S.M. Zubair, and A.A. Al-Farayedhi, Second-law-based thermoeconomic optimization of a sensible heat thermal energy storage system. Energy, 1993. **18**(6): p. 641-649.

38. Kuznetsov, A., A perturbation solution for heating a rectangular sensible heat storage packed bed with a constant temperature at the walls. International journal of heat and mass transfer, 1997. **40**(5): p. 1001-1006.
39. Prasad, A. and J. Nandi, A transient, conjugated, conduction-controlled, sensible-heat storage. Energy, 1992. **17**(4): p. 413-417.
40. Nallusamy, N., S. Sampath, and R. Velraj, Experimental investigation on a combined sensible and latent heat storage system integrated with constant/varying (solar) heat sources. Renewable Energy, 2007. **32**(7): p. 1206-1227.
41. Navarro, M.E., et al., Selection and characterization of recycled materials for sensible thermal energy storage. Solar Energy Materials and Solar Cells, 2012. **107**: p. 131-135.
42. Bauer, T., et al., Material aspects of Solar Salt for sensible heat storage. Applied energy, 2013. **111**: p. 1114-1119.
43. Medrano, M., et al., State of the art on high-temperature thermal energy storage for power generation. Part 2—Case studies. Renewable and Sustainable Energy Reviews, 2010. **14**(1): p. 56-72.
44. Fernandez, A., et al., Selection of materials with potential in sensible thermal energy storage. Solar Energy Materials and Solar Cells, 2010. **94**(10): p. 1723-1729.
45. Ferone, C., et al., Finite element method modeling of sensible heat thermal energy storage with innovative concretes and comparative analysis with literature benchmarks. Energies, 2014. **7**(8): p. 5291-5316.
46. Hasnain, S., Review on sustainable thermal energy storage technologies, Part I: heat storage materials and techniques. Energy conversion and management, 1998. **39**(11): p. 1127-1138.
47. Bradshaw, R.W., J.G. Cordaro, and N.P. Siegel. Molten nitrate salt development for thermal energy storage in parabolic trough solar power systems. in ASME 2009 3rd International Conference on Energy Sustainability collocated with the Heat Transfer and InterPACK09 Conferences. 2009. American Society of Mechanical Engineers.
48. Kearney, D., U. Herrmann, and P. Nava, Assessment of a molten salt heat transfer fluid in a parabolic trough solar field. Methodology, 2002. **2**: p. 3.
49. Xu, C., et al., Sensitivity analysis of the numerical study on the thermal performance of a packed-bed molten salt thermocline thermal storage system. Applied Energy, 2012. **92**: p. 65-75.
50. Energy, A.S.; Available from: http://www.archimedesolarenergy.it/molten_salt.htm.
51. Kuehn, T.H. and R.J. Goldstein, Numerical solution to the Navier-Stokes equations for laminar natural convection about a horizontal isothermal circular cylinder. International Journal of Heat and Mass Transfer, 1980. **23**(7): p. 971-979.
52. Clifford, C.E. and M.L. Kimber, Optimizing laminar natural convection for a heat generating cylinder in a channel. Journal of Heat Transfer, 2014. **136**(11): p. 112502.

53. Morgan, V.T., The overall convective heat transfer from smooth circular cylinders. Advances in heat transfer, 1975. **11**: p. 199-264.
54. Fand, R.M., E. Morris, and M. Lum, Natural convection heat transfer from horizontal cylinders to air, water and silicone oils for Rayleigh numbers between 3× 10 2 and 2× 10 7. International Journal of Heat and Mass Transfer, 1977. **20**(11): p. 1173-1184.
55. Lu, Y., et al., Natural convection heat transfer of molten salts around a vertically aligned horizontal cylinder set. International Communications in Heat and Mass Transfer, 2016. **76**: p. 147-155.
56. Corcione, M., Correlating equations for free convection heat transfer from horizontal isothermal cylinders set in a vertical array. International Journal of Heat and Mass Transfer, 2005. **48**(17): p. 3660-3673.
57. Ivanov, N., et al. Numerical modeling of buoyancy-induced fluid flow and heat transfer in a staggered tube bank. in 2010 14th International Heat Transfer Conference. 2010. American Society of Mechanical Engineers.
58. Inc., A., ANSYS introductory FLUENT training booklet.
59. T.Bello-Ochende, A.B., Constructal multi-scale cylinders with natural convection. nternational Journal of Heat and Mass Transfer, 2005. **48**(21): p. 4300-4306.
60. Kitamura, K., et al., Fluid flow and heat transfer of natural convection induced around a vertical row of heated horizontal cylinders. International Journal of Heat and Mass Transfer, 2016. **92**: p. 414-429.
61. Kanimozhi, B., et al., Review On Heat Transfer Enhancement Techniques in Thermal Energy Storage Systems. International Journal of Engineering Research and Applications, 2014. **4**(2): p. 144-149.
62. Fand, R.M. and J. Brucker, A correlation for heat transfer by natural convection from horizontal cylinders that accounts for viscous dissipation. International Journal of Heat and Mass Transfer, 1983. **26**(5): p. 709-716.
63. Kuehn, T. and R. Goldstein, Correlating equations for natural convection heat transfer between horizontal circular cylinders. International Journal of Heat and Mass Transfer, 1976. **19**(10): p. 1127-1134.
64. Seiichi, N. and O. Takuro, Heat transfer from a horizontal circular wire at small Reynolds and Grashof numbers—I: pure convection. International Journal of Heat and Mass Transfer, 1975. **18**(3): p. 387-396.
65. Seiichi, N. and O. Takuro, Heat transfer from a horizontal circular wire at small reynolds and grashof numbers—II: Mixed convection. International Journal of Heat and Mass Transfer, 1975. **18**(3): p. 397-413.
66. Churchill, S.W., Laminar free convection from a horizontal cylinder with a uniform heat flux density. Letters in Heat and Mass Transfer, 1974. **1**(2): p. 109-111.
67. Tsubouchi, T. and H. Masuda, Heat transfer by natural convection from horizontal cylinders at low Rayleigh numbers. Rep Inst High Speed Mech, 1967. **19**(190): p. 205-219.

68. Lu, Y., et al., Numerical simulation and experimental investigation of natural convection heat transfer of molten salt around fine wire. Science China Technological Sciences, 2013. **56**(7): p. 1651-1656.
69. Churchill, S.W. and H.H. Chu, Correlating equations for laminar and turbulent free convection from a horizontal cylinder. International journal of heat and mass transfer, 1975. **18**(9): p. 1049-1053.
70. Cesini, G., et al., Natural convection from a horizontal cylinder in a rectangular cavity. International Journal of Heat and Mass Transfer, 1999. **42**(10): p. 1801-1811.
71. Alinnawi, F.H.A., A.S.N. Alsaegh, and N.A. Hussein, Laminar Natural Convection In Square Enclosure Containing Different Cross Sections Of Inner Pipes With Internal Heat Generation. Energy. **2**: p. 3.
72. Kim, B., et al., A numerical study of natural convection in a square enclosure with a circular cylinder at different vertical locations. International Journal of Heat and Mass Transfer, 2008. **51**(7): p. 1888-1906.
73. Roychowdhury, D., S.K. Das, and T. Sundararajan, Numerical simulation of natural convective heat transfer and fluid flow around a heated cylinder inside an enclosure. Heat and mass transfer, 2002. **38**(7-8): p. 565-576.
74. Farouk, B. and S. Güçeri, Natural convection from horizontal cylinders in interacting flow fields. International Journal of Heat and Mass Transfer, 1983. **26**(2): p. 231-243.
75. Cianfrini, C., M. Corcione, and E. Habib, Natural convection from multiple horizontal cylinders arranged side by side. HEFAT 2007.
76. Warrington, R. and G. Crupper, Natural convection heat transfer between cylindrical tube bundles and a cubical enclosure. Journal of Heat Transfer, 1981. **103**(1): p. 103-107.
77. Chouikh, R., et al., Numerical study of the laminar natural convection flow around an array of two horizontal isothermal cylinders. International communications in heat and mass transfer, 1999. **26**(3): p. 329-338.
78. Sparrow, E. and J. Niethammer, Effect of vertical separation distance and cylinder-to-cylinder temperature imbalance on natural convection for a pair of horizontal cylinders. Journal of Heat Transfer, 1981. **103**(4): p. 638-644.
79. Bejan, A., A.J. Fowler, and G. Stanescu, The optimal spacing between horizontal cylinders in a fixed volume cooled by natural convection. International journal of heat and mass transfer, 1995. **38**(11): p. 2047-2055.
80. Sadeghipour, M.S. and M. Asheghi, Free convection heat transfer from arrays of vertically separated horizontal cylinders at low Rayleigh numbers. International journal of heat and mass transfer, 1994. **37**(1): p. 103-109.
81. Ashjaee, M. and T. Yousefi, Experimental study of free convection heat transfer from horizontal isothermal cylinders arranged in vertical and inclined arrays. Heat transfer engineering, 2007. **28**(5): p. 460-471.
82. Tokura, I., et al., An experimental study of free convection heat transfer from a horizontal cylinder in a vertical array set in free space between parallel walls. Journal of Heat Transfer, 1983. **105**(1): p. 102-107.

83. Hannani, S.K., M. Sadeghipour, and M. Nazaktabar, Natural convection heat transfer from horizontal cylinders in a vertical array confined between parallel walls. International Journal of Engineering, 2002. **15**(3): p. 293-302.
84. Warrington, R., et al., Boundary effects on natural convection heat transfer for cylinders and cubes. International journal of heat and mass transfer, 1988. **31**(6): p. 1322-1325.
85. Persoons, T., et al., Natural convection heat transfer and fluid dynamics for a pair of vertically aligned isothermal horizontal cylinders. International Journal of Heat and Mass Transfer, 2011. **54**(25): p. 5163-5172.
86. Dhaubhadel, M., J. Reddy, and D. Telionis, Penalty finite-element analysis of coupled fluid flow and heat transfer for in-line bundle of cylinders in cross flow. International journal of non-linear mechanics, 1986. **21**(5): p. 361-373.
87. Wung, T.-S. and C.J. Chen, Finite analytic solution of convective heat transfer for tube arrays in crossflow: Part I—Flow field analysis. Journal of Heat Transfer, 1989. **111**(3): p. 633-640.
88. Chen, C.J. and T.-S. Wung, Finite analytic solution of convective heat transfer for tube arrays in crossflow: Part II—Heat transfer analysis. Journal of Heat Transfer, 1989. **111**(3): p. 641-648.
89. Li, J.-W. and M.M. Chen, Computations of 2-D and 3-D regular arrays of cylinders and spheres in a flow field. Convective Heat Transfer in the Presence of an Obstructing Medium, 1990.
90. Wang, M. and J.G. Georgiadis, Conjugate forced convection in crossflow over a cylinder array with volumetric heating. International journal of heat and mass transfer, 1996. **39**(7): p. 1351-1361.
91. Bejan, A., The optimal spacing for cylinders in crossflow forced convection. Journal of heat transfer, 1995. **117**(3): p. 767-770.
92. Stanescu, G., A. Fowler, and A. Bejan, The optimal spacing of cylinders in free-stream cross-flow forced convection. International Journal of Heat and Mass Transfer, 1996. **39**(2): p. 311-317.
93. Tahseen, T.A., M. Ishak, and M. Rahman, Analysis of laminar forced convection of air for crossflow over two staggered flat tubes. International Journal of Automotive and Mechanical Engineering, 2012. **6**(1): p. 755-767.
94. Tillman, E. Natural convection heat transfer from horizontal tube bundles. 1976. ASME.
95. Keyhani, M. and T. Dalton, Natural convection heat transfer in horizontal rod-bundle enclosures. Journal of heat transfer, 1996. **118**(3): p. 598-605.
96. Hata, K., et al., Natural convection heat transfer from horizontal rod bundles in liquid sodium. Part 2: Correlations for horizontal rod bundles based on theoretical results. Journal of Nuclear Science and Technology, 2015. **52**(3): p. 342-354.
97. Hewitt, G.F. and J. Barbosa, Heat exchanger design handbook. Vol. 98. 2008: Begell house New York.
98. Razzaghpanah, Z., et al., Natural convection heat transfer from a horizontal row of finite number of heated circular cylinders immersed in molten solar salt. Journal of Energy Storage, 2019. **22**: p. 176-187.

99. Razzaghpanah, Z. and N. Sarunac, Natural convection heat transfer from a vertical column of finite number of heated circular cylinders immersed in molten solar salt. International Journal of Heat and Mass Transfer, 2019. **134**: p. 694-706.